Accelerating Wind Energy

A physical approach to monitor tower base fatigue loads using standard signals

Freark Jelmer Koopman B.Sc.

Master of Science Thesis

TU Delft Delft University of Technology

Vestas®

Challenge the future

Accelerating Wind Energy

A physical approach to monitor tower base fatigue loads using standard signals

Master of Science Thesis

For the degree of Master of Science in Sustainable Energy Technology at Delft University of Technology

Freark Jelmer Koopman

August 11, 2013

Faculty of Aerospace Engineering – Delft University of Technology

The work in this thesis was supported by Vestas Wind Systems A/S. Their cooperation is hereby gratefully acknowledged.

- Confidential -

Summary

Keeping track of the experience loads can be of great value for wind energy. If for instance lower loads are found than expected, the lifetime of a wind turbine could be extended beyond its design life. This will lead to a reduction in the cost of energy. Another advantage of so-called load monitoring is that design loads can be evaluated. This could lead to the conclusion that site conditions are different than expected, which means that either the turbine's operation needs to be altered or the design can be changed for future turbines. Furthermore load monitoring gives insight into turbine behaviour.

Loads can be measured directly with for instance strain gauges or optical fiber Bragg grating sensors. Installing these additional sensors can however be time consuming and expensive. Loads can also be monitored indirectly. In this case already available data is used to estimate the loads, omitting the need for extra sensors. Hence a system is wanted that uses the signals that are already available on wind turbines to describe the loads. It must be able to do so for all operating conditions.

Some research is already done into this subject. Most of it focuses on using artificial neural networks to link the available data to the experienced loads. These so-called black box models give however limited insight in the underlying process. What is wanted is a system that can predict the experienced loads for all circumstance, whilst giving as much insight as possible into turbine behaviour. Therefore a physical approach will be used to reach the following objective;

- Provide an accurate prediction of the tower base bending moment equivalent fatigue loads (10 min. 1 Hz and 1 year equivalent load ranges) by using the acceleration of the tower top.

The following steps are taken:

- The possibility of determining the tower bending moment from the tower top deflection is investigated with a homogeneous massless beam.
- It is investigated which steps need to be taken to find the tower top displacement from the tower top acceleration.

The results are validated with the aero-elastic code Flex5 and with measurements performed at two turbines from the Offshore Windfarm Egmond aan Zee.

For a homogeneous massless beam it is shown that predictions of the bending moment on the basis of tower top deflection and first eigenmode are exact if the only load is a horizontal force at the tower top. If moments or distributed loads are present, errors are introduced.

For wind turbines the loads other than the horizontal forces at the top are small in the fore-aft direction and may be neglected. In the side-side direction those can however be significant and need to be accounted for.

The deflection of the tower top must be found by integrating the measured acceleration twice. Integration of the low frequencies present in the acceleration signal leads to drift. A high-pass filter prior to the integration will prevent this from happening; a cut in frequency of 50 mHz can be used. The negative side effect is that filtering leads to information loss. In the fore-aft direction this needs to be compensated, which can be done with a thrust estimator. In the side-side direction no compensation is necessary.

Additionally, the acceleration signal is distorted from the measured gravity. It is shown that this will lead to overestimating the loads. This problem can be overcome with an iterative process between the estimated displacement and the measured acceleration.

For the Flex5 results the following conclusions are drawn.
The equivalent load range (10 min. 1 Hz) of the tower base bending moment from the tower top acceleration is:

- overestimated by 6% with a standard deviation of 3.5% in the fore-aft direction.
- overestimated by 3% with a standard deviation of 1.4% in the side-side direction.

The 1 year equivalent load range is:

- overestimated by 5% in the fore-aft direction.
- overestimated by 3% in the side-side direction.

For the OWEZ measurements conclusions need to be drawn with the following note. It is believed that one of the sensors from the turbine used to validate the results is installed in such a way that good results cannot be guaranteed. The prediction of the tower base bending moments will thus probably be better than the figures suggest.

The equivalent load range (10 min. 1 Hz) of the tower base bending moment from the tower top acceleration is:

- overestimated by 4% with a standard deviation of 11% in the fore-aft direction
- underestimated by 0.5% with a standard deviation of 7% in the side-side direction

The prediction of the 1 year equivalent load ranges is:

- overestimated by 7% in the fore-aft direction.
- overestimated by 3%in the side-side direction.

Contents

'There is nothing more deceptive than an obvious fact'

- Sherlock Holmes in 'The Boscombe Valley mystery'

1 Introduction

1.1 Wind energy

In Europe alone wind power has increased from 2% of the total installed power capacity in 2000 up to 11% in 2012, an increase of 93 GW, i.e. from 13 to 106 GW. In a normal wind year this is about 7% of European's gross electricity consumption. Furthermore, the annual installation of wind power has almost quadrupled in that same period, from 3.2 to 11.9 GW, figures representing a fast and steady growing industry. These are accompanied by the steady growth of installed turbines, from about 2 MW in 2000 to as big as 7.5 MW currently installed. [1]

That wind energy is such a rapidly growing market has mainly to do with government intervention. Without subsidies the price per kWh is still above market prices[1]. [2] It has therefore not yet made a definitive breakthrough. Upcoming countries for instance still rely heavily on coal for economic growth, mainly because it is the cheapest option [3].

Wind energy should be made as cheap as possible to increase its market share world-wide. One way of doing so is reducing its capital expenditure. That can be done by reducing material costs, i.e. using cheaper and/or less material.

Reducing the amount of material often also leads to reduced component strength. An optimum has to be found between the smallest amount of material and the biggest amount of strength. Eventually the components have to withstand the loads that may be expected during their operational life. Reasonable expectations are found in standards, where site conditions are divided into different classes. The expected operating conditions will by definition be more benign than the design class it was assigned to.

This implies that turbine loading during operation may be less severe than the design loads. This could lead to overdesigned turbines. Overdesigning means that more material is used than necessary, making wind turbines more expensive than necessary. To verify those thoughts however, the experienced loads should be monitored and compared with the design loads.

The costs of wind energy can also be reduced by increasing a wind turbine's energy yield. Monitoring the loads can help achieving that in different ways.

If loads are found that exceed expectations, the turbine's operation can be adjusted to ensure lowest possible energy costs for this particular situation. [4] The production can for instance be reduced to prevent more damage, or production can be ensured while waiting for maintenance or spare parts.

If the loads are however lower than expected the experienced fatigue will probably also be lower than expected. This means that a turbine's lifetime could be extended beyond its design life, increasing its total energy yield, thus reducing the cost of energy. Additionally, if it is expected that a turbine's lifetime can be extended, authorities have to be convinced that the actual fatigue damage is smaller than originally calculated.

Other possible advantages of fatigue load monitoring are that: it can be used for load reduction algorithms; it can help find abnormal turbine behaviour and loading information leads to better understanding of the impact of site and operational conditions.

[1] 0.04 €/kWh for coal vs. 0.058 €/kWh for wind in 2010. When environmental (CO_2) and regulation costs are taken into account it evens out at around 0.06 €/kWh [34]. Some even argue that wind energy will then be actually cheaper than conventional resources [30].

1.2 Previous work

Load monitoring is already done in other industries. For instance, dozens of papers can be found on monitoring the loads on bridges. Load monitoring can also be seen as a form of structural health monitoring, which seems to be the preferred term in civil engineering. In [5] already 40 different structural health monitoring projects on bridges are reviewed. Structural health monitoring can also be found in aircraft engineering. However, they are more focused on damage detection, with for instance systems as described in [6].

The biggest difference between these industries and the wind industry is that turbines are often installed in remote locations, especially with the current interest in offshore wind energy. This means that measuring the loads can be expensive and time consuming because extra sensors need to be installed [4] [7]. The need of additional sensors can be omitted by estimating the loads indirectly from other already available (i.e. measured) physical quantities[2], so-called indirect load monitoring.

Indirect load monitoring is again already done in civil engineering. A way to predict loads in bridges is given by Roberts et al. [8]. They combine a GPS signal with an acceleration sensor to predict bridge deflection. Also in aircraft engineering some applications can be found. In [9] different approaches are reviewed to predict the structural health of helicopter components from flight parameters. Load monitoring is also done on electric motors, where current signature analysis is done for the estimation of motor loadings and faults.

In the wind energy industry not much is found on indirect (fatigue) load monitoring. It seems that just 6 contributions to this topic were made. A large part of that is done by Cosack [4], he describes some of the possible approaches to use standard turbine signals for monitoring the loads.

An artificial neural network is the preferred method by Cosack and was part of his approach as well as the research done by Obdam et al. [10], Dittmar et al. ([11] from [4]) and Hofemann et al. [12].

Artificial Neural Networks can be trained with existing data to find the relation between certain in- and output. If the network is large enough it is able to describe complex relations with relatively simple functions.

Obdam et al. use neural networks in ECN's flight leader concept to determine the blade root and the tower base bending moments. Only a small amount of turbines, the flight leaders, are equipped with load measurement instruments. These measurements are related to their corresponding SCADA data with the use of an Artificial Neural Network. Combining the established relations with the SCADA data from the other turbines allows for a load reconstruction of the whole windfarm. For this approach, however, still some turbines have to be equipped with load measurement devices. [10]

Dittmar et al. used neural networks to determine the load cycle distribution of blade root bending moments. Rotational speed, electrical power and pitch angle acted as input. Their approach was tested on simulated and measured data with good success. [4]

Hofemann et al. also apply a neural network to reconstruct blade root bending loads. They however also tested the transferability of the method beyond one particular wind turbine or wind farm. They claim the results to be promising but not satisfying. Future improvements are planned to test the model in complex terrains and offshore. [12]

Artificial neural networks seem to give good results, but give limited insight in the process. Other than knowing which parameters found useful to act as input, not much can be said about what determines the size of the loads.

Physical Models use physical laws to the determine the size of the loads. The response of such a model can therefore be explained by basic physics. This can give more insight in the process than a neural network, which is basically a 'black box'.

[2] E.g. the power output could describe the wear of the rotor bearings, since it is directly related with the amount of rotor revolutions.

A physical based approach was applied in the UPWIND project [13], where the blade root and tower base bending were predicted with direct and indirect measurements. One proposed approach was further investigated, mainly focusing on tower base bending moment [14].

They describe a method for online load estimation with a state-space observer, using the tower top acceleration, power, rotational speed and pitch angle. The observer is used to estimate the states of a linear time-invariant model that is valid for a certain steady operating point. Good results were found for the loads regarding the first bending frequency.

However, only two load cases were investigated (i.e. at 6 and 18 m/s average wind speeds). Furthermore, slow varying loads were not well captured; it is not clear why that is the case.

A different approach to determine the blade root loads was used by Ochoa Algarín [15]. A load database was constructed according to the turbine state and with respect to wind speed and turbulence intensity. The results could be improved with using more variables as input for the database.

So-called state estimation means that the turbine's operation has to be categorized into suitable sub-states with corresponding representative loads. It can than also give results for turbine states that are difficult to assess. From there periodic state estimations one can reconstruct the loading history based on the states' corresponding loads.

Another approach is given by Veldkamp [16]. He suggests performing simulations for all relevant circumstances (this may very well be a couple of thousand) and correlating them with test results in a table. This table can then be used to predict the loads based on the monitored circumstances. An Artificial Neural Network can also be used to find the relationship between the calculated and measured loads.

1.3 Objective

It is clear that not much research is done into indirect load monitoring in the field of wind energy. However, the research that is done mainly focuses on using artificial neural networks. Although this approach gives promising results it gives limited insight in the underlying process.

What is wanted is a system that can predict all the experienced loads for all circumstances from already available signals, whilst giving insight into turbine behaviour.

This has led to the following objective:

- Provide an accurate prediction of the tower base bending moment equivalent fatigue loads (10 min. 1 Hz and 1 year equivalent load ranges) by using the acceleration of the tower top.

The following steps are taken:

- The possibility of determining the tower bending moment from the tower top deflection is investigated with a homogeneous massless beam.
- It is investigated which steps need to be taken to find the tower top displacement from the tower top acceleration.

The results are validated with the aero-elastic code Flex5 and with measurements performed at two OWEZ turbines

1.4 Organisation

In chapter 2 some background on fatigue is given. It is explained how fatigue can be quantified and how different load cycles are compared. Furthermore, it is explained how results should be interpreted.

Then, in chapter 3, it is investigated if the tower top displacement will be able to act as an input for the prediction of the tower base bending loads. This will be supported by the state-of-the-art BEM program Flex5. Different load cases are used for the verification of the applied approach.

Chapter 4 handles the integration necessary to find the tower top displacement from the tower top acceleration. Some background on numerical integration is given together with possible problems that can occur with integration. Again, Flex5 will be used to verify the approach for different load cases.

Chapter 5 gives the overall lay-out of the load estimation method and concludes on the theory and the results from the simulations.

The derived approach will be verified with data from measurements performed at the Offshore Windfarm Egmond aan Zee. An explanation about the wind farm and the measurements performed on the turbine can be found in chapter 6.

In chapter 7 the Flex5 results will be compared with measurements. The findings will be discussed and the method will be fine-tuned with data from one turbine. An independent data set from a second turbine will be used to validate the approach.

Finally conclusions and recommendations are given in chapter 8.

Some additional information is given in the appendices.

2 Methodology

2.1 Introduction to fatigue

The goal of this thesis is to give an accurate prediction of the fatigue loads. The reason for that is that fatigue plays an important role in the lifetime of a turbine. Wind turbines are slender structures with rotating parts that are excited by turbulent wind. Together with an operational life of 20-25 years it is not hard to imagine that wind turbines are subjected to a large number of load cycles (op to 10^9). Each load cycle will have a small contribution to the total fatigue damage.

To give some insight into why that is the case and how fatigue can be quantified some background on fatigue is given.

2.1.1 Material fatigue

Fatigue is the phenomenon that repeated cyclic loading, with stress amplitudes well below the yield limit, can cause a material/component to fail. So-called micro cracks occur that develop into larger cracks until failure occurs. [17]

The relationship between the stress amplitude and the corresponding number of cycles until failure occurs can be described by a S-N diagram, or Wöhler curve. A material specimen is subjected to cyclic loading with constant amplitude until failure occurs. When repeating the experiment with different stress amplitudes the complete diagram can be determined, Figure 2-1. Furthermore if the loading is too small to initiate a crack the lifetime is infinite, explaining the horizontal 'tail' of the curve, or 'knee'. If the loading is too big however (ultimate loading), one cycle will be enough to cause a failure, explaining the horizontal beginning.

Some indicative numbers are as follows. The two 'knees' are typically around 10^4 and 10^7 cycles and the fatigue limit (amplitude) is at roughly 1/3 of the ultimate strength. The slope of the curve in a log-log diagram (Wöhler exponent) is 1:4 for weld seams, 1:8 for nodular cast iron and 1:12 for blade materials (e.g. glass fibre reinforced plastics or epoxy) [18]

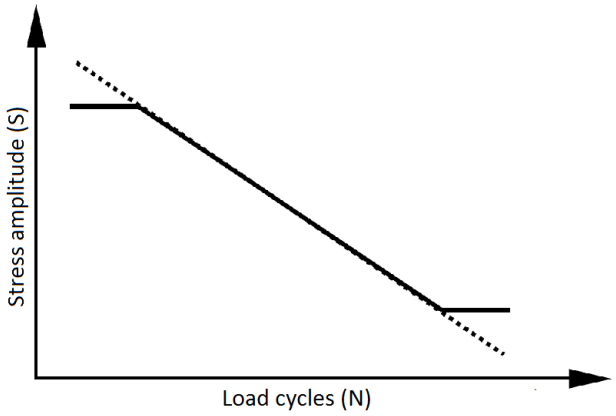

Figure 2-1 Example of an S-N curve with 'real' data (solid line) and an idealised curve (dotted line) [17]

For material testing the amplitude of the stress cycles is beforehand determined and the number of cycles can be easily counted. In operational conditions both the size and the amount of cycles will be measured passively. This will most probably result in a signal with a random order of varying stress cycles.

A so called rain-flow-counting algorithm can then be used to decompose the signal into single stress cycles with their corresponding amplitudes. These can then be grouped in a counting histogram with respect to for instance their mean and amplitude. This makes it possible to compare the loading with the test results. This process is shown in Figure 2-2.

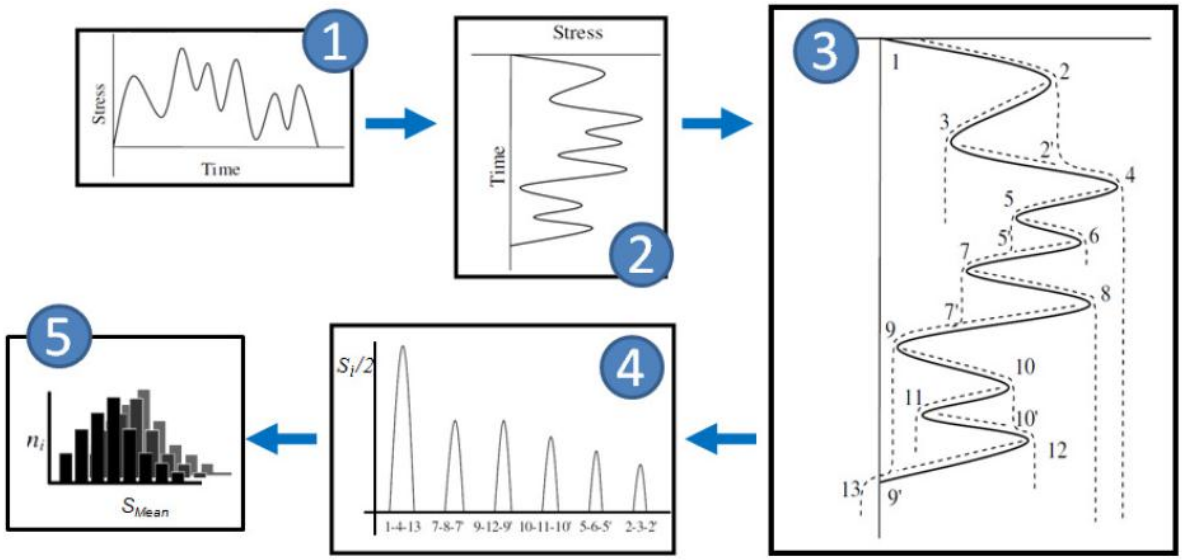

Figure 2-2 Load decomposition with rainflow counting, figure from [15]

In step 1 the original time series is given. In step 2 the plot is rotated to allow for the 'rain to fall onto the signal', which is shown in step 3. Each local maximum and minimum is given a number, in the example from 1 to 13. The 'rain' falls on each peak and the 'drops' roll and eventually fall down. The path each drop has followed before it is at the end of the signal or falls on another drop will determine the size of the cycle. All the cycles are gathered in step 4. If the signal was longer than most probably more cycles would be found with the same amplitude. These are then combined in a so-called counting histogram, step 5.

The counting histogram thus gives the amount and the size of the stress cycles. From there the S-N curve can be used to determine the experienced fatigue. A way to quantify the experienced fatigue is with using equivalent fatigue load ranges.

2.1.2 Equivalent loads

The equivalent load range is the constant amplitude fatigue load that produces the same fatigue damage as the original signal, when applied during a fixed number of cycles. That number can be chosen arbitrarily and different numbers will give a different outcome. It is a well-known concept in the field of fatigue and often used in wind turbine load analysis [19].

It is a way to reduce time series to a single number whilst keeping information about the experienced fatigue. A visualisation for better understanding is given in Figure 2-3. The histogram on the left represents the result of the rain-flow-count and the 'box' on the right represents the equivalent load. In this example the damage is visualised as the area under the histogram, which is the same as the area of the 'box' in the right plot.

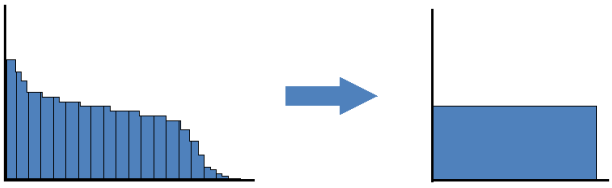

Figure 2-3 Principle of equivalent load range

For the calculation of equivalent loads (equation (2.1)) some assumptions are made. First of all a linear damage accumulation is assumed, i.e. the amount of damage is independent of the order of the load cycles. Also, the dotted line from Figure 2-1 is used to incorporate all the load cycles, where a double logarithmic scale is assumed. This means that even the cycles that are too small to initiate a crack are taken into account. Furthermore for welded seams, as in a turbine tower, it is assumed that due to residual stresses the mean of the load profile will hardly influence the fatigue. Tower fatigue is thus dominated by the stress amplitudes and not by the mean loading. [18]

Even though these assumptions are incorrect they may be made because the concept of equivalent loads is used to compare different load cases. This means that the error introduced by these simplifications will most likely exist in either of the equivalent loads, cancelling each other out. [20]

$$\Delta F_{eq} = \left[\frac{\sum_i \Delta F_i{}^m N_i}{N_{eq}}\right]^{1/m} \tag{2.1}$$

Where,

ΔF_{eq}	Equivalent load range
N_{eq}	Number of equivalent load cycles[3]
ΔF_i	Stress range cycle
N_i	Number of stress range cycles
m	Wöhler curve exponent (the inverse of the slope of a material's S-N curve)

Additionally the lifetime equivalent load can be calculated, it includes the probability of occurrence of a load case and is given in (2.2).

$$L_{eq} = \left(\sum_i \Delta F_{eq,U}{}^m p_U\right)^{1/m} \tag{2.2}$$

Where,

$F_{eq,U}$	Mean equivalent load range at (U)
U	Wind speed
p_U	Probability of (U)

The mean equivalent load range per wind speed can be found with equation (2.3). All the equivalent load ranges are binned according to their wind speed U

$$F_{eq,U} = \sum \left(\frac{\Delta F_{eq}(U)^m}{n(U)}\right)^{1/m} \tag{2.3}$$

Where,

$\Delta F_{eq}(U)$	Equivalent load range per wind speed
$n(U)$	Number of equivalent loads in (U)

[3] Often a 1 Hz equivalent load frequency is used, so for a time period of 10 min, N_{eq} would be 600. And

The probability of occurrence is given from a weibull distribution. Its probability density function is given by,

$$p(U) = \frac{k}{U}\left(\frac{U}{a}\right)^{k} e^{-(U/a)^{k}} \tag{2.4}$$

Where,

$$a = \frac{U_{average,year}}{0.89} \tag{2.5}$$

and,

k shape parameter $[-]$
U Wind speed $[m/s]$

In this thesis a shape parameter of 2 will be chosen with a yearly average wind speed of 10 m/s, which about right for the North Sea coast. [21]

2.2 Presentation of results

The fatigue damage equivalent load ranges, or equivalent loads, are used throughout this thesis to compare result. The comparison is done by calculating the ratio between the estimated and the measured equivalent loads, equation (2.6). Measured in this sense can also mean: as calculated in a simulation, i.e. Flex5 calculates the loads as if they were measured with a strain gauge.

Equivalent loads are used here to reduce any time series to a single number.

$$R_{\Delta Feq(Est/Meas)} = \frac{\Delta F_{eq}(Estimated)}{\Delta F_{eq}(Measured)} \tag{2.6}$$

This ratio is presented in a scatter plot versus a measured physical quantity (often wind speed is used), an example is given in Figure 2-4. If the investigated approach is correct the ratio will be 1. For the example given below the proposed approach could suffice, because

- the prediction of the equivalent load range (10 min. 1 Hz) of the measured quantity is possible with an accuracy of 100% with a standard deviation of 0.7%.
- the prediction of the 1 year equivalent load range is possible with an accuracy of 99%.

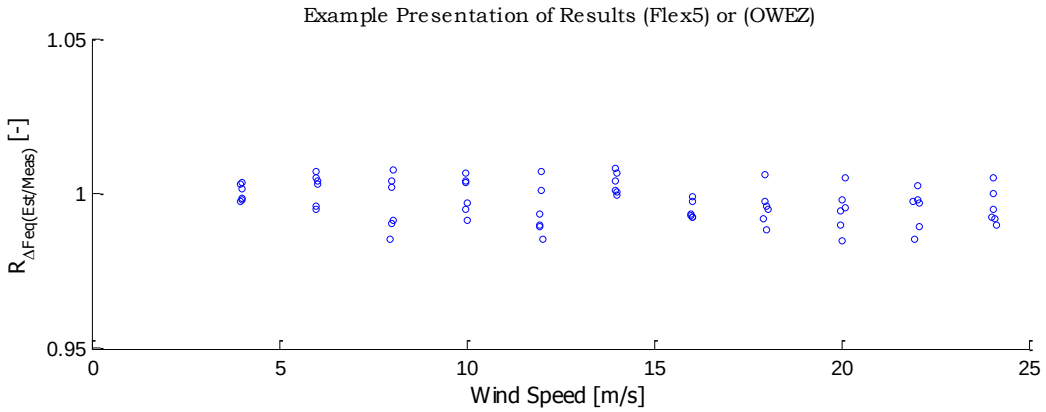

Figure 2-4 Example ratio of equivalent loads from a simulation (Flex5) (Ratio = Estimated/Measured). Data from the Offshore Windfarm Egmond aan Zee is indicated with (OWEZ)

2.3 General approach and terminology

Wind turbine simulations are performed with the aero-elastic code Flex5 (Appendix A). The turbine behaviour is simulated for 66 load profiles. Those are 10 min loadings of 6 different wind profiles at 11 mean wind speeds (i.e. 4, 6, 8…24 m/s). From a quick look at Figure 2-4 it can thus be easily concluded that the figure shows the results of Flex5, since the results are nicely divided over the different wind speeds

The so-called fore-aft and side-side direction will be treated separately, Figure 2-5.

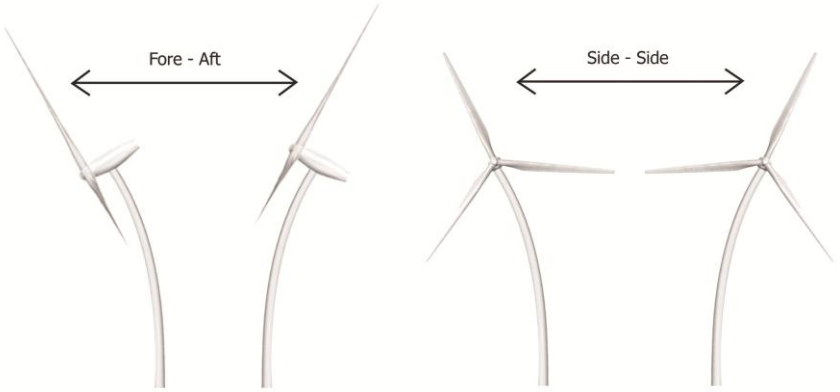

Figure 2-5 Exaggerated fore-aft and side-side bending of a wind turbine

On occasion the word 'filtered' is used. In this thesis it is used as short for 'a high (or low) pass Fourier filter is used'. The filter was made with using a Fast Fourier Transform, which is a standard Matlab routine. Additionally this routine can also be used for integration in the frequency domain. In Appendix B it is shown with the OWEZ data that similar results are found. Additional information about Fourier can also be found there.

The steps taken are visualised in a flow chart. It is only intended to give a better insight in the approach; it does not represent an actual model. The following blocks are used. The subscripts in the signal indicate for which direction (fore-aft (FA) or side-side (SS)) the process is used.

- Process

- Gain

- In- or output

- Summation 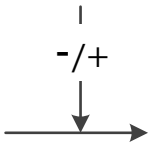

Furthermore, symbols and abbreviations will be explained in the main text where they first occur.

3 From deflection to tower base fatigue loads

The fatigue of the tower can be quantified by calculating the equivalent loads from the number and size of the stress cycles from the loads. The stress experienced by the material can be calculated from the bending moments.

In this chapter it is investigated with a homogenous massless beam if the deflection of the tower top can be used to estimate the bending moments at the tower base. The results will be validated with Flex5.

In chapter 4 the estimation of the deflection of the tower top will be treated.

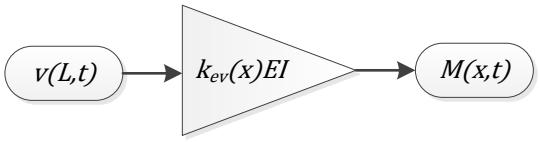

Figure 3-1 Flow chart to predict the bending moment from the tower top deflection

The basic idea is given in Figure 3-1. The deflection at the tower top $(v(L,t))$ is assumed to be directly related with a gain $(k(x)EI)$ to the bending moment $(M(x))$. How this relation is described and what the size of the gain is will be explained in the next section.

3.1 Beam theory

Any tower will in free oscillation, oscillate in all of its eigenfrequencies with their corresponding eigenmodes (i.e. a mode shape). Figure 3-2 shows two typical mode shapes that correspond to the first (at the left) and second eigenfrequency of a clamped beam.

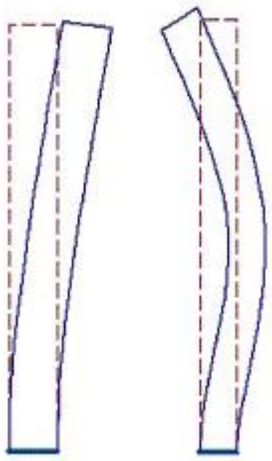

Figure 3-2 Examples of typical bending modes of a clamped beam

Mode shapes are a good way to approximate the actual bending mode of a beam or tower under loading. A combination of different mode shapes is often needed to improve the approximation. To what extent and how many of such mode shapes should be combined can be examined with a power spectral density plot[4]. Such a plot of the time series of the Fore-Aft bending moments of a turbine's tower is given in Figure 3-3. There it can be seen that the motion at the first eigenfrequency is dominant and that the second one is hardly visible.

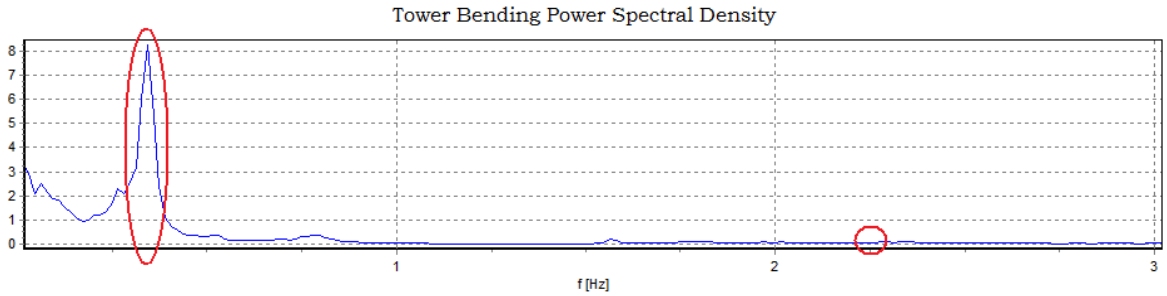

Figure 3-3 Power spectral density of the bending moment of a certain 10 min period

This means that the first eigenmode could be a good estimation of the actual bending mode. This means that the deflection of the tower top is a good estimator for the size of the bending[5]. To explain the principle the tower is assumed to be a homogeneous massless beam with a point mass on top (Figure 3-4).

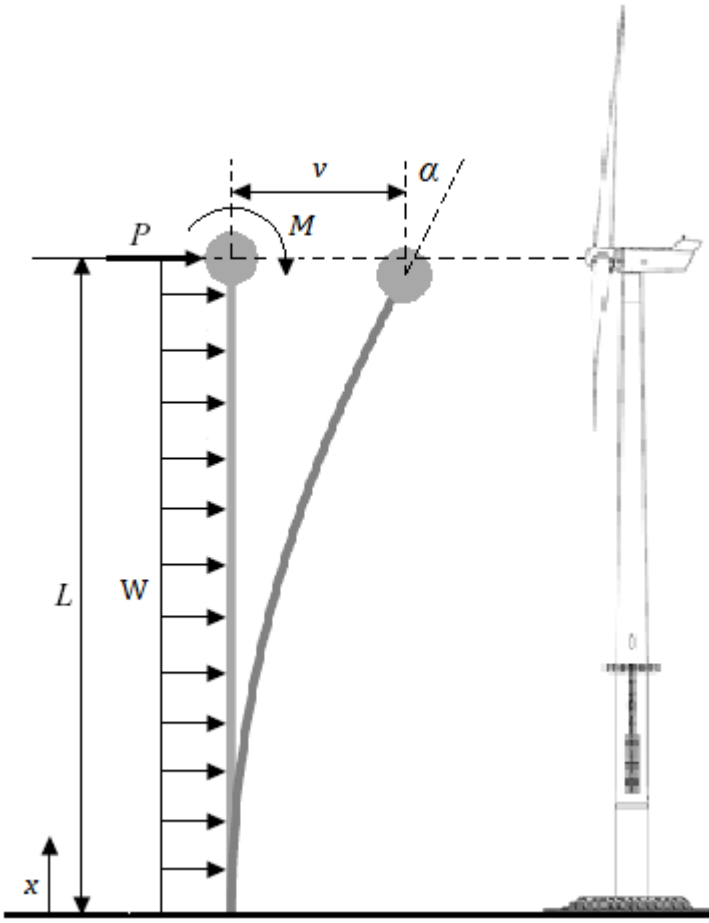

Figure 3-4 Free body diagram of a clamped beam (left) representing the turbine tower (right) in its first mode shape (exaggerated) under horizontal Fore-Aft loading.

[4] Some additional information about power spectral density can be found in Appendix B.

[5] If the second eigenmode would be dominant the deflection at the middle of the tower would be of interest.

The mode shape is estimated with the assumption that only the force (P) is applied to the tower top $(x = L)$. That means that the bending moment (M) and distributed loading (W) are neglected. For a wind turbine this would mean that it is assumed that the thrust force of the rotor dominates the turbine loading. The first mode shape is then described by eq. (3.1)-(3.3).

$$v_{ev}(x) = \frac{3Lx^2 - x^3}{2L^3} \tag{3.1}$$

$$\alpha_{ev}(x) = \frac{6Lx - 3x^2}{2L^3} \tag{3.2}$$

$$\kappa_{ev}(x) = \frac{3(L - x)}{L^3} \tag{3.3}$$

Where,

v_{ev}	Generalised deflection $[-]$
x	Distance from bottom $[m]$
L	Tower/Beam length $[m]$
α_{ev}	Generalised rotation $[-]$
κ_{ev}	Generalised curvature $[m^{-2}]$

The local bending moment $(M(x))$ is a product of the local curvature and the bending stiffness eq. (3.4).

$$M(x) = \kappa(x)EI \tag{3.4}$$

Where,

$$\kappa(x) = \kappa_{ev}(x)v(L,t) = \frac{3(L - x)}{L^3}v(L,t) \tag{3.5}$$

and,

E	Elasticity $[Pa]$
I	Area moment of inertia $[m^4]$

Combined they lead to a linear relationship between tower top deflection and bending moment anywhere on the tower, eq. (3.6).

$$M_{est}(x) = \kappa_{ev}(x)EIv(L,t) \tag{3.6}$$

Remember that equation (3.6) is true when the moment at the tower top and distributed loading on the tower are neglected. This can only be done if these loadings are small with respect to the thrust force or if the mode shape described in equation (3.1) is also valid for a nonzero bending moment and distributed load.

The moment at the tower top is a result of the overhanging weight of the nacelle and blades. Its contribution to the total bending moment is at low wind speeds (i.e. where the thrust force is relatively low) almost 20%, which is too big to neglect[6].

The distributed loading on the tower is the drag from the wind on the tower. Its contribution to the total bending moment is at high wind speeds (i.e. where the wind drag on the tower is highest) close to 10%, which is also too big to neglect.

It thus needs to be checked if the given mode shape suffices for this type of loading. In equations (3.7)-(3.14) it is shown that it is not able to describe the loading of the thrust force, bending moment and tower drag.

Whenever a force (P) and a moment (M) are applied at $x = L$ and a distributed load (W) is applied to the whole tower the work (or generalised force, F_{gen}) is given by,

$$F_{gen} = P v_{ev}(L) + M \alpha_{ev}(L) + \int_0^L W v_{ev}(x) dx = P + M \frac{3}{2L} + W \frac{3L}{8} \qquad (3.7)$$

The generalised stiffness is given by,

$$\mathrm{K}_{gen} = \frac{3EI}{L^3} \qquad (3.8)$$

If it is assumed that the deflection will come from the horizontal component of the thrust force only (i.e. $M = W = 0$), the following formula will hold.

$$v(L) = \frac{F_{gen}}{\mathrm{K}_{gen}} = \frac{PL^3}{3EI} \qquad (3.9)$$

If only the moment is considered (i.e. $P = W = 0$) the following holds,

$$v(L) = \frac{F_{gen}}{\mathrm{K}_{gen}} = \frac{ML^2}{2EI} \qquad (3.10)$$

and if only the uniform distributed loading of Figure 3-4 is considered (i.e. $P = M = 0$) the displacement becomes,

$$v(L) = \frac{F_{gen}}{\mathrm{K}_{gen}} = \frac{3WL^4}{8EI} \qquad (3.11)$$

The latter three equations, (3.9) - (3.11), are also known as the so-called 'vergeet-me-nietjes' and can be found in any textbook on mechanics. Combined they lead to the total deflection, equation (3.12).

[6] This contribution will become lower at higher wind speeds because the thrust force will increase, while the bending moment decreases due to increasing tilt angles. The difference should peak at rated wind speed.

$$v(L) = \frac{8PL^3 + 12ML^2 + 3WL^4}{24EI} \tag{3.12}$$

The curvature can be derived from eq. (3.5) and (3.12),

$$\kappa(x) = \left(\frac{P}{EI} + \frac{3M}{2EI \cdot L} + \frac{3WL}{8EI}\right)(L - x) \tag{3.13}$$

leading to the following bending moment, from eq. (3.4) and (3.13).

$$M_{est}(x) = P(L - x) + M\frac{3(L - x)}{2L} + W(L - x)\frac{3L}{8} \tag{3.14}$$

However, the exact bending moment is calculated as the integral of all the external forces from L to x minus the integral of mass times acceleration. That will in equilibrium, when the acceleration is zero, reduce to basic mechanics, eq. (3.15).

$$M_{exact}(x) = P(L - x) + M + W(L - x)\frac{(L - x)}{2} \tag{3.15}$$

This shows that the two approaches give different results. Obviously, equation (3.15) is correct. The problem is that the shape function described earlier and used for the derivation of equation (3.14) cannot be used for this loading. [22] The estimated bending moment should be corrected with,

$$\Delta M = M_{exact}(l) - M_{est}(l) = M\left(\frac{3x - L}{2L}\right) + W(L - x)\left(\frac{L - 4x}{8}\right) \tag{3.16}$$

For a homogenous massless beam, the bending moments can be calculated from the top deflection if the moment at the top end and the distributed loading are known, equation (3.17).

$$M(x) = \frac{3EI(L - x)}{L^3}v(L) + M\left(\frac{3x - L}{2L}\right) + W(L - x)\left(\frac{L - 4x}{8}\right) \tag{3.17}$$

This means that, for the most interesting location, where the bending moment is maximum at $x = 0$ the error is

$$\Delta M = -M/2 + WL^2/8 \tag{3.18}$$

The two terms are opposing, thus there is reason to believe that at some point near the tower base the predicted bending moment from the tower top deflection will be accurate. It depends however on the sign of the loading.

To summarize, for a homogenous massless beam the bending moment anywhere on the beam cannot be described by knowing the tower top deflection. However, for this approach the mode shape determines how the external loadings are treated. For the example above this meant that the moment at the tower top and the tower drag also need to be known. They should be added, with a certain correction factor that follows from the mode shape (eq. (5.2)), to the linear relationship between the deflection and the bending moment, eq. (3.6), which yields to eq. (3.17).

This approach is summarised in the flow chart of Figure 3-5.

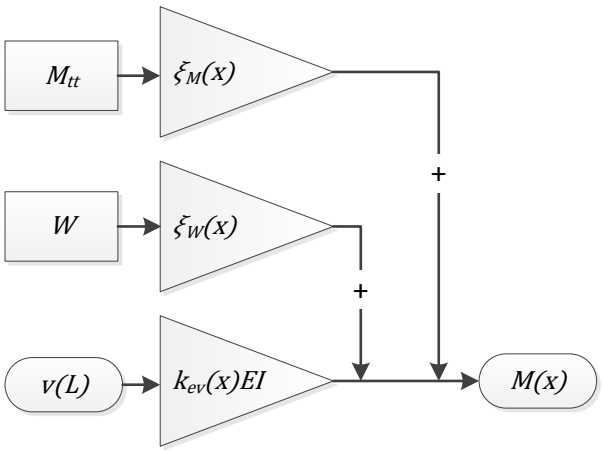

Figure 3-5 Flow chart for finding the bending momemt from the tower top deflection

3.2 Flex5 results (Static analysis)

3.2.1 Fore-Aft direction

In Flex5 the assumption of a homogenous massless beam is incorrect because an actual wind turbine tower with varying mass and stiffness is used. The mode shape given in the previous section (eq. (3.1)) will probably give wrong results. Better results will be found if the mode shape that describes the first eigenmode of the tower is used.[7]

Equation (3.6) is used to see how well the assumed mode shape can describe the actual loading. The mean values of the calculated time series from the Flex5 program (Appendix A) are used to compare results. The ratio between the estimated and measured bending moment (eq. (3.19)) should be exactly 1, if the calculations are right.

$$R_{BM} = \frac{\bar{M}_{est}}{\bar{M}_{meas}} \tag{3.19}$$

It is not expected that R_{BM} is indeed 1 for all load cases, since the single mode shape will most probably not be able to describe all the loads acting on the tower. The reason for this was given in section 3.1. There it was shown that the bending moment at the tower top and the distributed loading from the wind on the tower distort the results.

To see to what extent that is the case, the simulations are done with different assumptions:

- normal conditions (Real [o]);
- without a moment at the tower top (G=0 [*]);
- without the bending moment and distributed load on the tower (G=Cd_{twr}=0 [□]).

[7] In Appendix B a method to is given to find the Eigen mode of a beam or tower. However, the mode shape calculated by Flex5 is used; the approach given in Appendix B gives similar results though.

The moment is omitted by removing gravity. The distributed load is omitted by setting the tower drag coefficient to zero. The results are shown in Figure 3-6.

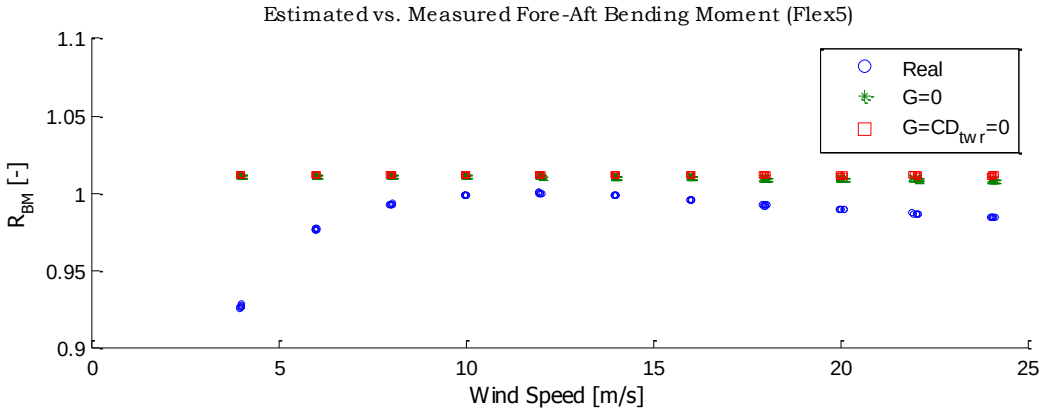

Figure 3-6 Ratio between the mean values of the estimated and measured bending moments for real conditions (Real); without gravity (G=0) and without gravity and tower drag (G=Cd_{twr}=0). (Flex5) (Ratio = Estimated/Measured)

The wind loading on the tower hardly influences the results and will therefore be neglected. Neglecting the moment at tower top however, does result in significant errors and should be accounted for. The Fore-Aft moment at the tower top is,

$$M_{tt,FA} = mGd\cos(\alpha) \tag{3.20}$$

Where,

m Mass of the nacelle, hub and blades $[kg]$
G Gravitational constant $[m/s^2]$
d Distance between centre of gravity and tower midpoint $[m]$
α Tower top rotation $[rad]$

The bending moment at the tower top is thus not constant, which makes it hard to predict. However, the rotation is considered to be very small, so equation (3.20) can be simplified to equation (3.21).

$$M_{tt,FA} = mGd \tag{3.21}$$

This moment should be taken into account when calculating the bending moment at the tower base, which leads to the following relationship between the tower top deflection and the tower base bending moments.

$$M_{est,FA}(x) = \kappa_{ev}(x)EIv_{FA}(L) + \xi(x)M_{tt,FA} \tag{3.22}$$

Where,

ξ correction factor[8] $[-]$

[8] This factor depends on the assumed mode shape. It was derived in equation (5.2) for the example in section 3.1, for other mode shapes/examples it is easiest found iteratively.

The result of using equatin (3.22) is shown in Figure 3-7. It can be seen that it gives good results, but there is still a small overestimation of the bending moments, about 1%. Since the size of that error is small and more importantly, constant for all load cases, the cause of the error is not further investigated.

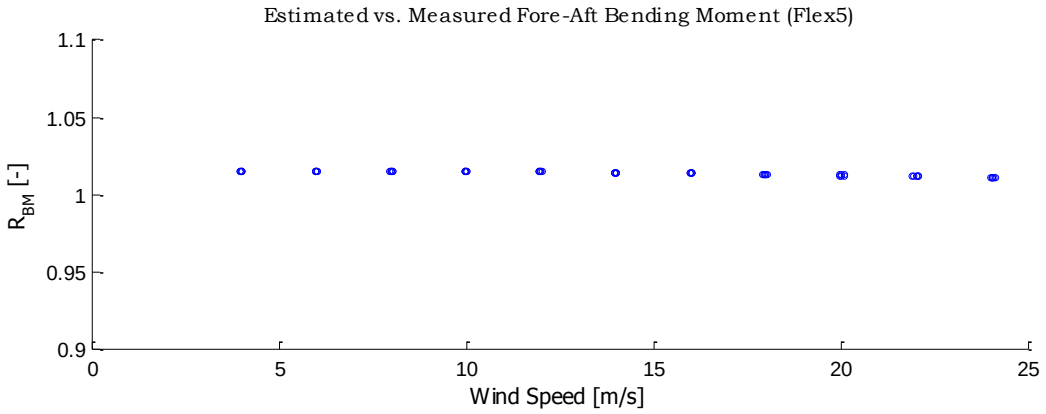

Figure 3-7 Ratio between the mean values of the estimated Fore-Aft bending moment (corrected for overhanging nacelle weight) and the measured bending moment (Flex5) (Ratio = Estimated/Measured)

In Figure 3-8 the approach is summarised. The curvature from the eigenmode of a turbine tower can be used to estimate the bending moment from the deflection at the tower top. The relationship is however not linear as equation (3.6) and Figure 3-1 suggest. The moment at the tower top, from the overhanging weight of the nacelle and blades, distorts the results. It can be accounted for if added as a constant with a correction factor that can easiest be found iteratively.

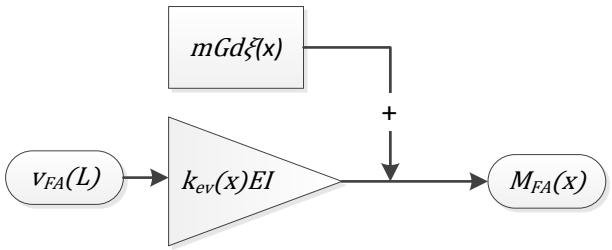

Figure 3-8 Flow chart for finding the fore-aft bending moment from the tower top deflection. The influence of the wind loading may be removed and the correction from the tower top may be added as a constant.

3.2.2 Side-Side direction

The theoretical approach in section 3.1 showed that the distributed loading on the tower and the bending moment at the tower top may not be neglected when the bending moment is predicted from the tower top deflection. In the Fore-Aft direction the distributed loading comes from the wind drag of the tower. The bending moment comes from the overhanging weight of the nacelle and blades. If they were neglected the bending moments were underestimated.

For the Side-Side direction the wind loading may be neglected, because even in the Fore-Aft direction it was hardly visible. The moment at the tower top comes from the rotor torque, if it is neglected the results in Figure 3-9 are found. Figure 3-9 shows the ratio between the linear relationship between deflection and bending moment, equation (3.6) and the actual bending moment. The first Eigen mode of the tower is again used to determine the curvature.

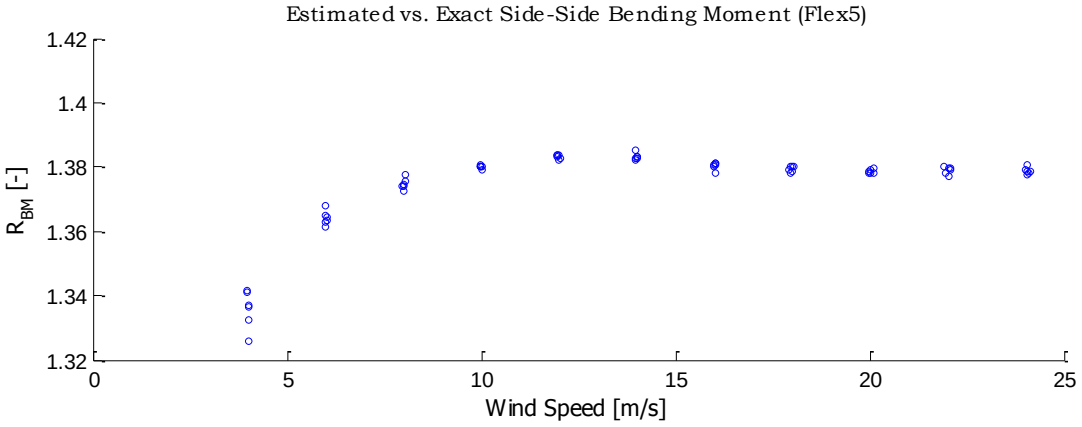

Figure 3-9 Ratio between the mean values of the estimated and exact Side-Side bending moment (Flex5) (Ratio = Estimated/Measured)

It shows that the bending moments are overestimated with more than 30%. The overestimation becomes more or less constant above rated wind speed, i.e. where the torque is constant. The horizontal force and the bending moment act in the same direction, unlike with Fore-Aft bending, therefore the bending moments are overestimated. It is clear that the moment at the tower top may not be neglected.

The bending moment at the tower top comes from the torque (T_{static}) of the rotor and is given as,

$$M_{tt,SS} = T_{static} = \frac{P}{\Omega} \tag{3.23}$$

Where the power[9],

$$P = \frac{P_{el}}{\eta(P_{el}, \Omega)} \tag{3.24}$$

and,

P_{el} Electric power $[W]$
Ω Rotor speed $[rad/s]$
η Combined drive train and generator efficiency $[-]$

The Side-Side bending moment can thus be described as follows.

[9] This holds for the static case, hence the *static* under script at the Torque. For the dynamic case the inertia of the rotor and drivetrain should also be taken into account.

$$M_{est,SS}(x) = \kappa_{ev}(x)EIv_{SS}(L) - \xi(x)M_{tt,SS} \quad (3.25)$$

Remember that the bending moment is in the same direction as the actual bending, therefore the moment at the tower top is subtracted instead of added, as was done for the fore-aft bending. The result of equation (3.25) is given in Figure 3-10, where ξ is the scale factor from the assumed mode shape and is again found iteratively. The difference between the actual moment at the tower top (from Flex5) and the estimated moment at the tower (from eq. (3.23)) is also shown in Figure 3-10.

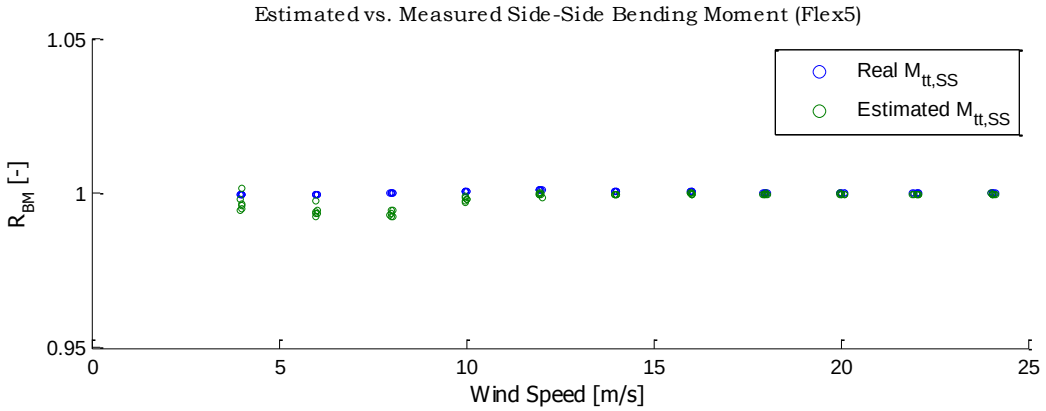

Figure 3-10 Ratio between the mean values of the estimated and the measured Side-Side bending moment, where the estimated bending moment is corrected with the real and estimated tower top bending moment. (Flex5) (Ratio = Estimated/Measured)

It shows that the Side-Side bending moment can be described with the tower top deflection if the bending moment at the tower top $(M_{tt,SS})$ is known. When the real tower top bending moment is used estimated tower base bending moment is exactly the same as the actual tower base bending moment. For the estimated tower top bending moment from estimating the Torque the bending moments are slightly under predicted below rated wind speed. That means that the torque is slightly overestimated.

For calculating the torque the mechanical as well as the electrical efficiency of the generator is guessed, i.e. interpolated from a lookup table that varies with power and rotational speed. It could be that at the point where both are constantly changing, i.e. below rated wind speed, the generator's efficiency is underestimated. Eventually the error is less than 1% and it can therefore be stated that the torque estimator performs well.

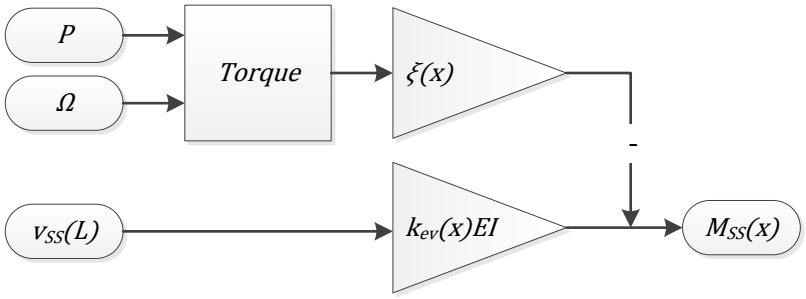

Figure 3-11 Flow chart for finding the side-side bending moment from the deflection. The torque needs to be subtracted from the linear relationship to prevent overprediciotn

3.3 Flex5 results (Dynamic analysis)

3.3.1 Fore-Aft

In the previous section it was proved that for the turbine tower the bending moment can be calculated from the tower deflection if the moment at the tower top is known (eq. (3.22)). Therefore, also the equivalent loads of the estimated bending moments should coincide with the equivalent loads from the exact bending moments.

However, accounting for the fore-aft bending moment at the tower top only adds a constant to the linear relationship between deflection and bending (eq (3.6)). It thus only influences the mean value of the estimated bending moment, which has no effect on the equivalent loads (eq. (2.1)); for welded seams it is believed that the amplitudes of the stress cycles are dominant and the mean values may be neglected. A linear relationship between deflection and bending moment may be used; although wrong, its use is justified whenever equivalent loads are considered.

The ratio between the equivalent loads of the estimated and the measured bending moments (equation (3.26)) is given in the figure below, Figure 3-12.

$$R_{\Delta Feq(Est/Meas)} = \frac{\Delta F_{eq}(M_{est,FA})}{\Delta F_{eq}(M_{measured,FA})} \tag{3.26}$$

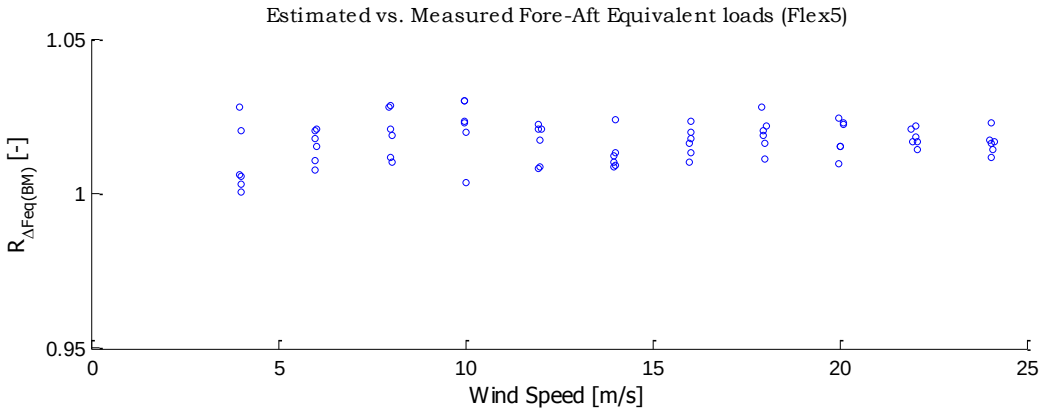

Figure 3-12 Ratio between the equivalent loads from the estimated and the exact fore-aft bending moments (Flex) (Ratio = Estimated/Measured)

The mean value of the results is again overestimated by about 1%, just like in Figure 3-7. Secondly, some scatter is introduced. A better look at the estimated and exact bending moment shows that the estimated bending moment (or, deflection with a certain gain) shows less high frequency content, Figure 3-13.

A possible explanation is the following: the bending moment is calculated as the product of force and distance, where the deflection is calculated from integration of force divided by mass. Integration can act as a low-pass filter, resulting in fewer high frequency cycles, explaining the scatter in Figure 3-12.

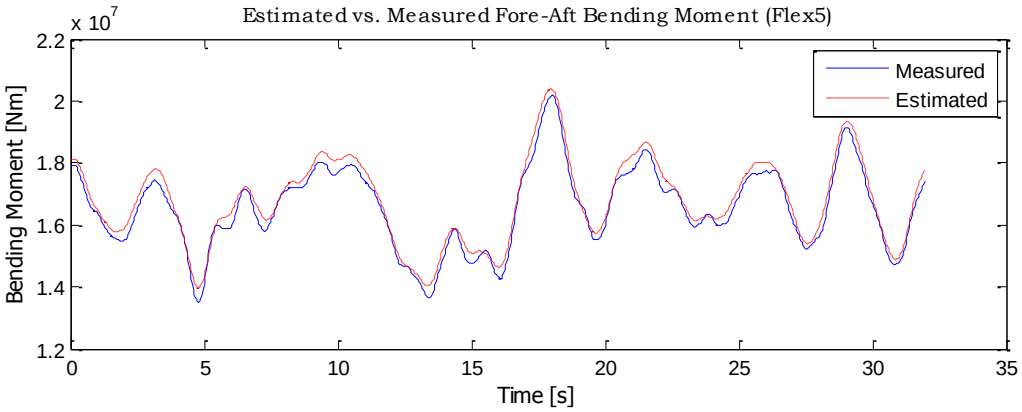

Figure 3-13 Estimated vs. Measured bending moments (Flex5)

To summarize, the equivalent loads of the fore-aft bending moments of a wind turbine can be estimated by solely knowing the deflection of the tower top. This is verified with Flex5, where a linear relation between tower deflection and bending moment is investigated. The approach overestimates the fore-aft bending moments with ~1% with a standard deviation of 0.68%.

That means that for the dynamic case in the fore-aft direction whenever tower fatigue is considered the original flow chart of Figure 3-1 is valid, Figure 3-14

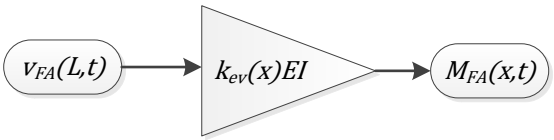

Figure 3-14 Flow chart to find the fore-aft bending moment from the tower deflection, for the dynamic case a correction with the tower top bending moment is not necessary.

3.3.2 Side-Side direction

Unlike the fore-aft tower top bending moment the Side-Side moment due to torque is not constant. For calculating the equivalent loads of the side-side bending moment the torque should thus be taken into account. This is done with using equation (3.23)-(3.25). For the dynamic case however, also power is needed to accelerate the rotor, drivetrain and generator. The power from the rotor is thus better described with equation (3.27)[10].

$$P = \frac{P_{el}}{\eta(P_{el}, \Omega)} + J\dot{\Omega} \tag{3.27}$$

Where,

J Inertia $[kgm]$
$\dot{\Omega}$ Angular acceleration $[rad/s^2]$

The dynamic torque can thus be described as

$$T = \frac{1}{\Omega}\left(\frac{P_{el}}{\eta(P_{el}, \Omega)} + J\dot{\Omega}\right) \tag{3.28}$$

[10] The drivetrain, generator and rotor are taken as one, where they actually are 3 separate, but coupled systems.

The estimated and exact equivalent loads of the side-side tower base bending moments are compared in Figure 3-15 by using equation (2.6). The estimated bending moment is calculated in three different ways i.e. with:

- A linear relationship between deflection and bending moment, equation (3.6) ('Linear' [○]);
- Corrected with the estimated tower top moment, equation (3.25),
  - where static torque is considered, equation (3.24) ('T_{static}' [*]);
  - where dynamic torque is considered, equation (3.28) ('$T_{dynamic}$' [□]).

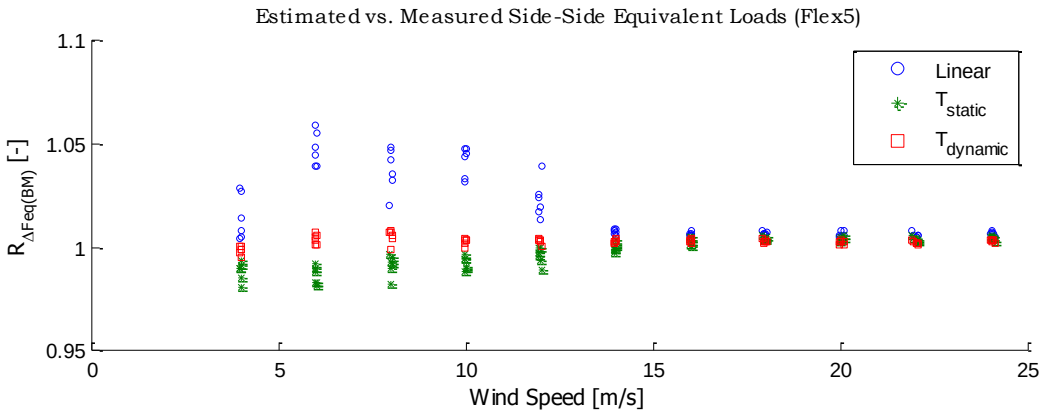

Figure 3-15 Ratio between the equivalent loads of the estimated and measured Side-Side bending moments, where the estimated equivalent loads are given without any corrections (Linear), with simplified torque correction (T_{static}) and with improved torque correction ($T_{dynamic}$) (Flex5) (Ratio=Estimated/Measured)

For the calculating the equivalent loads of the Side-Side bending moments a linear relationship between bending and tower top deflection may not be assumed. It should be corrected with the moment at the tower top, which is the torque from the rotor. It can be calculated from the generator's power output and the rotor's rotational speed. The best results are found where the inertia from the rotor and drivetrain are taken into account; albeit as a very rough estimation.

The approach is again summarised in a flow chart, Figure 3-16.

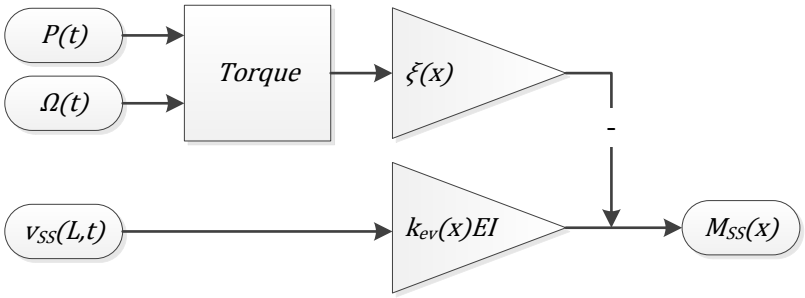

Figure 3-16 Flowchart for finding the side-side bending moment from the tower top deflection. In the dynamic as well as the static case the linear relationship should be corrected with torque.

4 From acceleration to deflection

The actual deflection of the tower top is unknown in real life. It must be found by double integration of the tower top acceleration, which is measured on many modern turbines. There are different ways of digital integration of an acceleration signal. Some of them will be discussed in the next section. There are some difficulties with integrating measured acceleration that will be discussed in subsequent sections.

It is important to remember that at the end the equivalent loads of the integrated signal should coincide with the one from the bending moments. It is therefore not necessary to know the exact deflection, as long as the rain-flow-count gives similar results.

The basic approach to start from is given in Figure 4-1.

Figure 4-1 Flow chart to find the tower top deflection from the tower top acceleration

4.1 Integration methods

The easiest method of integration of a signal is rectangular integration. This is a simple cumulative sum of all the data points of the signal times the rectangle width, i.e. divide by its sampling frequency. The difference equation is given in equation (4.1).

However the trapezoidal rule is always superior because it achieves higher accuracy with the same amount of work. It uses the average of two data points for integration. Its difference equation is given in equation (4.2). An example of both is given in Figure 4-2.

$$y(n) = \frac{1}{f_s}\sum_{k=0}^{n} x(n-k) = y(n-1) + \frac{1}{f_s}x(n) \tag{4.1}$$

$$y(n) = y(n-1) + \frac{1}{2f_s}[x(n-1) + x(n)], n > 0 \tag{4.2}$$

Where,

f_s Sampling Frequency

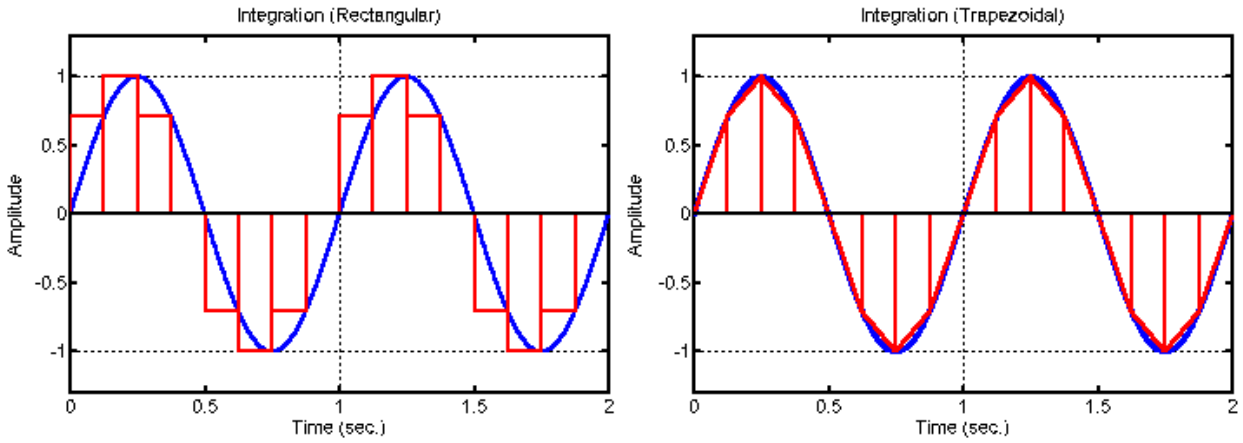

Figure 4-2 Example of rectangular (left) and trapezoidal (right) integration from [23]

There are other and more elaborate methods of integration, e.g. Fourier, but for now the trapezoidal rule will be used to discuss the problems of integration. More on Fourier can be found in Appendix B.

4.2 Initial conditions

The initial conditions are the integration constants C_1 and C_2, from numerical integration, equations (4.3) - (4.5). They are respectively the initial speed and initial displacement.

$$a(t) = Ampl * \sin(2\pi\omega t) \tag{4.3}$$

$$\int a(t)dt = vel(t) = -\frac{1}{2\pi\omega} Ampl * \cos(2\pi\omega t) + C_1 \tag{4.4}$$

$$\iint a(t)\, dt^2 = x(t) = -\left(\frac{1}{2\pi\omega}\right)^2 Ampl * \sin(2\pi\omega t) + C_1 t + C_2 \tag{4.5}$$

Where,

a	Acceleration $[m/s^2]$
t	Time $[s]$
$Ampl$	Amplitude $[-]$
ω	frequency $[Hz]$
vel	Velocity $[m/s]$
x	Displacement $[m]$
C	Integration constant $[-]$

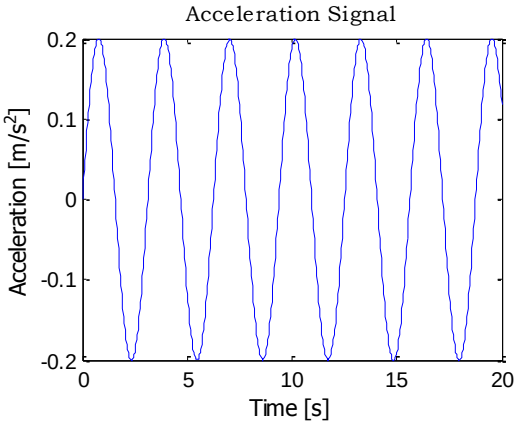

Figure 4-3 Sinusoid representing the acceleration of a tower top

When the initial conditions are unknown, significant errors can occur after integration. An example is given Figure 4-4, where the acceleration signal from Figure 4-3 is integrated. It can be seen that after the first integration step (the left plot) the mean value (i.e. C_1 in equation (4.4)) is half the amplitude of the actual velocity, where it should be zero. If that is integrated, it will lead to an unbound increase of displacement x.

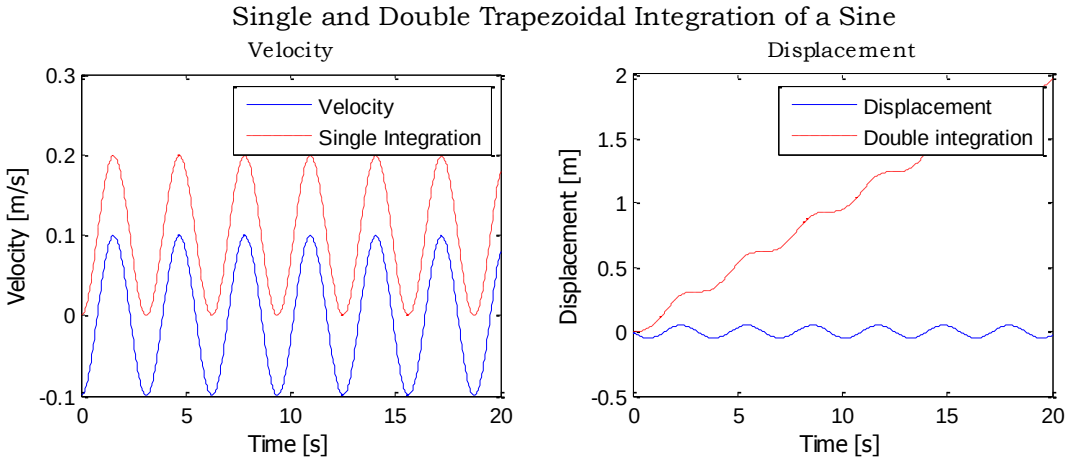

Figure 4-4 Integration of a sine to velocity (left) and displacement (right) using rectangular and trapezoidal integration

An infinite x is impossible since the oscillation of a tower top is considered, so C_1 must be 0. Furthermore, for simplification, justified in the previous chapters (section 0), an oscillation around zero mean may be assumed. Thus a zero initial displacement can be considered, i.e. $C_2 = 0$. This can be implemented is by adjusting the mean value to zero after each integration step. This is done in Figure 4-5.

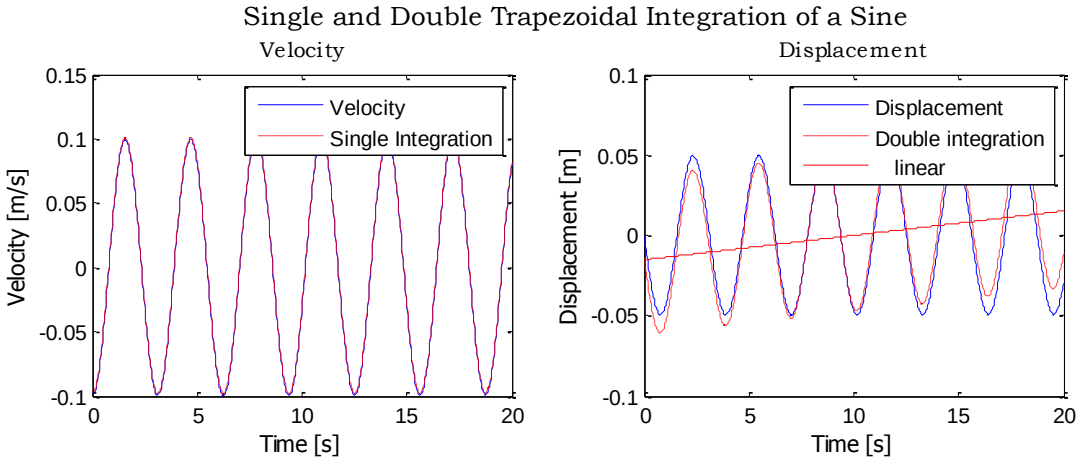

Figure 4-5 Integration of a sine to velocity (left) and displacement((right) using rectangular and trapezoidal integration with subtracting the mean after each integration step.

By only adjusting the mean of the signal an error after the 2nd integration will occur. That comes from the fact that an oscillating function with zero acceleration at $t = 0$, has a maximum velocity at $t = 0$, so the assumption of zero initial velocity is invalid. Therefore the initial condition should be added instead of simply adjusting the mean. That is, the constant in equation (4.4) will result in a linear trend after integration, equation (4.5), which is missed when only the mean is subtracted. A way to overcome this in this example is to subtract the best linear fit.

The results in Figure 4-5 imply that the starting point of the integration influences the error. If, for instance, the acceleration signal would be integrated from maximum acceleration, i.e. at zero initial velocity, no integration error would occur after the first integration step. This can be shown by integrating a cosine, which is done in Figure 4-6. In the right plot, it is visible that the initial displacement is nonzero.

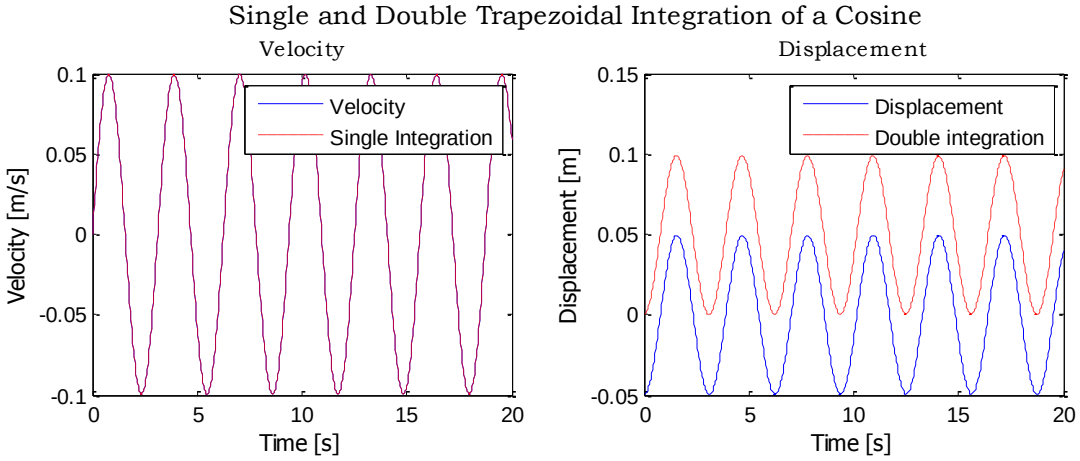

Figure 4-6 Integration of a cosine to velocity (left) and displacement (right) using rectangular and trapezoidal integration.

To summarize, not knowing or incorrect initial starting assumptions may lead to large integration errors. These can be prevented by setting the mean of the signal to zero prior to each integration step. This is justified, since the actual mean of the signal is not at our interest.

4.3 Drift from bias

Whenever acceleration is measured with a sensor there will always be a small bias in the signal. This is basically a small offset in the mean value, which leads to large integration errors, so-called drift. This was also seen in the right plot of Figure 4-4, where the initial conditions were neglected.

The numerical approach below shows that errors increase quadratic with time after double integration, equations (4.6)-(4.8). A small dc offset (DC_0) is added to the acceleration signal given earlier in equation (4.3). The result can be seen in Figure 4-7.

$$a(t) = Ampl * \sin(2\pi\omega t) + DC_o \tag{4.6}$$

$$\int a(t)dt = v(t) = -\frac{1}{2\pi\omega} Ampl * \cos(2\pi\omega t) + DC_o t + C_1 \tag{4.7}$$

$$\iint a(t)\, dt^2 = x(t) = -\left(\frac{1}{2\pi\omega}\right)^2 Ampl * \sin(2\pi\omega t) + \frac{1}{2} DC_o t^2 + C_1 t + C_2 \tag{4.8}$$

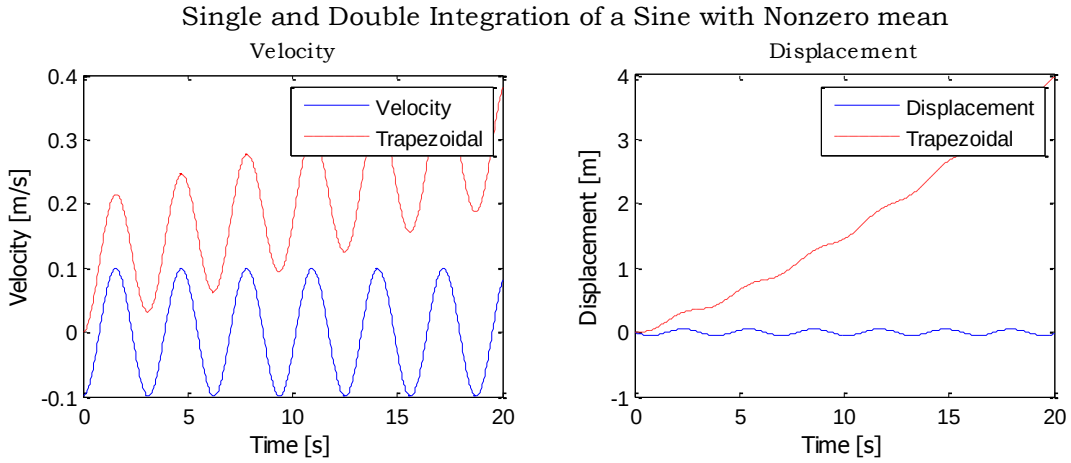

Figure 4-7 Integration of a cosine with a small positive mean to velocity (left) and displacement((right) using rectangular and trapezoidal integration.

As expected, after the first integration a linear trend is visible, which results in a quadratic ramp after the second integration. This effect can be mitigated by setting the mean of the original signal to zero, i.e. removing the dc offset. It will then give the results shown in Figure 4-5. It may therefore be treated the same way as the unknown initial conditions.

4.4 Noise

Sensor measurements will most probably contain noise. An example is given in equation (4.9) and Figure 4-8, where the maximum amplitude of the noise (N) is 20% of the signal's amplitude.

$$a(t) = Ampl * \sin(2\pi\omega t) + N(t) \tag{4.9}$$

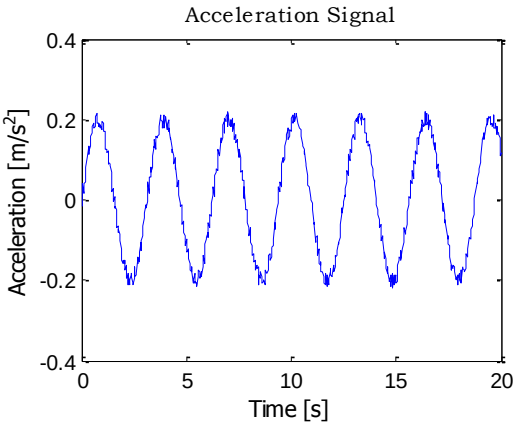

Figure 4-8 Sinusoid representing the acceleration of a towertop with measured noise

Noise can be seen as unwanted frequency components in the signal. High frequencies will give low amplitudes after integration. This can be seen in equation (4.5). Integration thus has a low-pass filtering effect on the signal, which removes the unwanted high frequencies from the noise.

However, there are also low frequency components present in the noise, which are blown up after integration. In Figure 4-9 the signals length is increased to show that indeed the unwanted high frequencies are removed and that the low ones lead to integration errors.

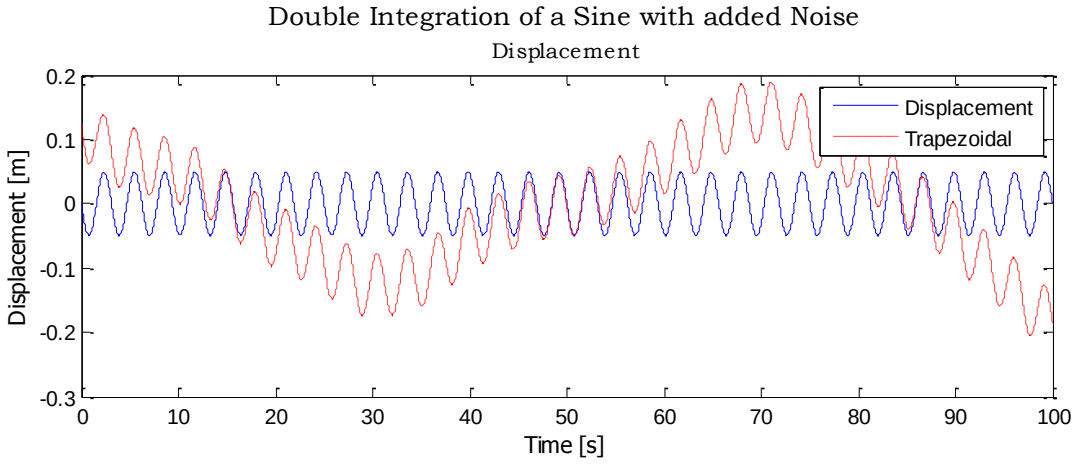

Figure 4-9 Double integration of a sine with added noise

A high-pass filter can be used to remove the low frequency components from the noise before integration. In the next figure a Fourier filter (Appendix B) was used prior to each integration step to remove the low frequency components. This gives good results and the influence of noise is hardly visible. Only at the beginning and end of the signal some small errors are visible, Figure 4-10

These errors are however so small that they hardly influence the rain-flow-count, i.e. both signals result in the same equivalent load. Therefore applying a high-pass filter prior to each integration step will suffice to remove the influence of noise.

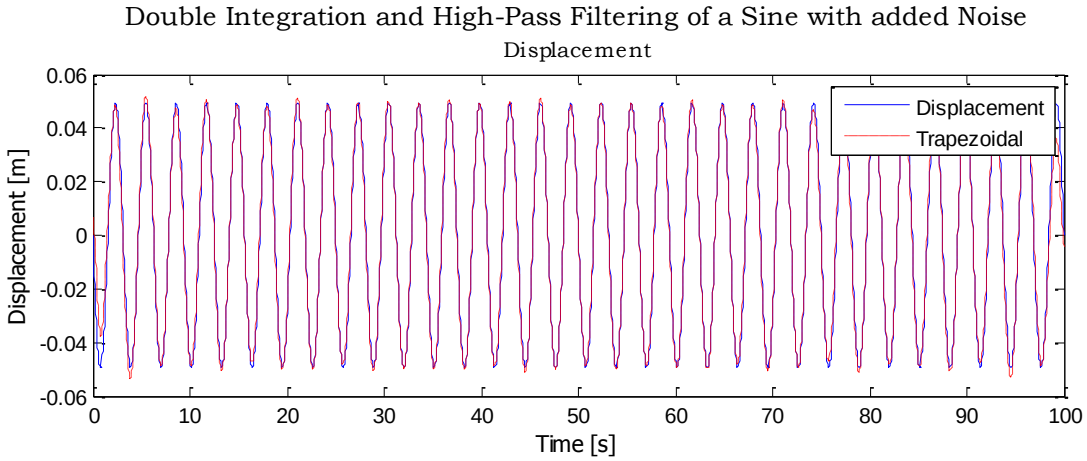

Figure 4-10 Double integration of a sine with added noise and a high-pass filter after each integration step

To summarize, noise can be seen as an unwanted signal with high and low-frequency components on top of the actual signal. The high-frequencies are removed after integration since it acts as a low-pass filter. The low frequency components can be removed by adding a high-pass filter prior to each integration step. Only at the beginning and end of the signal small discrepancies are visible but they do not lead to a difference in the equivalent load calculations.

4.5 Flex5 results (Horizontal Acceleration)

In previous sections a perfectly predictable oscillation of the tower top was considered. This is not to be expected to be seen in the actual acceleration of the tower top, which is a result from the thrust and/or torque of the rotor and mass and stiffness of the tower. The thrust and/or torque are again a result of the pitch angle, rotor speed and wind speed. All of them are known, more or less, except for the latter, which can be seen as complete stochastic. Eventually this will result in a semi-stochastic acceleration signal. In the next section it is investigated how the integration performs with a semi-stochastic signal. The results will be treated in the Fore-Aft and in the Side-Side direction in subsequent sections.

The true horizontal acceleration of the tower top is used.

4.5.1 Semi-Stochastic signals

The real Fore-Aft acceleration of the tower top acceleration from Flex5 is considered to be a semi-stochastic signal, shown in Figure 4-11. The signal seems to be more or less random; it does however seem to oscillate with certain constant frequencies and has a zero mean.

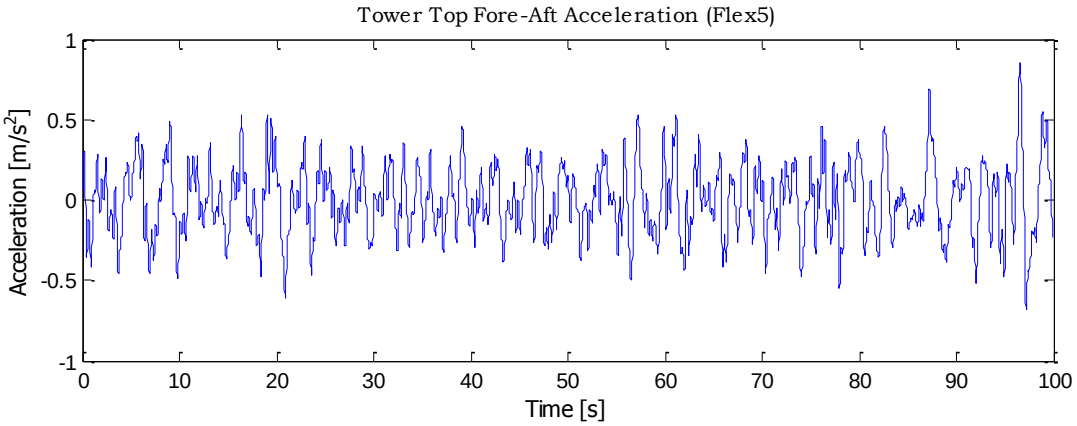

Figure 4-11 Tower top acceleration (Flex5)

There is no noise, bias or whatsoever in the signal, since it is the output from a theoretical model and not measured data. That means that only the initial conditions are unknown. The problems that can occur with unknown initial starting conditions can be overcome by setting the mean of the signal to zero before each integration step, section 4.2, page 26.

The error after double integration is quite large, Figure 4-12 and looks like drift or a random walk, which also happened after integrating a stochastic signal like noise. The assumption that there are no errors in the signal might also be wrong. Aliasing can have a significant effect on the integration. In [24] it is shown that it can lead to low frequency errors, even with simulated data.

A high-pass filter in the frequency domain can be used to overcome that problem. Subtracting a moving average might also work, since that also acts as a high-pass filter, but in the time domain.

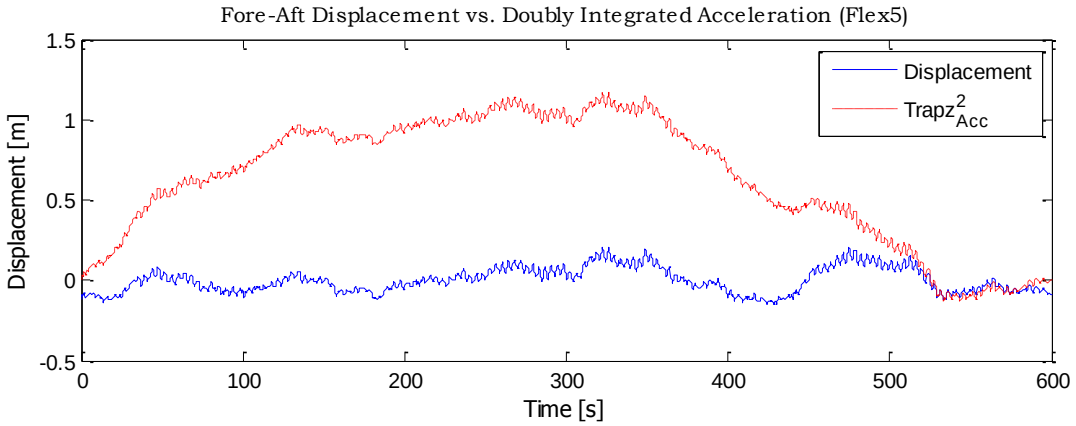

Figure 4-12 Double trapezoidal integration ($\text{Trapz}^2_{\text{Acc}}$) of the real tower top fore-aft acceleration vs. the tower top displacement (Flex5)

The two approaches are given in Figure 4-13. For the filter in the frequency domain the best results are found with a cut-in-frequency of 4 mHz. For the moving average approach that is found with a

moving average length of 132 s, which corresponds approximately to high pass filtering with 4 mHz.[11]

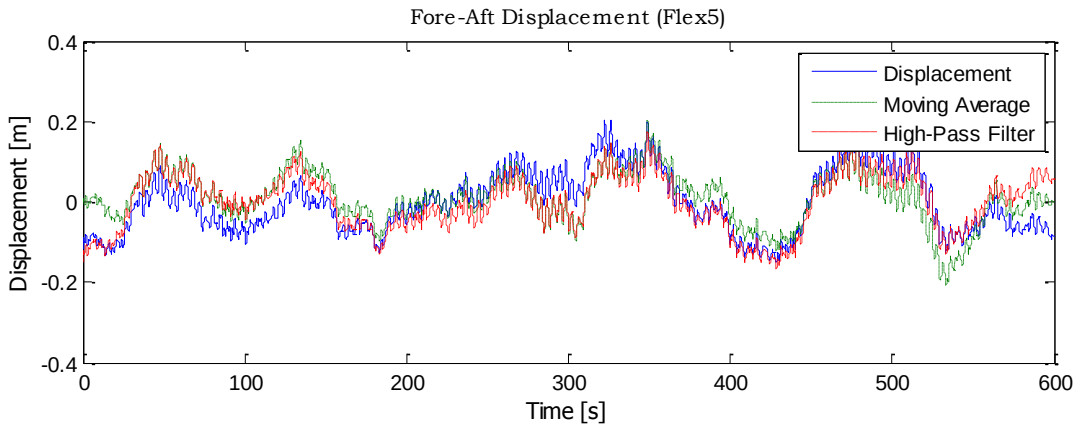

Figure 4-13 Double integration of the real tower top fore-aft acceleration vs. the tower top displacement, where the acceleration is filtered in the frequency domain (High-Pass filter) and in the time domain (Moving Average) (Flex5)

The results for the different load cases are given in Figure 4-14, where the ratios between the equivalent loads (ΔF_{eq}) from the estimated and the exact tower top displacement are given, equation (4.10).

$$R_{\Delta Feq(X)} = \frac{\Delta F_{eq}(X_{est})}{\Delta F_{eq}(X_{exact})} \qquad (4.10)$$

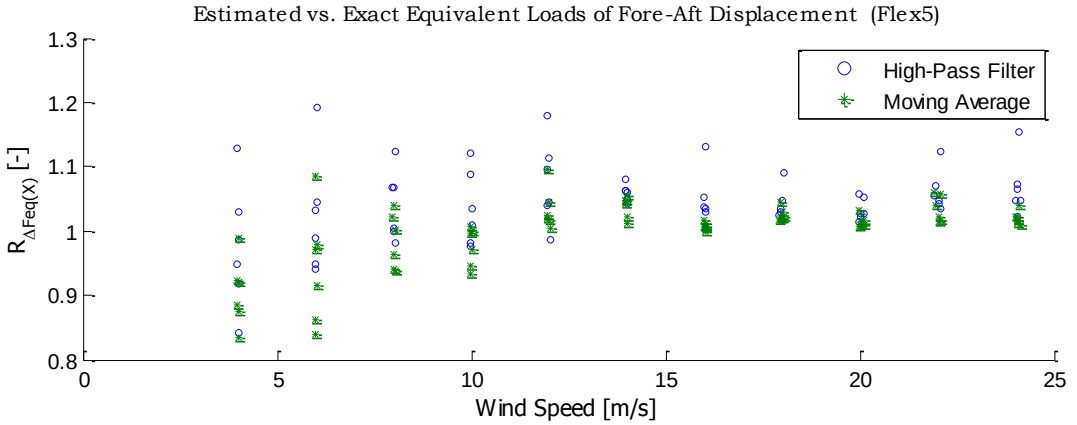

Figure 4-14 Ratio of equivalent loads between the integrated real acceleration and the actual fore-aft displacement of the tower top, where the acceleration is filtered in the frequency domain (High-Pass filter) and 'filtered' in the time domain (Moving Average) (Flex5) (Ratio = Estimated/Exact)

Subtracting a moving average gives better results than a high-pass filter, but still, at low wind speeds the spread of the error is almost 25%, varying between over- and underestimation. For the approach with the high-pass filter the spread is almost 40%. Varying the cut-in frequency or moving average length does not lead to significant improvement of results.

The frequencies just above 4 mHz are thus also not well described. This leads to an unpredictable estimation of the equivalent loads. Especially at below rated wind speeds it is hard to say how big the error will be. It can basically be concluded that integrating unpredictable (i.e.

[11] 'Best results' are found by comparing equivalent loads.

stochastic) signals will give unpredictable results, where the low frequencies lead to the biggest errors. Furthermore the low frequencies could come from aliasing. [24]

Removing also the frequencies just above 4 mHz before integration gives more predictable results. In Figure 4-15 an example is given where all the frequencies considered low are removed, i.e. frequencies below 50 mHz. The drift is completely removed and the high frequency cycles match; essential low frequency cycles are now completely missed though. It causes a significant underestimation of the equivalent load, about 40%.

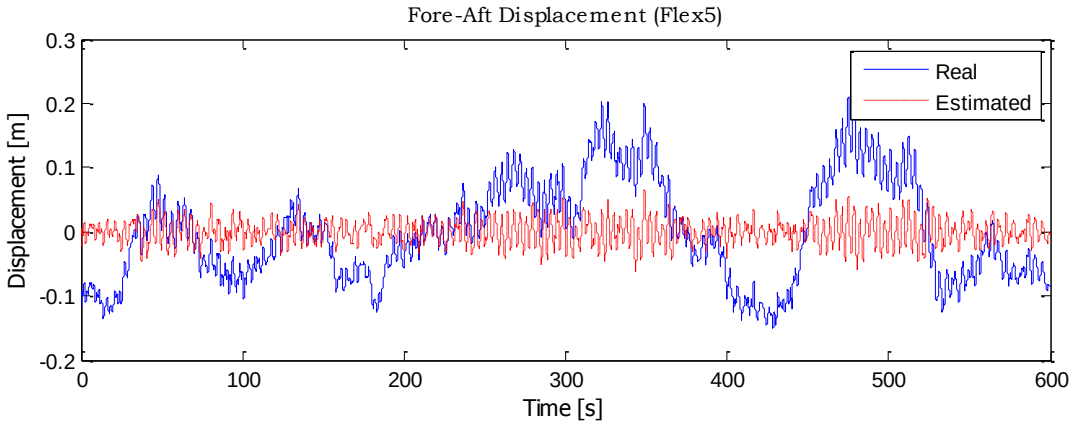

Figure 4-15 Double integration of the Fore Aft acceleration after being high-pass filtered in the frequency domain (estimated) vs. the real tower top displacement (Flex5)

To summarize, straightforward integration of the semi-stochastic signals can lead to drift, or so-called random walk. This can be overcome by removing the low frequencies causing the drift. This can be done with a high-pass filter, Figure 4-16

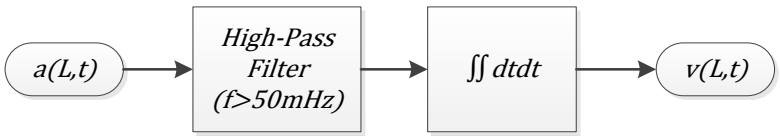

Figure 4-16 Flow to chart for finding the deflection from the acceleration, a high-pass filter needs to be added to prevent drift.

The problem is that removing the low frequencies will lead to significant underestimation of the equivalent loads. The missed low frequencies thus need to be compensated. There is however no problem with tower dynamics since the tower's eigenfrequency is much higher, i.e. ~ 0.3 Hz.

4.5.2 Fore-Aft low frequency compensation

Integrating signals with low frequency content leads to drift. This can be partially compensated by removing a running average after the integration. The low frequencies are still not very well described with this adjustment. A more drastic approach is to remove all low frequencies with a high-pass filter prior to each integration step. This has as side-effect that the equivalent loads are underestimated, because there are also low frequencies present in the actual tower top displacement. They need to be accounted for, since the underestimation varying between 0 to almost 60% (Figure 4-17).

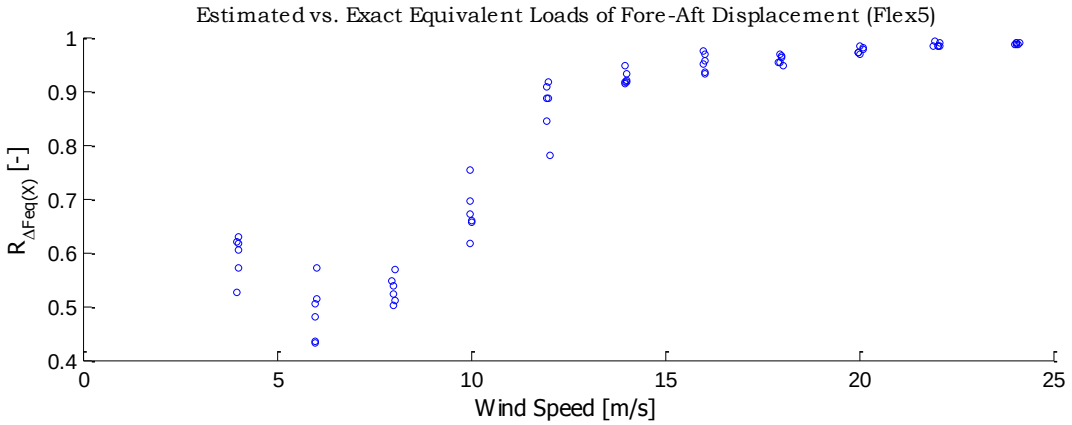

Figure 4-17 Ratio of equivalent loads between the estimated and the actual tower top displacement. A high-pass filter with a cut-in frequency of 50 mHz was used (Flex5) (Ratio = Estimated/Exact)

The underestimation is especially big at low wind speeds and seems to diminish above rated wind speed. Apparently at higher wind speeds fewer low frequencies are present in the tower displacement. This difference is also visible if the power spectral density plots of the tower displacement at low and high wind speeds are compared. The discrepancy can be ascribed to the low-pass-filtering effect of the rotor.

The rotor's inertia is so large that it will not respond to high frequency changes in the wind. It can be compared with a capacitor in an electric circuit. That stores energy when accelerated and restores it with deceleration. It accordingly prevents fast variations of the rotor speed, making it in essence a low-pass filter. [25] This effect decreases with increasing wind speeds, because the controller is designed to keep a constant rotor speed above rated wind speed.

The missed cycles could be added after integration and before the rain-flow count to ensure a good estimation of the equivalent loads. A signal has to be found, which has the same low frequency cycles as the actual fore-aft displacement. Thrust force can act as the low frequency input, since the tower top displacement is directly related when bending moments are neglected, equation (4.11).

$$v_{FA}(L) = \frac{F_{thrust}}{K} \tag{4.11}$$

Where,

$$K \cong \Omega^2(m_{nac} + m_{rotor} + m_{hub} + 0.25 * m_{tower}) \tag{4.12}$$

Only the low frequency components of the thrust are of interest, therefore it is filtered with a low-pass filter. Its frequency is set at the same value as was used for the high-pass-filter used for the acceleration signal, i.e. 50 mHz. The result is shown in Figure 4-18, where it is visible that the low-frequency components of the thrust match the ones from the displacement, as expected.

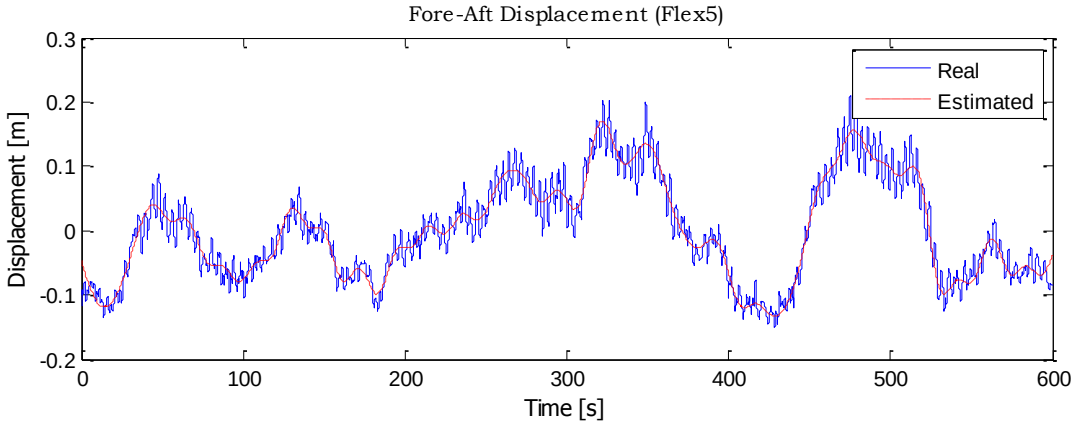

Figure 4-18 Fore-Aft displacement of the tower top together with the estimated dipslacement from the thrust calculated by Flex5

The combined integrated acceleration and thrust (respectively the red dotted lines from Figure 4-15 and Figure 4-18) describes the actual tower displacement very well, Figure 4-19.

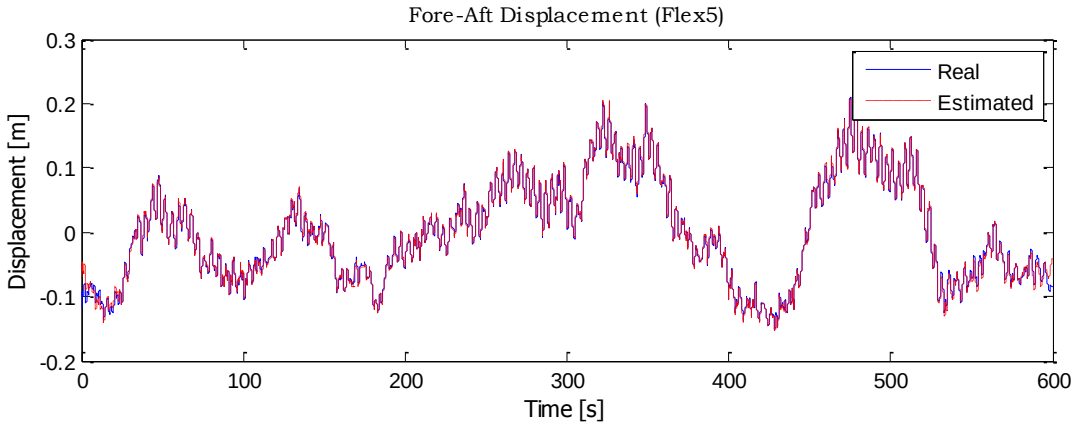

Figure 4-19 Combination of the thrust (calculated by Flex5) (red line Figure 4-18) and integrated acceleration (red line Figure 4-15) together with the actual displacement (Flex5)

For this single load case the equivalent load is overestimated by less than 1%. The results for all the load cases are given below. In Figure 4-20 the ratios of equivalent loads are given, where it is visible that this approach gives good results. The equivalent loads are overestimated with about 1% with a standard deviation of 0.004[12].

[12] It even gives better results than where the exact tower top deflection is known, Figure 3-12.

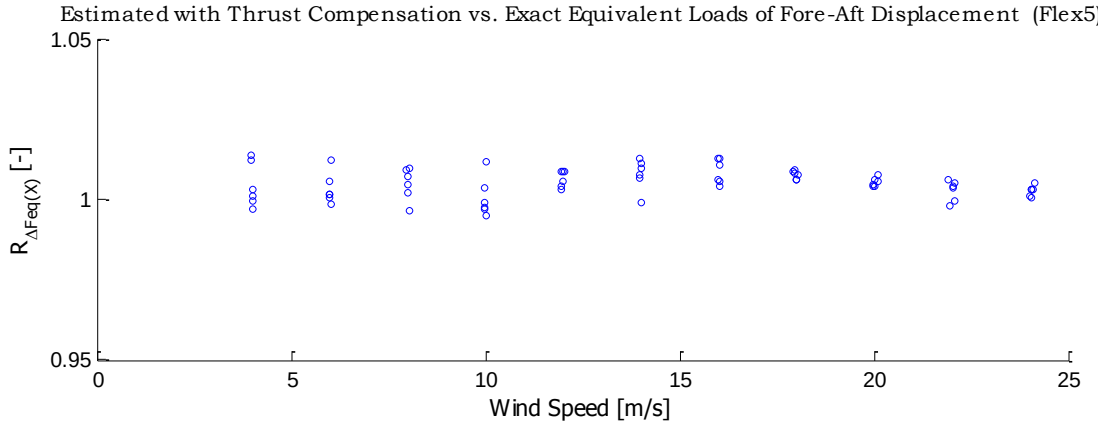

Figure 4-20 Ratio of equivalent loads between the estimated displacement and the actual fore-aft displacement, where the low frequencies of the estimated results are compensted with the actual thrust (Flex5)

This approach would suffice if the thrust was known, which is not the case in real-life. There is however not much written in the field of thrust estimation, therefore the most straightforward approach will be tested. A very simple thrust (T) estimator is the following, equation (4.13).

$$T = {}^{1}/_{2}\,\rho U_{\infty}^{2} A C_t \tag{4.13}$$

Where,

ρ Air density $[kg/m^3]$
U_∞ Undisturbed wind speed $[m/s]$
A Rotor swept area $[m^2]$
C_t Thrust coefficient $[-]$

The only unknown in equation (4.13) is the thrust coefficient[13], which is the ratio of the actual thrust force and the wind force. The actual thrust force is a combination of the lift and drag of the rotor blades. These depend on wind speed, rotor speed, pitch angle and blade characteristics. This means that the thrust coefficient is constantly changing during turbine operation.

Flex5 can calculate the thrust coefficient for certain conditions and it is given as a combination of the tip speed ratio (λ) and pitch angle. Where the tip speed ratio is given as a combination of rotor and wind speed, equation (4.14), and the pitch angle is measured.

$$\lambda = \frac{\Omega R}{U_\infty} \tag{4.14}$$

Where,

Ω Rotor speed $[rad/s]$
R Rotor radius $[m]$

The simple thrust estimator uses equation (4.13) and a thrust coefficient table from Flex5 to find the unknown C_t. The inputs for the thrust estimator are; the undisturbed wind speed; the rotor rotational speed and pitch angle. The inertia of the wake (and hence the change in induced wind speeds) is not taken into account.

[13] Actually, on actual turbines undisturbed wind speed is also unknown.

The low frequency cycles of the estimated and actual thrust at 12 m/s wind speed are given in Figure 4-21.

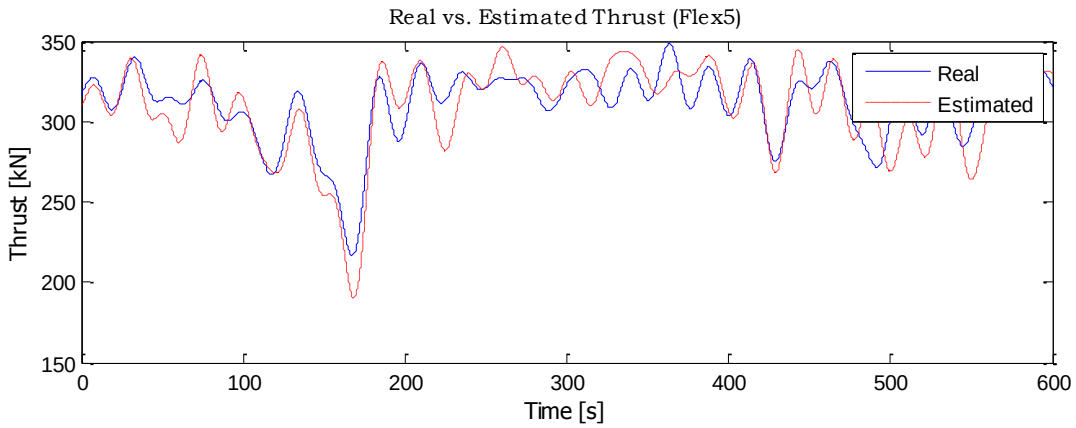

Figure 4-21 Real and estimated thrust, where both signals are filtered with a low-pass filter (Flex5)

The thrust estimator gives bigger low frequency amplitudes, i.e. its standard deviation is almost 25% higher than the actual thrust's! This leads to the following ratio of equivalent loads. With the thrust estimator as low frequency input the equivalent loads of the fore-aft displacement are overestimated by almost 30% at low wind speeds. This decreases to about 10% at high wind speeds, there where the low frequency cycles become less dominant.

The results are improved with reducing the influence of the thrust estimator. This results in less overestimation at lower wind speed; it can be reduced to about 10%, Figure 4-22.

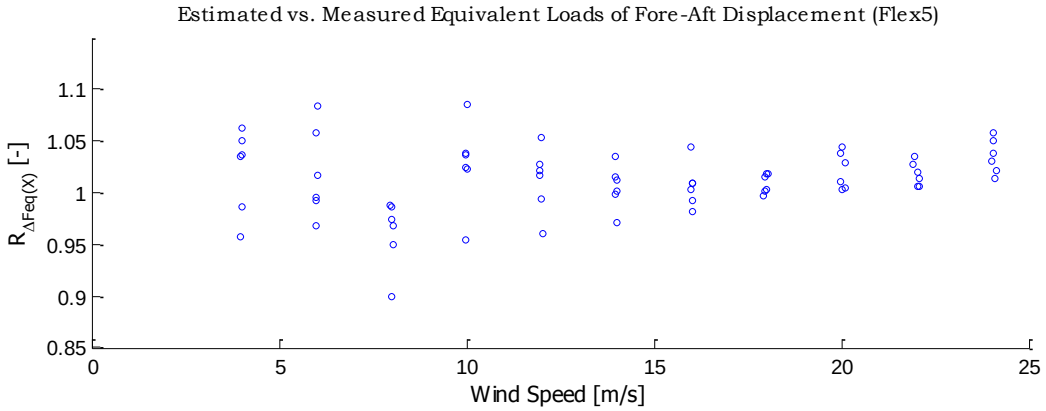

Figure 4-22 Ratio of equivalent loads between the estimated and the actual fore-aft displacement, where the estimated displacement is corrected with the low frequencies from the estimated thrust (Flex5) (Ratio=Estimated/Measured)

The displacement is overestimated with about 1% with a standard deviation of about 3%. If one remembers that these are results from a theoretical model it is easily stated that this approach might not work in real life. This estimator is for instance very sensitive to the undisturbed wind speed. In real life that is also unknown.

It is expected that an improved thrust estimator would give better results. However, due to time constraints no further effort is put into improving the thrust estimator; a whole thesis could be based on the matter.

The findings are summarised in Figure 4-23. The missed low frequencies can be very well compensated by adding low frequency components to the integrated signal. The best results were found if the low frequency components from the actual thrust signal are used, which is not an

available signal on actual turbines. It was therefore estimated with a basic thrust estimator. The fore-aft displacement is overestimated by 1% with a standard deviation of 3%.

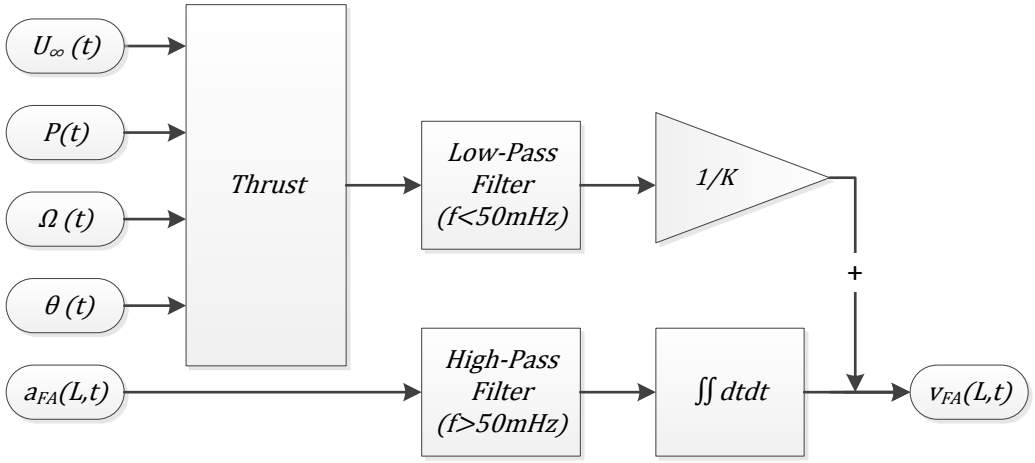

Figure 4-23 Flow chart for finding the fore-aft tower top deflection from the acceleration. Additional input from the thrust is needed to compensate for the high pass filter. Note the difference in sign between the two filters.

4.5.3 Side-Side low frequency compensation

A high-pass filter is needed to before the acceleration signal can be integrated to prevent drift. This has as side effect that essential low frequencies are missed, eventually leading to underestimation of the equivalent loads. This can be compensated by adding similar low frequencies from another signal after integration.

In the Fore-Aft direction this can be done with using the thrust force, since it dominates the Fore-Aft bending displacement. In the Side-Side direction the bending moment at the tower top is dominant, i.e. it accounts for almost 90% of the total displacement. Therefore it could be a good estimator of the low frequency components of the tower top displacement. If it is assumed that the deflection is only a result from the tower top bending moment, the displacement can then be described by equation (4.15), from equation (3.25).

$$v_{SS}(L) = \frac{\big(1+\xi(x)\big)T}{\kappa_{ev}(x)EI} \tag{4.15}$$

The low frequency components (<50 mHz) from the torque match the ones from the tower displacement, Figure 4-24.

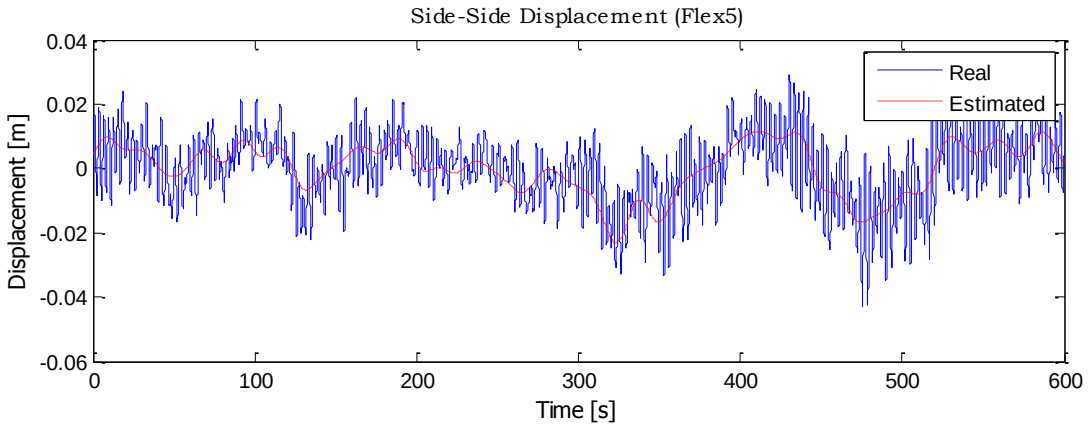

Figure 4-24 Side-Side displacement of the tower top and the estimated displacement from the tower top bending moment (Flex5)

The ratio of the equivalent loads between the estimated displacement and actual displacement (equation (4.10)) is given in Figure 4-25. To show if the assumption that all low frequencies can be compensated from the tower top moment, three different cases are shown in Figure 4-25:

- without low frequency correction (Direct [o]);
- with low frequency correction from the estimated torque (T [*]);
- with low frequency correction from the estimated torque and horizontal force (T - $F_{tt,ss}$ [□])[14].

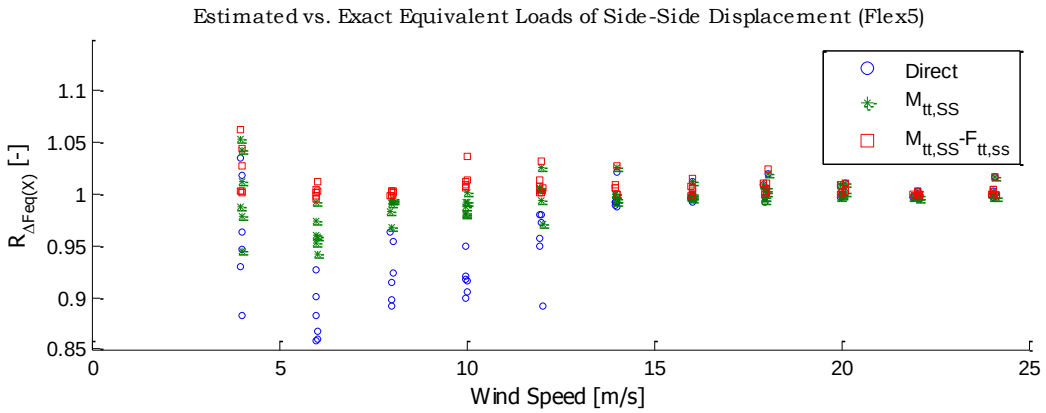

Figure 4-25 Ratio of equivalent loads between the estimated and the exact Side-Side displacement, where the estimated signal: is not corrected ('Real'); is corrected with the bending moment ('$M_{tt,SS}$') and is corrected with the bending moment and tower top force ('$M_{tt,SS}$-$F_{tt,SS}$') (Flex5) (Ratio=Estimated/Exact)

The 'dip' at below rated wind speeds is less steep than with the fore-aft displacement. This means that in the side-side direction the low frequencies are less dominant. They contribute to about a maximum of 15% of the loads. It is also visible that the low frequencies from the tower top force contribute to about 5% of the loading; the remaining 10% comes from the tower top bending moment.

The actual force and bending moment at the tower top are unknown and should thus be estimated. The bending moment at the tower top is a result from the torque of the rotor. Thus $M_{tt,ss} = T$ and the torque estimation from equation (3.23) can be used. The force at the tower top is a lot harder to predict since it comes from the wind speed. Since it only accounts for about 5% of the displacement and it will be neglected.

In Figure 4-26 it can be seen that the low frequencies from the torque are a good estimation of the side-side displacement of the tower top. The equivalent loads of the displacement are underestimated with a little less than 2%.

[14] The best results are found when the low frequencies from the bending moment and horizontal force are subtracted.

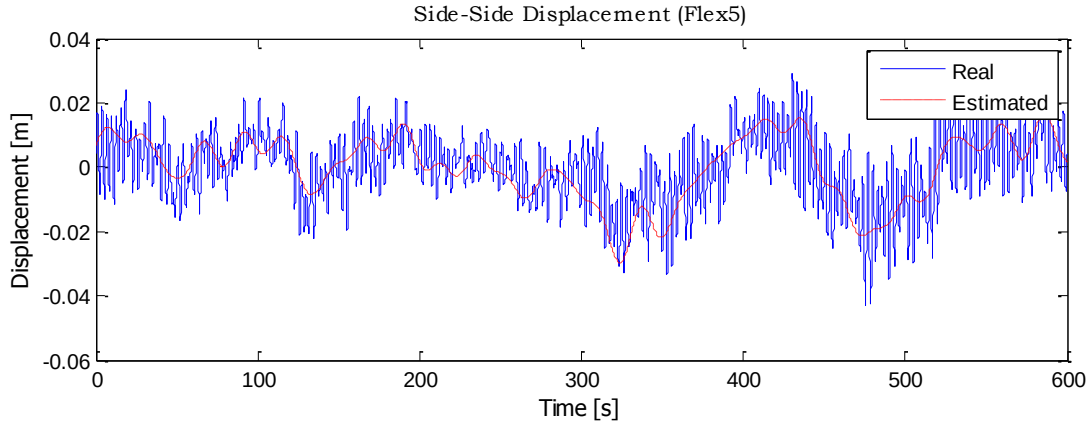

Figure 4-26 Side-Side displacement together with the estimated displacement form the torque (Flex5)

With solely the torque as low frequency compensation the following results are found for all the load cases, where the equivalent loads of the estimated and actual side-side displacements are compared, Figure 4-27.

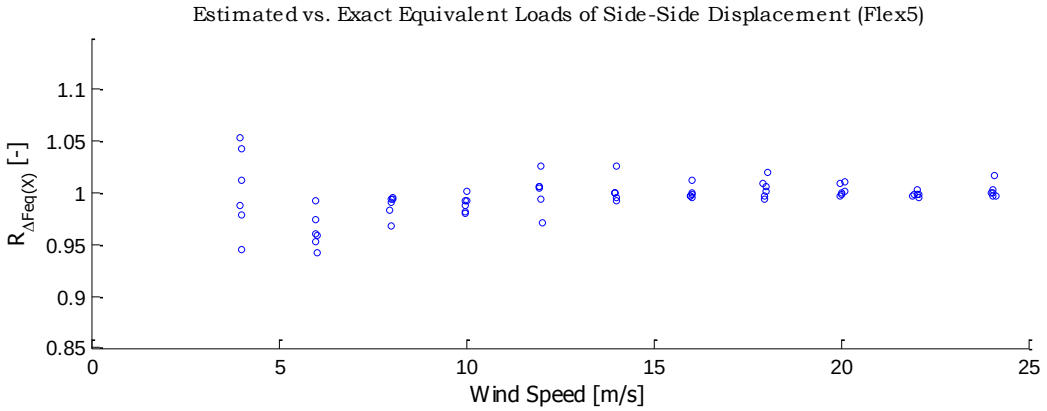

Figure 4-27 Ratio of equivalent loads between the estimated ant the exact Side-Side displacement Side-Side, where the estimated displacement is corrected with the estimated torque (Flex5)(Ratio=Estimated/Real)

From this analysis it can also be concluded that the acceleration signal can be omitted, since the side-side bending moment can be calculated from the torque (equation (4.15) with $M_{tt,ss} = T$). That is however not completely the case. Since the torque is calculated from the power output, it does not give a good estimation of the high frequencies. That is because the power is a low frequency representation of the torque due to the inertia of the whole system.

The high frequencies can be compensated by including the inertia of the system (as was done in equation (3.27) in section 3.3.2), which is subject to some assumptions and does not lead to the desired result. It thus seems better to use the acceleration signal to estimate the high frequencies and the torque for the low ones.

The proposed approach is again summarised in a flow chart, Figure 4-28. the acceleration signal of the side-side direction also has to be filtered to prevent drift. The missed low frequencies can be compensated by the torque estimator. The equivalent loads of the actual displacement can be predicted with a standard deviation of about 2%.

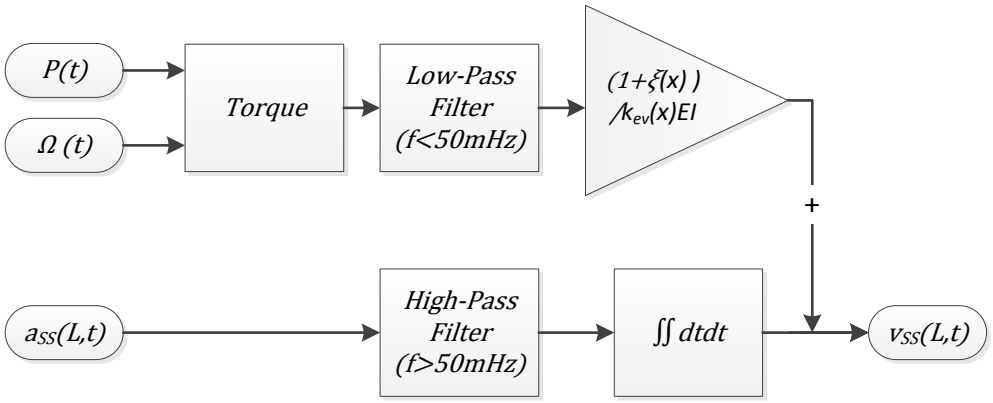

Figure 4-28 Flow chart for finding the side-side deflection of the tower top from the acceleration. Additional input from the torque is needed. Note the sign change between the two filters.

4.6 Flex5 results (Measured acceleration)

In previous sections the real horizontal tower top acceleration was used. This is not possible in real life and it needs to be measured with an acceleration sensor, i.e. an accelerometer. In this section the difference between real and measured acceleration will be treated. These are again Flex5 results, thus a perfect accelerometer is used.

Since the tower top, thus also the sensor, rotates under bending, some gravity will be measured by the sensor, disturbing the signal[15]. In addition, due to its misalignment with the horizontal axis, less acceleration is measured. See the free body diagram in Figure 4-29 and equation (4.16).

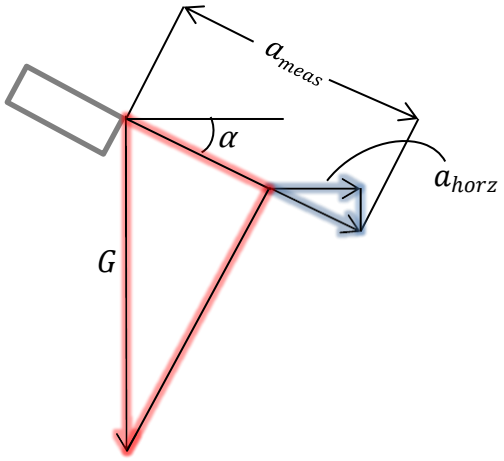

Figure 4-29 Free body diagram of the acceleration sensor

From geometry, (in Figure 4-29)

$$a_{horz} = (a_{meas} + G\sin(\alpha))\cos(\alpha) \tag{4.16}$$

Where,

a_{horz} Horizontal acceleration $[m/s^2]$

[15] Actually, acceleration sensors are often used for measuring rotation, or tilt.

a_{meas} Measured acceleration by sensor $[m/s^2]$
G Gravitational constant $[9.81\ m/s^2]$
α Rotation $[rad]$[16]

For small changes in tilt angles the influence of gravity seems negligible, since then $\cos(\alpha)\sim 1$ and $\sin(\alpha)\sim 0$. What will remain is a small DC-offset from the average tilt, which could be corrected by setting the mean of the signal to zero, equation (4.17).

$$a_{est} = a_{meas} - \bar{a}_{meas} \tag{4.17}$$

The real and the estimated (equation (4.17)) Fore-Aft acceleration are shown in Figure 4-30.

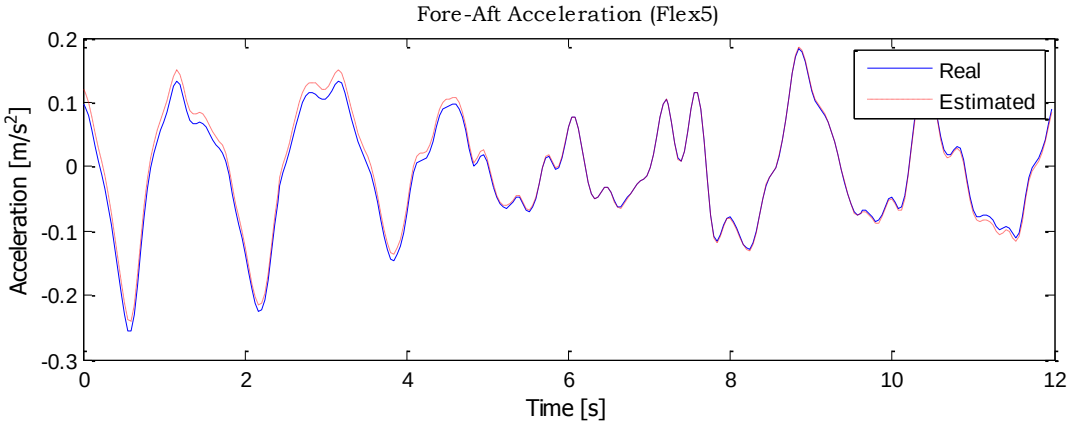

Figure 4-30 Actual Fore-Aft acceleration of the tower (solid line) and the simplified relationship (dotted line) (Flex5)

At a first glimpse, the simplification seems to be valid. The estimated line shows some bigger peaks, but the difference is small; the standard deviation is about 3% bigger. This can lead to a significant error after double integration. To check if that is indeed the case the measured acceleration is used to predict the fore-aft displacement.

The same approach as in section 4.5 is used for the result shown in Figure 4-31. The acceleration signal is filtered and the mean values of both signals are set to zero. The low frequency components from the thrust are added after the second integration to compensate for the high-pass filter needed for integration.

[16] The counter clockwise tilt angle is considered positive.

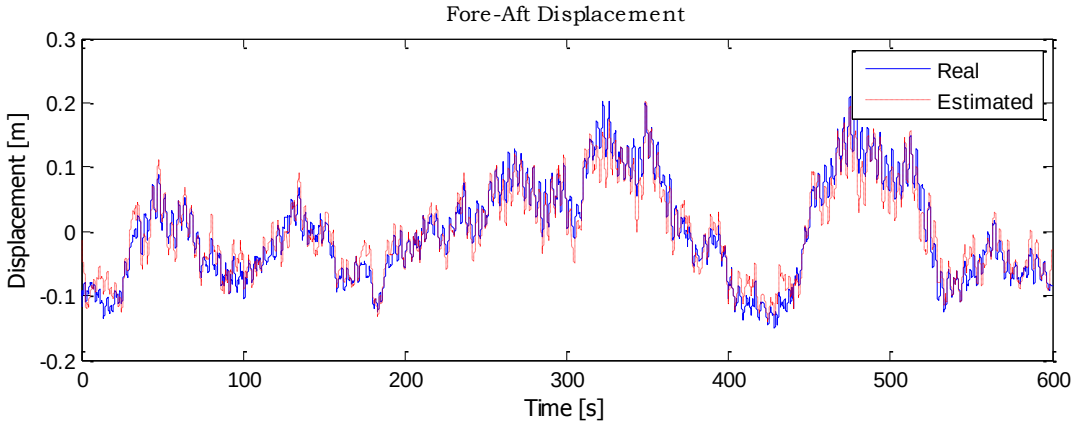

Figure 4-31 Integrated measured acceleration (dotted line) and the actual displacement (solid line), where the estimated displacement is corrected with the low frequencies from the actual thrust (Flex5)

The estimated displacement from the acceleration sensor overestimates the tower displacement. The equivalent load is overestimated by about 12% for this load case. The result for all load cases is given below, Figure 4-32, where it can be seen that the error as well as the scatter between different load cases at the same wind speed is increased.

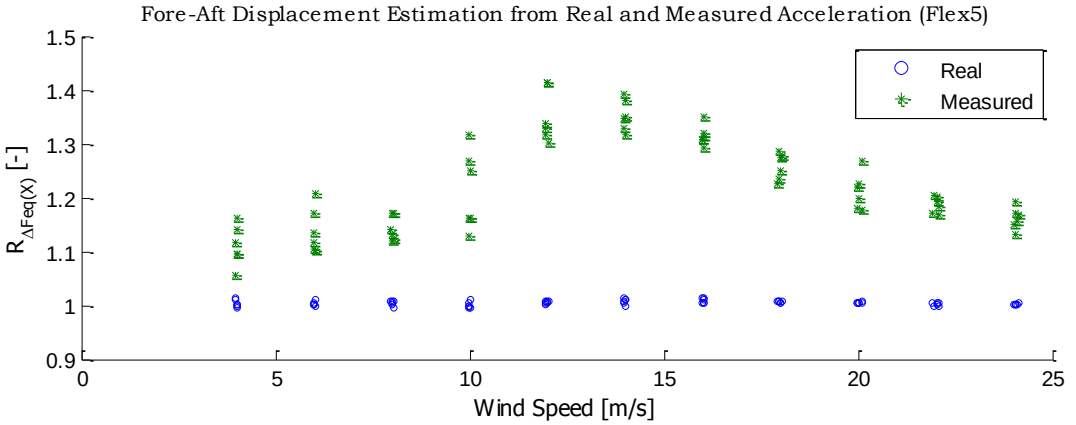

Figure 4-32 Ratio of equivalent loads between the estimated and real fore-aft displacement, where the displacement is estimated from the Real and the Measured acceleration. (Flex5) (Ratio=Estimated/Real)

The error shows a similar relationship with wind speed as the tilt angle, i.e. the size of the error seems to increase with increasing tilt. This implies that gravity has quite a significant influence on the results, because at bigger tilt angles more gravity is measured. To check if that is indeed the case the gravity is set to zero.

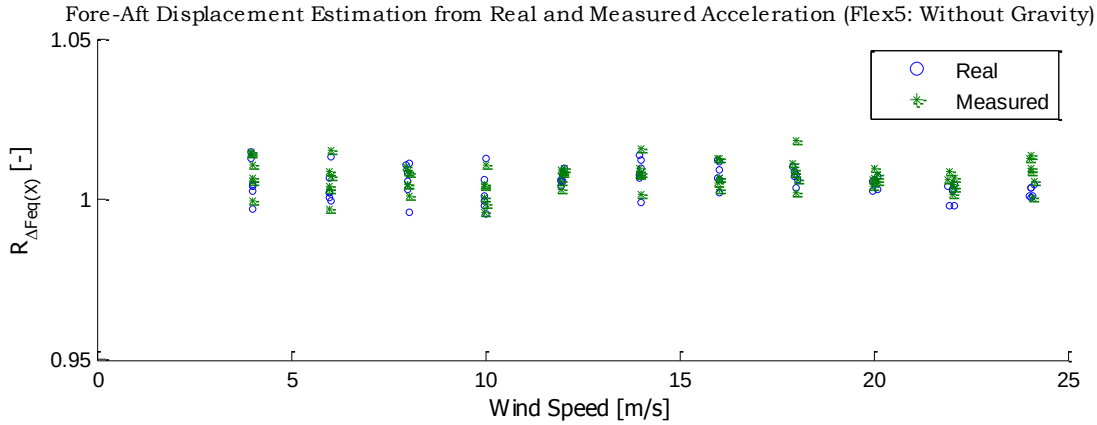

Figure 4-33 Ratio of equivalent loads between the estimated and real Fore-Aft displacement, where the displacement is estimated from the Real and the Measured acceleration and the gravity is set to zero. (Flex5) (Ratio=Estimated/Real)

Without gravity the measured and the actual acceleration give the same results, Figure 4-33[17]. It can thus be concluded that the cause of the overestimation seen in Figure 4-32 is caused by the gravity measured by the sensor.

In Figure 4-34 it can be seen that gravity adds low frequency content to the signal. In previous sections (section 4.5, p. 31) it was shown that integration of low frequencies leads to errors. Additionally these low frequencies are introduced by the gravity measured by the sensor i.e. they are not in the actual fore-aft acceleration, increasing the error in predicting the displacement.[18]

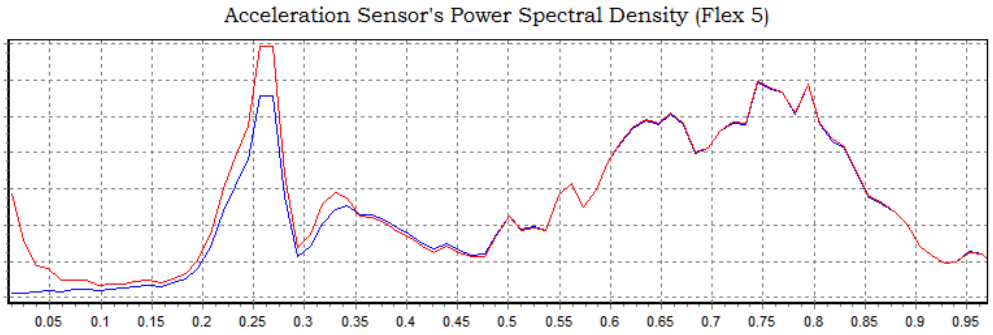

Figure 4-34 Power spectral density plot of the real and measured Fore-Aft acceleration (Flex5)

A numerical example shows how big that error could become. The tilt output of Flex5 is used, where a half cycle of about 7 s is found, the tilt varies between 0.01 and 0.02 radians, Figure 4-35.

[17] The side effect of setting the gravity to zero is that the bending moment at the tower top is also neglected (this was also done in section 3.2 on p. 12). That resulted in an overestimation of the displacement from the thrust correction. Therefore to get the results of Figure 4-33 the size of the thrust correction needed to be decreased by ~5%, i.e. increasing the size of K in equation (4.11). No further attention will be given to this phenomenon because the example is only used to show the influence of gravity on the measured acceleration.

[18] It is also visible that the peaks at the rotational speed and tower Eigen frequency are also bigger for the measured acceleration. By removing the gravity also the bending moment from the weight of the nacelle and blades is removed. This will influence the total bending and thus also the results of Figure 4-34. Therefore the conclusions drawn from the plot cannot be decisive.

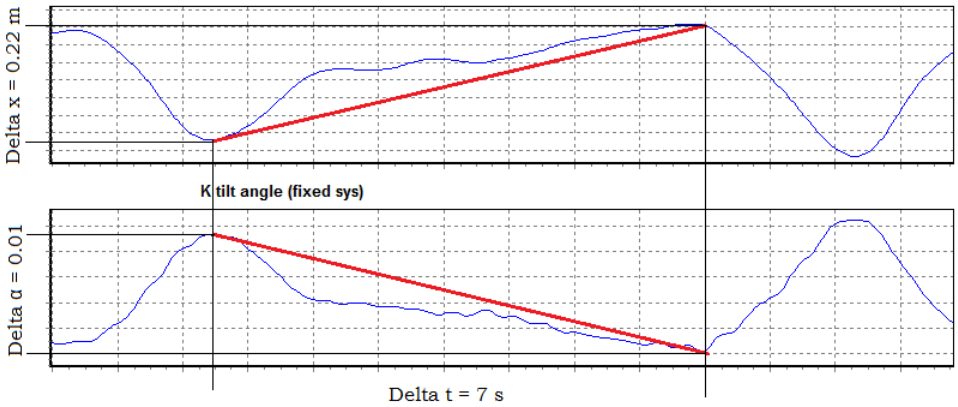

Figure 4-35 Tilt angle (bottom) and Fore Aft displacement (Top) (Flex5)

During this cycle the measured gravity has changed between 0.098 m/s^2 and 0.196 m/s^2. This means that there is an imaginary change in acceleration of 0.014 m/ s^2/s. That is,

$$a_g = 0.014t \tag{4.18}$$

which leads to an imaginary change of velocity,

$$vel_g = \int a_g dt = 0.007t^2 \tag{4.19}$$

resulting in an imaginary displacement,

$$x_g = \int v_g dt = 0.00233t^3 \tag{4.20}$$

which for t= 7 s leads to a half cycle of almost 80 cm that is 4 times more than the actual displacement. Even though the initial conditions are ignored, it shows that the gravity could have a significant influence on the prediction of the displacement.

Another example is given in Figure 4-36, where the tilt angle is converted to measured gravity and integrated, i.e. the influence of gravity is,

$$x_g = \iint 9.81\sin(\alpha)\, dtdt \tag{4.21}$$

The signal is filtered with a high pass-filter prior to the integration to prevent drift. This means that some of low frequency cycles present in the tilt signal are omitted. The previous example (equation (5.2)-(4.20), showed that these cycles can cause significant errors. Even without the extreme low frequency cycles the equivalent load from the imaginary displacement due to the gravity as big as 27% of the equivalent load from the real displacement.

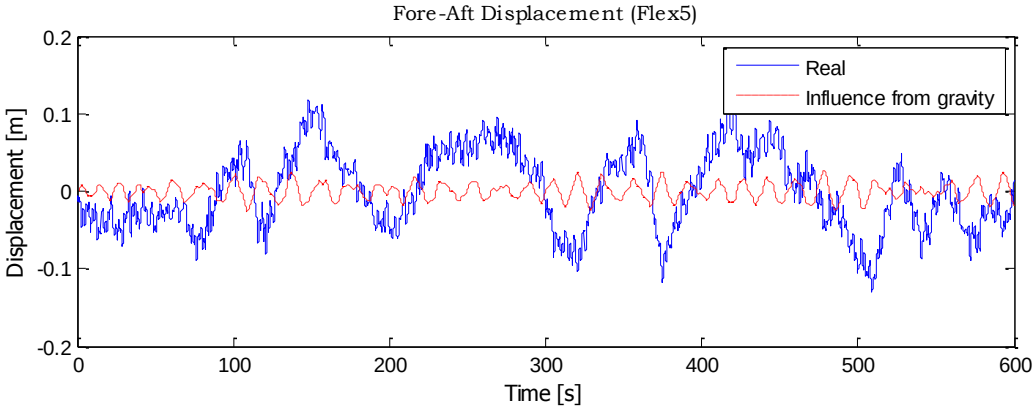

Figure 4-36 Real tower top Fore-Aft displacement and the Fore-Aft displacement if the measured gravity was integrated (Flex5)

From the examples above it can be concluded that gravity influences acceleration. These errors in the acceleration signal can become significant after integration and need to be removed. That can be done if the rotation of the tower top is known, because then the amount of gravity measured can be quantified. This is shown in Figure 4-36 and the gravity can be accounted for with equation (4.16). The rotation at the tower top is however unknown, thus a different approach is needed.

The measured gravity can also be corrected with an iterative process, which is given below equations (4.22) and (4.23)). This approach works as follows. The measured tower top acceleration is a result of the horizontal acceleration and the influence of gravity, or:

$$a_{meas} = a_{horz} + G a_{ev} v(L,t) \tag{4.22}$$

Where the tower top displacement,

$$v_{est}(L,t) = \iint a\, dtdt \tag{4.23}$$

In theory this could give the real acceleration and eventually the actual tower top displacement. First the displacement is estimated from integrating the measured acceleration. Then, from equation (4.22), the horizontal acceleration can be estimated by subtracting the influence of the gravity from the measured acceleration. The acceleration found is again integrated (equation (4.23)) to find a new estimation of the tower top displacement. The steps can be retaken until v_{est} converges, Figure 4-37.[19]

[19] Remember that for the integration the acceleration signal is filtered to prevent drift.

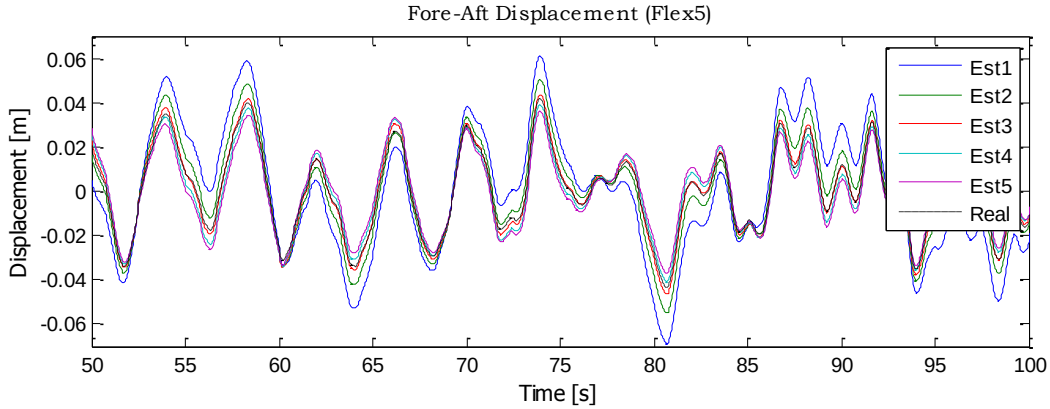

Figure 4-37 Estimated and real Fore-Aft displacement, where the estimated displacement comes from 5 iteration steps (Est 1-5) (Flex5)

The displacement indeed converges towards the actual tower top displacement in 5 iteration steps. The biggest displacement comes from the first integration, i.e. the outlying value in Figure 4-37. Each additional iteration step will give a smaller displacement and will eventually converge, but the result is sensitive to the generalised rotation. If it is too big the results will diverge and if it is too small it will hardly converge.

It seems however that the equivalent load will always converge to a very small number if the amount of iteration steps is increased. In Figure 4-38 the amount of steps is increased to 500. The standard deviation of the estimated displacement is shown for each iteration step. The horizontal line gives the standard deviation of the actual Fore-Aft displacement.

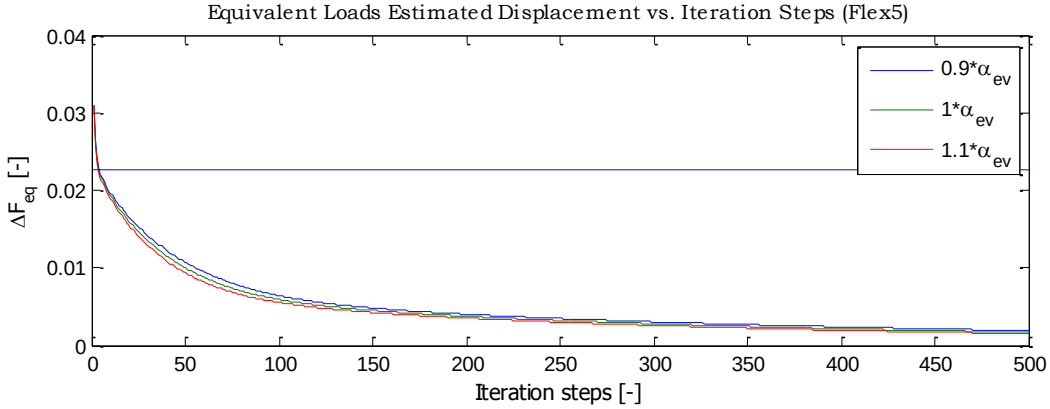

Figure 4-38 Equivalent loads of the estimated displacement vs the amount of iteration steps together with the equivalent laod of the actual Fore Aft displacement (Flex5)

Ideally the iteration diverges towards the point where the equivalent loads of the actual and the estimated displacement are the same. That is where the horizontal line crosses the other lines. It is hardly visible in the plot above, but the lines intersect already after 3 iteration steps.[20]

The point found on the intersection will be used to see how this approach works for the Flex5 results of the Fore-Aft and Side-Side displacement.

To summarise, the acceleration sensors in the tower top measure gravity due to tilt. This has a negative effect on the estimation of the Fore-Aft displacement. For some cases the equivalent loads of the actual displacement are overestimated by more than 40%.

[20] Many different numbers for the general rotation where tried but none would converge to the right standard deviation. It could be that the filter needed for integration distorts the results. This phenomenon will not be further investigated because it is believed that the results from using less iteration steps will suffice.

The problem can be solved if the rotation of the tower top is known, this is however not the case. Therefore another approach is necessary. A process is proposed that estimates the real acceleration from the estimated displacement. The estimation of the real acceleration can be used to find a new displacement. These steps can be retaken until the result converges. The best result for the example given in this section is found when 4 iteration steps are used.

The additional gravity compensation is added to the approach described in Figure 4-16. The iterative approach is represented as a feedback loop, Figure 4-39.

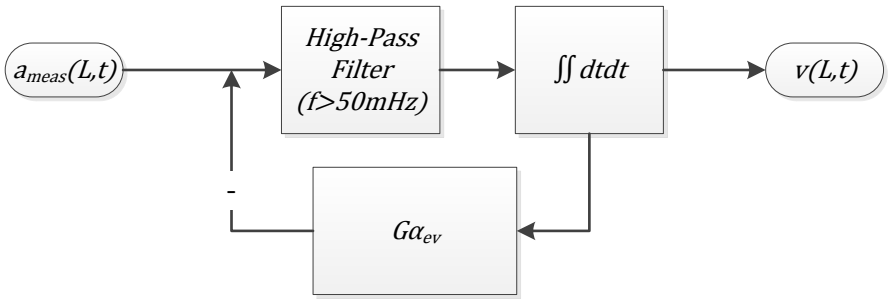

Figure 4-39 Flow chart for finding the displacement from the measured acceleration. The measured acceleration is compensated with the found displacement.

In the next sections the applicability of this approach is tested for the fore-aft and side-side directions. First the fore-aft direction will be treated; this was also used for the examples in this section.

4.6.1 Fore-Aft

As shown in the previous section, gravity has a significant influence on the measured acceleration. Although the error seems small, it leads to a significant overestimation of the displacement. This can be solved by an iterative process described in equations (4.21) and (4.22). For the single load case in the previous section four iteration steps led to the exact estimation of equivalent load of the actual tower top displacement; that was only for the frequencies above 50 mHz though.

In the figure below it can be seen how the approach also works for the other load cases. In Figure 4-38 the results are plotted for estimating the tower Fore-Aft displacement with low frequency compensation from the thrust, i.e. the same approach as in section 4.5.2. Three different approaches are given:

- with the real Fore-Aft Acceleration ('Real' [○]);
- with the measured acceleration,
  - without any correction ('Meas' [*]);
  - with iterative tilt correction ('$Meas_{Corr}$' [□]).

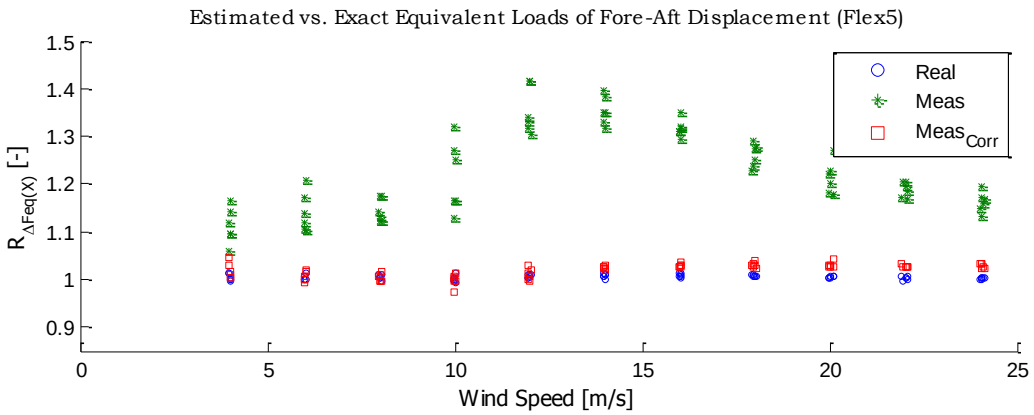

Figure 4-40 Ratio of equivalent loads between the estimated and real fore-aft displacement, where the displacement is estimated from the Real, the Measured and the Corrected measured acceleration. (Flex5) (Ratio=Estimated/Real)

For the gravity compensation with 4 iteration steps almost the same results as with the real acceleration are found. The equivalent loads of the displacement are overestimated by less than 2% with a standard deviation of 1.4%.

4.6.2 Side-Side

The error from measuring gravity is in the Fore-Aft direction significant. In the Side-Side direction the tilt (or roll) angles will be a lot smaller. The results for the Side-Side direction are given in the same way as was done in the Fore-Aft direction

In Figure 4-41 the results are plotted for estimating the tower Side-Side displacement with low frequency compensation from the torque, i.e. the same approach as in section 4.5.3 Three different results are given:

- with the real Fore-Aft Acceleration ('Real' [○]);
- with measured acceleration,
  - without any correction ('Meas' [*]);
  - with iterative tilt correction ('$Meas_{Corr}$' [□]).

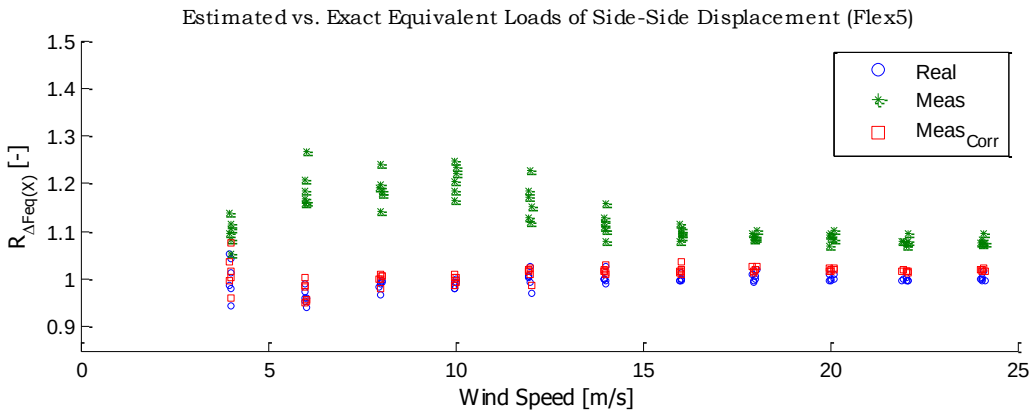

Figure 4-41 Ratio of equivalent loads between the estimated and real Side-Side displacement, where the displacement is estimated from the Real, the Measured and the Corrected measured acceleration, (Flex5) (Ratio=Estimated/Real)

For the iterative tilt correction almost the same results as with the real acceleration are found. The equivalent loads of the Side-Side displacement are overestimated by 1% with a standard deviation of a little less than 2%.

5 From acceleration to tower base fatigue loads (Flex5 results)

In chapter 2.3 an approach was given to estimate the bending moments from the tower top deflection. In chapter 4 the tower top deflection was estimated from the acceleration signal. In this chapter both results are combined to estimate the equivalent loads of the bending moments from the tower top acceleration. The flow chart used to explain the approach will in this section be divided into the fore-aft and the side-side direction to prevent a good overview.

Just like in the previous chapters the Fore-Aft and Side-Side directions will be treated separately.

5.1 Fore-Aft direction

For the dynamic analysis in the Fore-Aft direction a linear relationship between the tower top deflection and tower base bending moments may be assumed. This was concluded in section (3.3.2). Therefore equation (5.1) is used to compare the results. A high pass-filter (50mHz) is applied prior to the integration to prevent drift, section 4.3.

$$R_{\Delta Feq(BM)} = \frac{\Delta F_{eq}(k(x) * EI \iint a_{tt} dt)}{\Delta F_{eq}(M_{meas}(x))} \tag{5.1}$$

Where,

ΔF_{eq}	Equivalent load (from equation (2.1))
$k(x)$	Curvature $[m^{-2}]$
EI	Stiffness $[Nm^2]$
a_{tt}	Measured tower top acceleration $[m/s^2]$
M	Bending moment $[Nm]$

Without any further corrections the Fore-Aft bending moment is over predicted as well as under predicted. These errors can be ascribed to two phenomena.

The underestimation comes from the missed low frequency cycles as a result from the high pass filter. This is ascribed to the low-pass filtering effect of the rotor. This effect diminishes at higher wind speeds because the pitch control is designed to keep a constant rotor speed above rated wind speed.

The missed low frequencies can be compensated with the low frequencies from the rotor thrust. The thrust is however unknown and can be estimated with equation (4.13). The thrust coefficient C_t is calculated by Flex5 for different pitch angles and the tip speed. Data from the resultant table is interpolated to estimate the thrust coefficient and subsequently the thrust.

$$T = {}^{1}/_{2}\,\rho U_{\infty}^{2} A C_t \tag{4.13}$$

With the low frequency compensation the standard deviation of the results is much lower, but the mean value is increased. The over estimation comes from the fact that the accelerometer measures

gravity when tilted. This effect was described in section 4.6. The problem can be solved by iteration between equation (4.23) and (4.22).

$$a_{horz} = a_{real} + G a_{ev} v(L,t) \tag{4.22}$$

Where the tower top displacement,

$$v_{est}(L,t) = \iint a\, dtdt \tag{4.23}$$

With the iterative approach the influence of gravity is hardly visible any more. The results of the steps above are summarised in Figure 5-1, where

- the acceleration signal is filtered prior to the integration step ('Filtered' [○]);
- the filtered acceleration is iterated ('Iteration'[*]);
- the filtered acceleration is iterated and compensated with the estimate thrust ('Thrust' [□]).

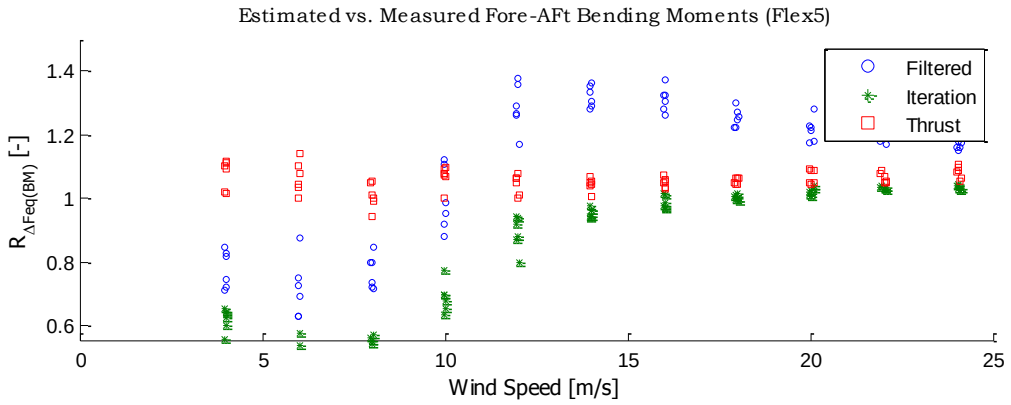

Figure 5-1 Ratio of equivalent loads between the estimated and the measured Fore-Aft Bending moments, where the bending moment is estimated from integration of the filtered tower top acceleration (Filtered) with thrust compensation (Thrust) and where the acceleration corrected for gravity (Iteration) (Flex5) (Ratio=Estimated/Measured)

To conclude on the Flex5 results in the fore-aft direction:

- The equivalent load range of the tower base bending moment from the tower top acceleration is overestimated by 6% with a standard deviation of 3.5%.
- The 1 year equivalent load range of the tower base bending moment from the tower top acceleration is overestimated by 5%.

The steps that need to be taken to find the bending moment from the measured acceleration are, for the fore-aft direction, summarised in Figure 5-2.

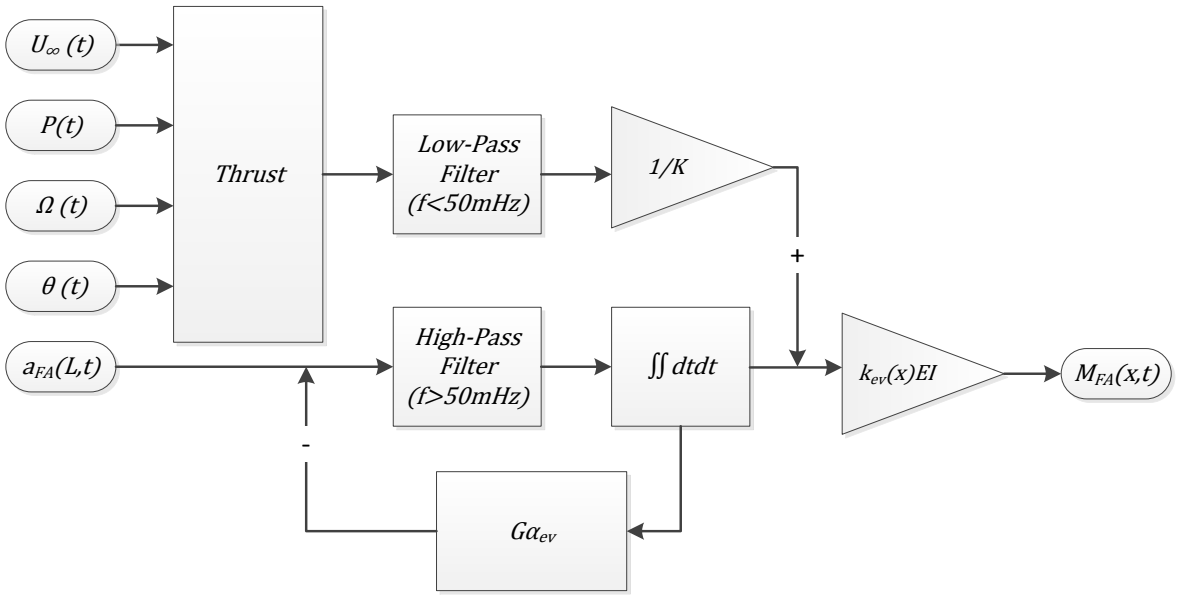

Figure 5-2 Flow chart for finding the bending moment from the acceleration in the Fore-Aft direction

The biggest scatter is introduced by the simplified thrust estimator. It is believed that a more sophisticated thrust estimator will give better results. This is however beyond the scope of this thesis.

5.2 Side-Side direction

For the dynamic analysis in the side-side direction a linear relationship between the integrated acceleration and the tower base bending moment may not be assumed. In section 3.3.2 it was shown that the bending moments will then be overestimated because of the assumed mode shape. That is because the torque of the rotor dominates the bending moment. It should therefore be accounted for. The torque can be described by equation (3.28),

$$T = \frac{1}{\Omega}\left(\frac{P_{el}}{\eta(P_{el},\Omega)} + J\dot{\Omega}\right) \tag{3.28}$$

Where the efficiency (η) is both the mechanical and electrical efficiency of the generator and depends on the rotational speed and the power output. The inertia (J) is a rough estimation of the combined inertia of the rotor drivetrain and generator, although wrong the simplification suffices for its purpose in this thesis.

The torque is however also needed for the low frequency compensation. Just as in the Fore-Aft direction the bending moments are underestimated because of the missed low frequencies due to the filter. These low frequencies can be compensated by torque.

To summarise, the integrated acceleration underestimates the tower top deflection because of the missed low frequencies due to the filter. The deflection however, over estimates the bending moments because of the mode shape assumed. This means that for the side-side bending moments the relationship between the acceleration and deflection is can be described by equation (4.23), from equation 3.25 and 4.16,

$$M_{est,SS}(x) = \kappa_{ev}(x)EIv_{SS}(L) - \xi(x)M_{tt,SS} \tag{3.25}$$

with the low frequency compensation described by,

$$v_{SS}(L) = \frac{\big(1+\xi(x)\big)T}{\kappa_{ev}(x)EI} \tag{4.15}$$

and with the assuming that the moment at the tower comes from the torque

$$M_{est,SS}(x) = \kappa_{ev}(x)EI\left(\iint a_{ss}\,dtdt + \frac{\big(1+\xi(x)\big)T}{\kappa_{ev}(x)EI}\right) - \xi(x)T \tag{5.2}$$

which can be simplified to

$$M_{est,SS}(x) = \kappa_{ev}(x)EI\iint a_{ss}\,dtdt + T \tag{5.3}$$

The results are shown in Figure 5-3, where the same steps are taken as with the fore-aft displacement, those are:

- the acceleration signal is filtered prior to the integration step ('Filtered' [○]);
- the filtered acceleration is iterated ('Iteration'[*]);
- the filtered acceleration is iterated and compensated with the estimated torque ('Torque' [□]).

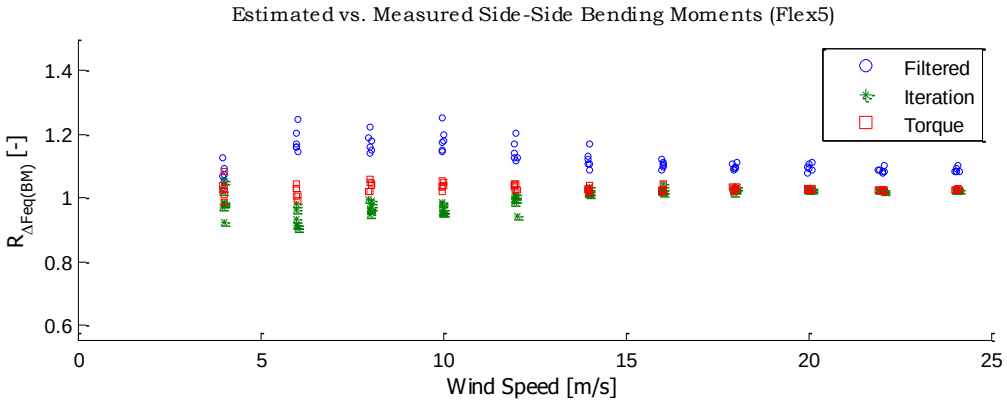

Figure 5-3 Ratio of equivalent loads between the estimated and the measured side-side Bending moments, where the bending moment is estimated from integration of the filtered tower top acceleration (Filtered) with torque compensation (Torque) and where the acceleration is corrected for gravity (Iteration) (Flex5) (Ratio=Estimated/Measured)

To conclude on the Flex5 results in the side-side direction:

- The equivalent load range of the tower base bending moment from the tower top acceleration is overestimated by 3% with a standard deviation of 1.4%.
- The 1 year equivalent load range of the tower base bending moment from the tower top acceleration is overestimated by 3%.

Without the torque compensation similar results are found:

- The equivalent load range of the tower base bending moment from the tower top acceleration is estimated exact with a standard deviation of 3.6%.
- The 1 year equivalent load range of the tower base bending moment from the tower top acceleration is overestimated by 2%.

This makes the approach a lot more straightforward. The steps that need to be taken as well as the steps that can be omitted are summarised in Figure 5-4.

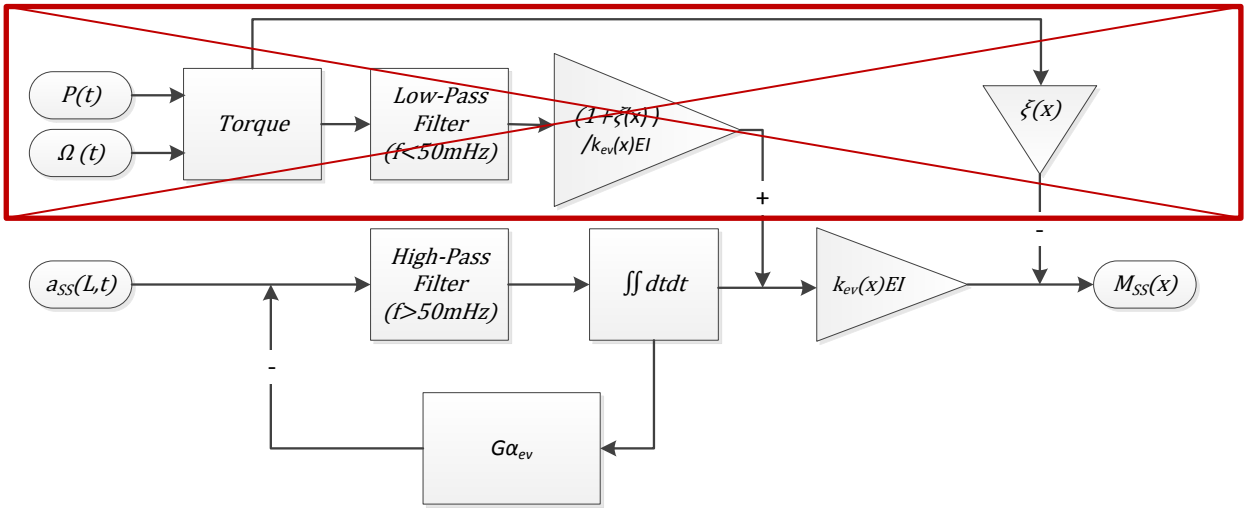

Figure 5-4 Flow chart for finding the side-side bending moment from the acceleration. The influence of torque may be neglected since it hardly influences the results.

6 Measurements

The results from previous chapters will be validated with the measurement performed on turbines from the Offshore Wind farm Egmond aan Zee.

In this chapter a description about the wind farm and the measurement campaign will be given. Only the raw data of the sensors is available. This has to be translated to the physical quantities used in the rest of the thesis to allow for a comparison of results. The transfer functions needed to do so are given in section 6.2.

Furthermore, in Flex5 more or less ideal conditions are considered. For a good comparison of results similar conditions need to be compared. The method used to find similar operating conditions for the OWEZ turbines is given in section 6.3.

6.1 Egmond aan Zee Windfarm (OWEZ)

A feasibility study was carried out in 1997 on the development and construction of a 100 MW offshore wind farm. The initiative was a result of the Dutch government's identification of offshore wind as being the largest feasible renewable energy resource in the Netherlands. This study, conducted by SenterNovem (formerly Novem), concluded that such a project would only be economically viable if sufficient subsidies were granted. This initiated the demonstration project now known as Offshore Windfarm Egmond aan Zee.

In 2002 a 50/50 joint venture between Shell and Nuon, called NoordZeeWind (NZW) awarded the site concession via a public tender. In 2005 a joint venture between Vestas and Ballast Nedam, called Bouwcombinatie Egmond, signed for the realisation of the windfarm. It comprises one meteorological mast and 36 Vestas V90 turbines yielding an installed power of 108 MW, between 10 and 18 km from the coast of Egmond aan Zee, Figure 6-1.

Figure 6-1 Location of the Offshore windfarm Egmond aan Zee (OWEZ)

6.1.1 Construction

The design of the support structure was performed by Infra Consult and Engineering, an in-house engineering company of Ballast Nedam. Further calculations on the tower and the total wind turbines were done by Vestas.

A monopile of 45 metres long with a diameter of 4.6 meters and an average thickness of 50 mm is used as a foundation, weighing approximately 230 tons. It is driven about 30 meters into the soil and protected by anodes to prevent corrosion. The anodes are connected to a ring which also holds

the j- tubes. A transition piece holding a boat landing and I-tubes is lowered into the monopile. The slightly smaller diameter allows for small corrections of possible inaccuracies of the vertical angle of the monopile. A grouted connection holds the transition piece in its place. See Figure 6-2

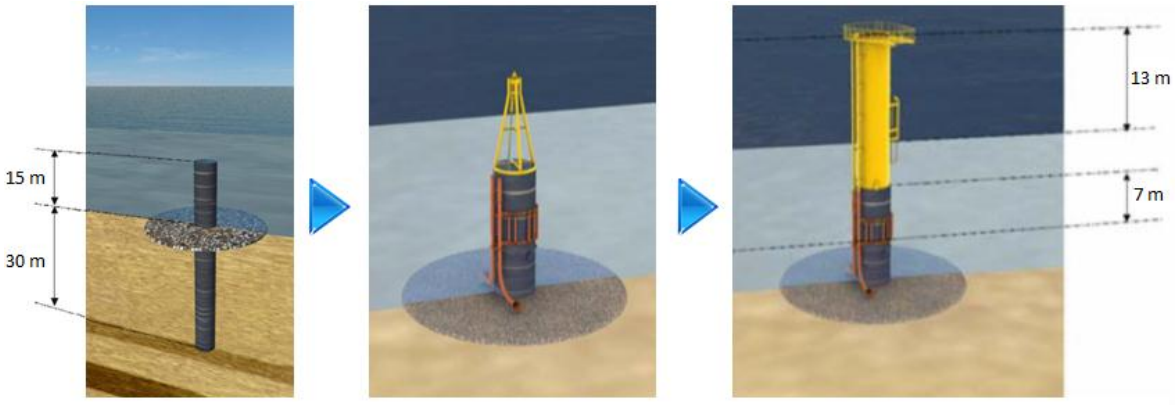

Figure 6-2 Foundation installation sequence [26]

On top of the transition piece, 13 meters above mean sea level, the turbine's tower is installed. The 55 m. long tower holds the nacelle, resulting in a hub height of 70 meters above mean sea level, Figure 6-3.

Figure 6-3 Installation of a turbine at the offshore wind farm Egmond aan Zee

6.1.2 Monitoring and evaluation program (MEP)

To gain insight in the development of offshore wind energy in the Netherlands an extensive Monitoring and Evaluation Program (MEP) became part of the project, often referred to as NSW-MEP (Near Shore Wind MEP). Part of the program is gaining insight in the technology. Therefore additional measurements are done, in the environment as well as on the turbines.

Just outside the wind farm a meteorological mast (Met Mast) was erected, which is able to measure the sea and weather conditions. The Met Mast consists out of a similar foundation as the wind turbines, with a triangular lattice tower on top. Instruments are installed at 21.6, 70 and 116 meters above mean sea level and at three wind directions (i.e. 300º (NW), 60º (NE) and 180º (S)). Able to measure wind speeds over the entire rotor diameter. The distance between the measurement devices and the tower is sufficient to keep the wind speed measurements within 5% inaccuracy. The wind speed is measured with cup anemometers and sonic wind meters at each level and wind direction [27].

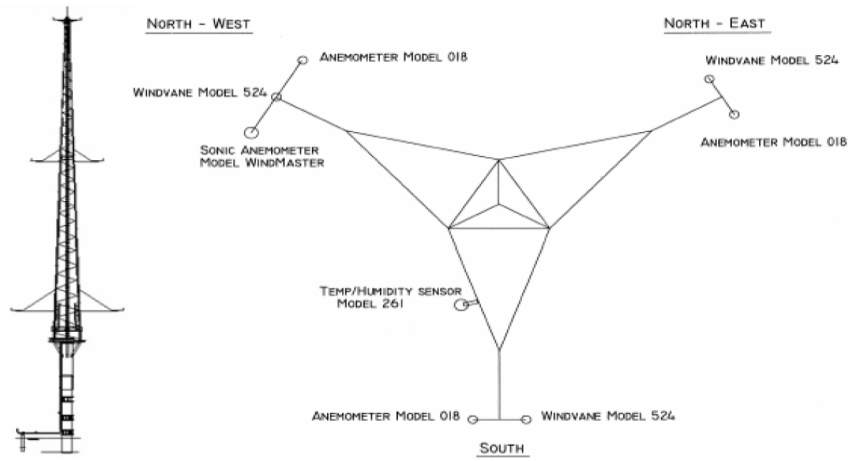

Figure 6-4 Front view of OWEZ MetMast (left), top view of sensors and their position at 21.6 m above MSL (right) [27].

Furthermore turbines 7 and 8, Figure 6-5, are equipped with extra sensors to measure the loads. Amongst others the acceleration of the tower top and the bending moments near the tower base are measured.

The turbines are variable speed pitch controlled Vestas V90 turbines. Each has a rated power of 3 MW and a rotor diameter of 90 m. Additional info about the Vestas V90 turbine can be found in the construction request of the Zuidlob windfarm (NL) [28]

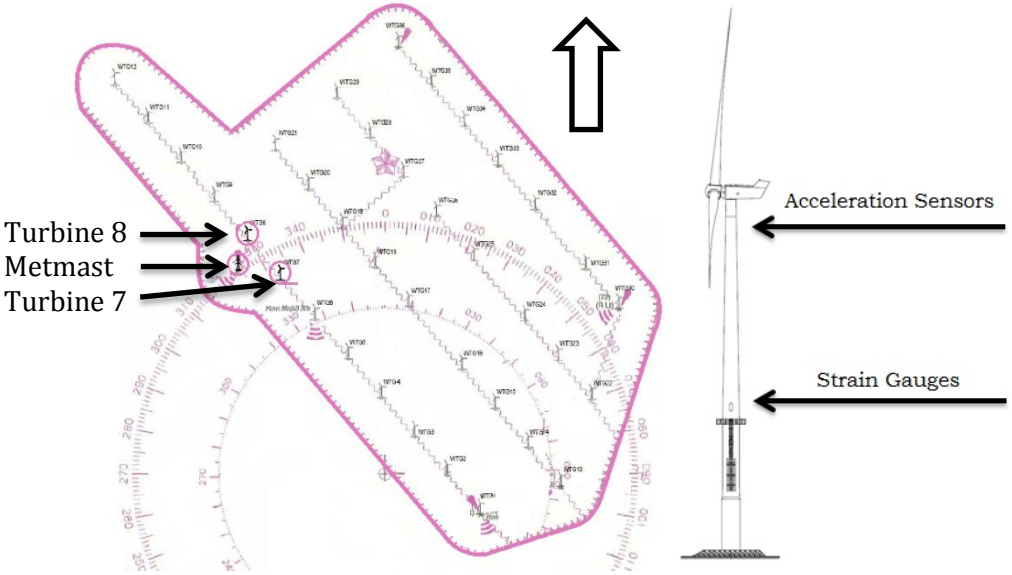

Figure 6-5 OWEZ site lay out and position of Turbines 7,8 and the MetMast

6.2 Transfer functions

Most of the signals are already given in the right physical quantity. The output of the strain gauges and accelerometers are however given in $\mu V/V$. They therefore need to be transferred into the right physical quantities. The transfer functions are described below.

6.2.1 Strain gauges

To go from any signal (S) to a desired value, in this case the tower bending moment (M_b), a transfer function is needed. A general layout is given in equation (6.1), where the signal is adjusted with a certain offset (O) for calibration and multiplied by a gain (G), giving the physical relationship between the output and the desired value.

$$M_b = G(S - O) \tag{6.1}$$

The gain should be a bending-moment/voltage relationship, because a voltage drop is measured. For the tower bending moment strain gauges are used, Figure 6-6. Due to bending of the material the strain gauge, depending on the alignment, elongates or shortens, resulting in a change in electrical resistance. When a voltage is applied to the gates, on the right side of the strain gauge, the change in resistance will result in a voltage drop, which is either positive or negative, depending on the direction of the tower's bending. This voltage drop is the sensor's output given as the ratio between the voltage drop and the nominal voltage.

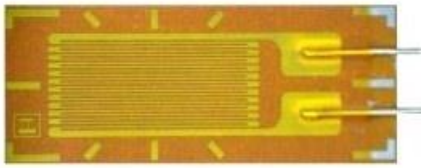

Figure 6-6 Example of a single strain gauge

The bending-moment/voltage relationship can be acquired by basic mechanics. First a bending moment/strain relationship is acquired and then combined with a strain/voltage relationship to get to the desired transfer function.

The tower bending moments come from Hooke's law (6.2) and the basic formula for a cylinder stress under bending (6.3) and can be found in any book about material mechanics.

$$\sigma = \varepsilon E \tag{6.2}$$

$$\sigma = \frac{M_b D}{2I} \tag{6.3}$$

Where:

σ	Stress $[Pa]$
ε	Strain $[m/m]$
E	Elasticity modulus $[Pa]$
M_b	Bending moment $[Nm]$
D	Diameter[21] $[m]$
I	Area moment of inertia $[m^4]$

[21] Note that the diameter depends on the strain gauge's placement on the tower.

Combining equations (6.2) and (6.3) yields the moment/strain relationship, equation (6.4).

$$\frac{M_b}{\varepsilon} = \frac{2EI}{D} \tag{6.4}$$

Furthermore strain gauges are connected with a so called Wheatstone bridge (Figure 6-7) to be able to measure the very small voltage drops over the strain gauges.

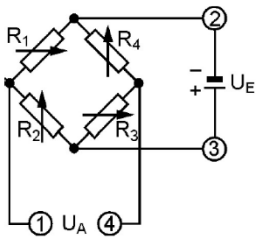

Figure 6-7 Example of a Wheatstone bridge circuit used for strain gauges

Where the resistances (R_i) represent the strain gauges and their resistance depends on their elongation (ε). The relationship of the voltages (U_A) and (U_E) describe the strain with the following relationship, equation (6.5).

$$\frac{U_A}{U_E} = \frac{1}{4}\left(\frac{\Delta R_1}{R_1} - \frac{\Delta R_2}{R_2} + \frac{\Delta R_3}{R_3} - \frac{\Delta R_4}{R_4}\right) \tag{6.5}$$

Furthermore,

$$\frac{\Delta R_i}{R_{i,0}} = k\varepsilon_i \tag{6.6}$$

Where,

k Gauge factor $[-]$

Under the assumption that the four strain gauges in one bridge are similar, the relative elongation depends solely on the Poisson's ratio (υ) of the inspected material. So equation (6.5) can be simplified into equation (6.7).

$$\frac{U_A}{U_E} = \frac{k}{4}B\varepsilon \tag{6.7}$$

Where the so-called bridge factor,

$$B = 2 + 2\upsilon \tag{6.8}$$

Since,

$$\varepsilon_1 = \varepsilon_3 = \varepsilon \text{ and } \varepsilon_2 = \varepsilon_4 = -\upsilon\varepsilon \tag{6.9}$$

Combining equations (6.4) and (6.7) gives the total transfer function to get from the sensor's output to the bending moment, equation (6.10) and is essentially the gain (G) in equation (6.1).

$$\frac{M_b}{U_A/U_E} = \frac{8EI}{DkB} \tag{6.10}$$

In case of multiple strain gauges the orientation of the different strain gauges needs to be taken into account to get to the tower's North-South (NS) and East-West (EW) bending. When a 90° offset between the different strain gauges is assumed equation (6.11) holds.

$$\begin{pmatrix} M_{NS} \\ M_{EW} \end{pmatrix} = \begin{pmatrix} \cos\beta_t & \sin\beta_t \\ -\sin\beta_t & \cos\beta_t \end{pmatrix} \begin{pmatrix} M_{b,1} \\ M_{b,2} \end{pmatrix} \tag{6.11}$$

Where,

β_t Offset angle to the north [°]

6.2.2 Accelerometers

The tower acceleration sensors directly measure acceleration so the transfer function is more straightforward and similar to equation (6.1), equation (6.12). The offset in this case comes from sloppy installation and/or calibration. The gain is given by the sensor's manufacturer.

$$Acc = G(S - O) \tag{6.12}$$

Where,

Acc Acceleration $[mm/s^2]$

And for coinciding coordinate systems

$$\begin{pmatrix} Acc_{NS} \\ Acc_{EW} \end{pmatrix} = \begin{pmatrix} \cos\beta_t & -\sin\beta_t \\ \sin\beta_t & \cos\beta_t \end{pmatrix} \begin{pmatrix} Acc_1 \\ Acc_2 \end{pmatrix} \tag{6.13}$$

6.3 OWEZ data processing

6.3.1 Statistical analysis

From March until October 2007 28,881 files are available, each containing measured signals (mostly) at 32 Hz of 82 sensors divided over 2 turbines. Giving a lot of data points which can be cumbersome to work with. Therefore all the signals are converted to their corresponding statistical parameters, amongst others; minimum, maximum, mean and standard deviation. These are used for data verification, to find the files with the least amount of unforeseen externalities, i.e. that match the operating conditions of Flex5.

6.3.2 Data verification

It has to be made sure that the available data is realistic and represents the actual working conditions one is looking for. Some faulty data is easily filtered. Sensor faults are detected by abnormal high or low sensor output (i.e. -99999 or 99999). Other 'faults' are a little harder to find

and need some understanding of wind turbine operation, but still, finding them is rather straightforward.

The files are filtered for:

- Sensor faults (Mean = ±99999)
- High wind (Mean > 30 [m/s])
- Yaw activity (Standard deviation > 2 [^{0}]
- Rotor speed (Mean > 17 [rpm] and Standard deviation > 0.4 [rpm])
- Power output (Mean < 0.5 [MW] or Mean > 4 [MW])
- Yaw angle (Varying with demand)

To give some more understanding of the process some scatterplots are made, showing the relationship of the bending moment with respect to the wind speed and yaw angle. These scatterplots are made from the data from the test turbine, i.e. Turbine 7 (see Figure 6-5).

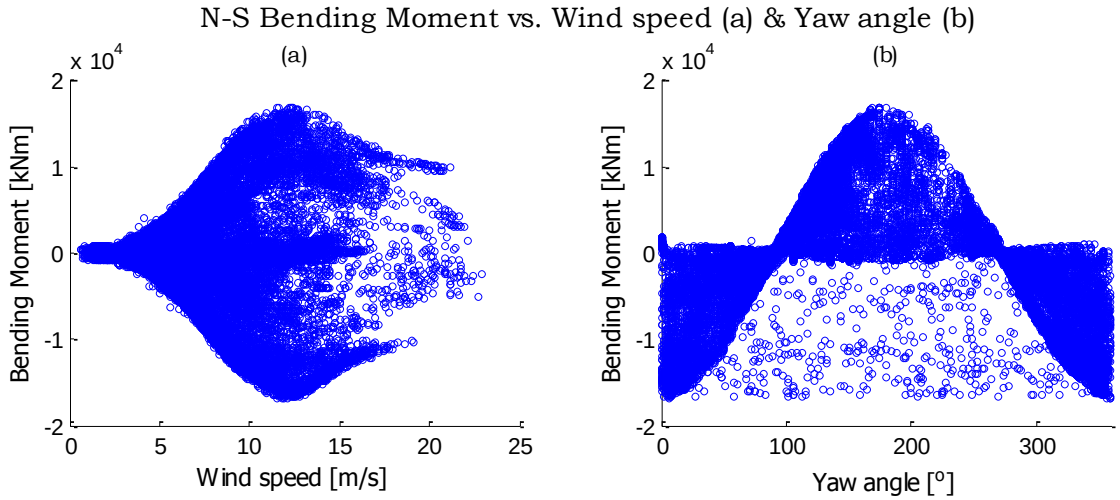

Figure 6-8 North-South Bending Moment vs. Wind speed & Yaw angle after filtering for high wind and sensor faults

From the left plot (a) in Figure 6-8, it can be seen that the maximum absolute bending moments occur at a little below rated wind speed. This is due to the fact that above a wind speed of about 10 m/s, the blades are pitched to control the power output, resulting in reduced loads, see also Figure 6-9[22]. The values between the maximum and minimum values represent the cases where the wind direction doesn't align with the strain gauges, i.e. no pure north-south or south-north bending.

From the right plot (b) it can be seen that the maximum absolute N-S bending moments occur at 0^0 and 180^0 angles. The outlying values probably come from some yaw activity crossing the $0^0/360^0$ line, resulting in wrong mean yaw angles. E.g. a yaw displacement from 355^0 to 5^0 results in a wrong average yaw angle of 180^0 instead of 0 or 360^0. Filtering for 'high' yaw activity will hopefully clear the outlying values. Figure 6-10 shows that this indeed is the case.

[22] The horizontal line at about 35° pitch angle represents idling. That is where the blades are pitched to feather, i.e. high pitch angles, at all wind speeds.

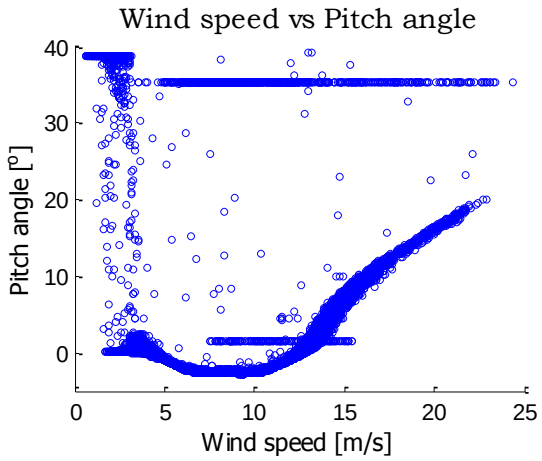

Figure 6-9 Wind speed vs. Pitch angle. Above ~10 m/s the blades are pitched for power output control.

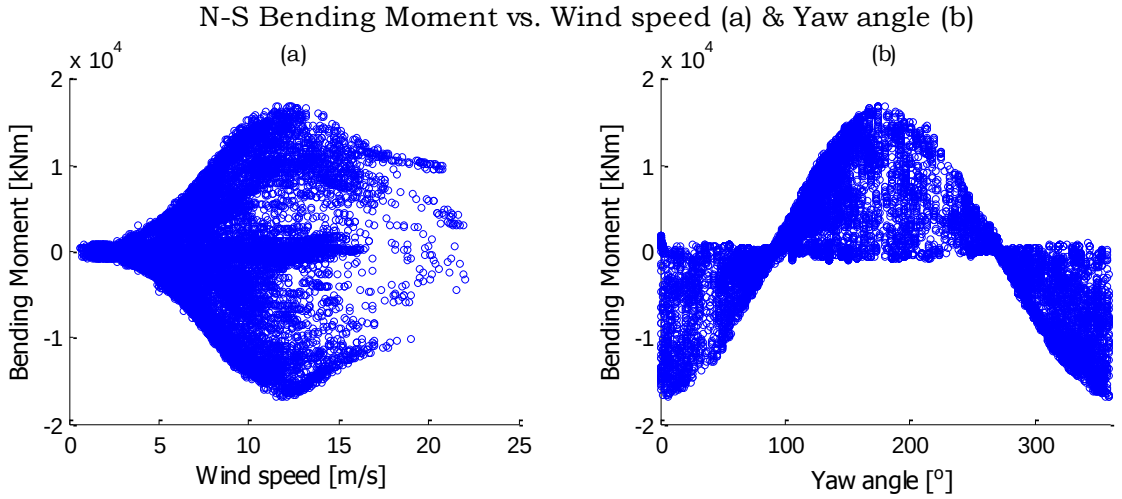

Figure 6-10 North - South Bending Moment vs. Wind speed & Yaw angle after filtering for high wind, sensor faults and 'high' yaw activity.

Furthermore constant operation conditions are preferred for better comparison between situations. Therefore also the periods with a lot of rotor activity (due to extreme turbulence or increasing wind speeds) are filtered, Figure 6-11. This will thus most likely also comprise situations with increasing wind speeds, wind gusts etc.

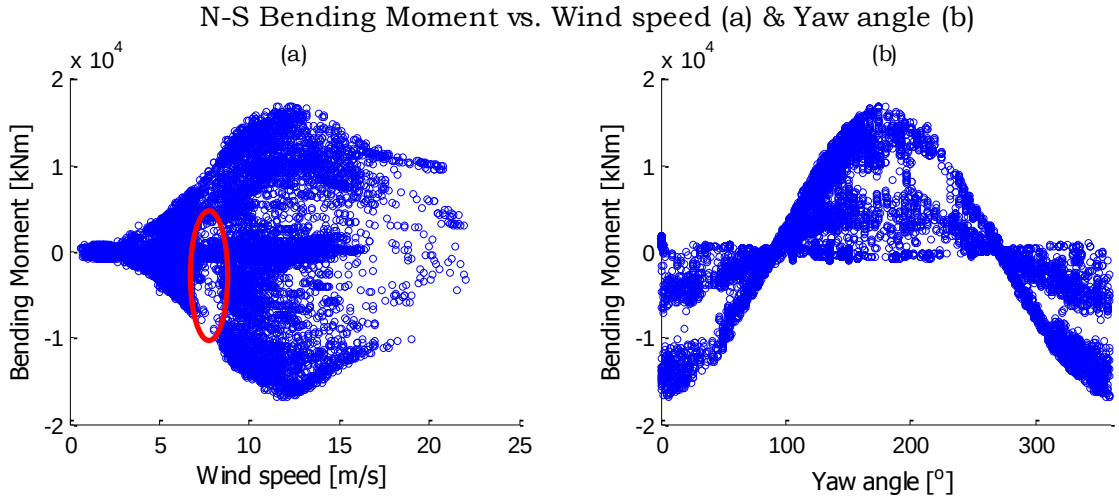

Figure 6-11 N-S Bending Moment vs. Wind speed & Yaw angle after filtering for high wind, sensor faults, 'high' yaw activity and high rotor activity

In the left plot (a) of Figure 6-11 a distinct gap can be seen at around 8 m/s, especially at negative bending moments. In the right plot (b) of it can be seen that this corresponds to yaw angles of about 320° – 120°, neglecting the East-West winds. Those angles correspond to wake conditions. Apparently that leads to higher rotational activity at lower wind speeds. It is also the region where there is hardly any pitch activity.

Also idling conditions need to be filtered, since these can give a wrong picture of the loads for certain wind speeds. Therefore also a filter is applied for abnormal power production, i.e. at little or above rated power.

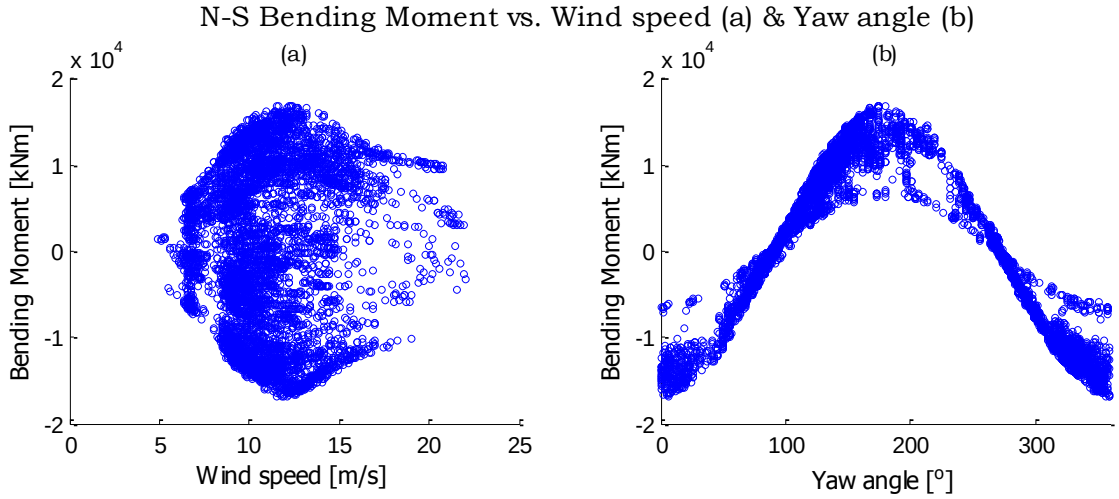

Figure 6-12 N-S Bending Moment vs. Wind speed & Yaw angle after filtering for high wind, sensor faults, 'high' yaw and rotor activity and abnormal power production.

As expected all the values below 6 m/s are cleared since that is more or less in start-up conditions and not reaching the 0.5 MW limit, left plot (a) in Figure 6-12.

It is believed that the remaining files are selected in such a way that no abnormal working conditions are left. But to make a proper analysis that corresponds to the Flex5 conditions only pure North-South wake free bending is considered, or East-West for that matter. Another filter is used to find the conditions between 170^0 and 190^0, Figure 6-13. In this case is thus only the south-north bending moments are considered, resulting in only the maximum values of the left plot.

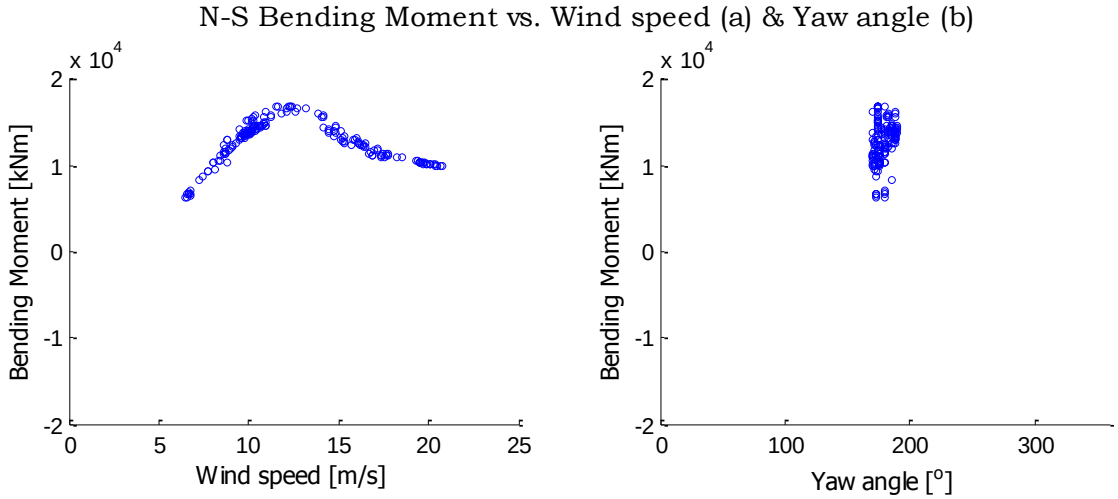

Figure 6-13 N-S Bending Moment vs. Wind speed & Yaw angle after filtering for high wind, sensor faults, 'high' yaw and rotor activity, abnormal power production and pure South-North wake free conditions.

For the test turbine (i.e. turbine 7), the number of files is reduced from 28,881 to only 179, i.e. about 30 h of data. For the pure East-West wake free bending the number of files is reduced to 357, i.e. about 60 h of data.

For the validation turbine (i.e. turbine 8) the amount of files is reduced to 501, i.e. almost 85 h of data. For the pure East-West bending the number of files is reduced to 201, i.e. almost 35 h of data.

7 Measurement results

The data from the measurement campaign described in chapter 6 will be used to test the theoretical approach derived with Flex5 on real turbines. Two independent data sets are available, i.e. from turbine 7 and turbine 8.

First the transferability between results from the simulations and the measured data will be investigated. The approach will be fine-tuned for best results. The new approach will be used to check to transferability between similar turbines. This is done with the independent dataset from turbine 8.

In chapter 5 the approach derived in chapters 3 and 4 was applied to the simulation software Flex5. There it was seen that in the Fore-Aft as well as the Side-Side direction a linear relationship between the tower top deflection and the tower base bending moment may be assumed.

There are some differences between Flex5 and the measurements that need mentioning.

The placing of the acceleration sensors is different between Flex5 and the measurements. The acceleration sensors from OWEZ are mounted in the tower top, Figure 6-5. In Flex5 however the acceleration is measured at the rotor axis, which is about 1 m above the tower top. This difference in height is accounted for as follows, equation (3.6) is rewritten as,

$$M_{est}(x) = \kappa_{ev}(x) EI \frac{v(L,t)}{v_{ev}(h)} \tag{7.1}$$

Where,

$v_{ev}(h)$ Generalised deflection at the point where the acceleration is measured $[-]$

The low frequency compensation and the generalised angle for the gravity correction also need to be corrected with this ratio, $\left(1/v_{ev}(h)\right)$.

The air density in Flex5 is constant. For OWEZ the air density is and is about 1.25 $[kg/m^3]$ with a standard deviation of about 1.5%.[23] That is, the difference between the maximum and minimum air density is about 7%.

Air density has a linear relation with thrust and will thus influence the results of the thrust estimator. For now a constant air density is assumed, since it is expected that the scatter introduced by the unknown undisturbed wind speed will be significantly larger.

Finally the measurements are performed at an offshore windfarm. This means that there is an additional loading on the tower induced by the waves and current. This is not accounted for during the theoretical approach.

The possible influence is investigated briefly in Appendix D. A thorough analysis is however beyond the scope of this thesis. Additionally, no wave buoy data is available for the measurements, meaning that the theory could not be verified by the measurements.

[23] Air density, $\rho = {}^{p}/_{RT}$ with R taken with the specific gas constant for dry air.

7.1 Test (Turbine 7)

Because of the placing of the sensors only the North-South-North and the East-West-East conditions are used. Sensor faults and abnormal turbine behaviour are also not taken into account. The process for finding the proper load cases is described in section 6.3. It is believed that the remaining files represent similar operating conditions as the load cases used for Flex5.

This means that for the test turbine 28,881 files have been reduced to 1,176 files. Each file contains measurements over a time span of 10 min. That means that 196 h of data is used. These are distributed over the yaw angles shown in Figure 7-1.

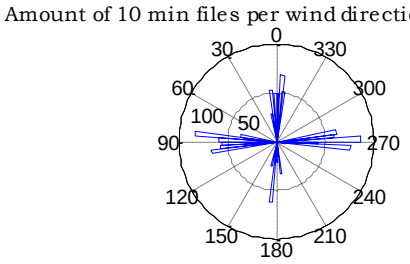

Figure 7-1 Amount of data used for the test turbine (T7), the radius of the circle gives the amount of files, where the circle represents the corresponding yaw angle. The yaw angle is measured counterclockwise, i.e. East = 270° (OWEZ T7)

First the general approach from Figure 7-2 will be used in the fore-aft as well as in the side-side direction, i.e. without any of the corrections derived in previous chapters. This is done to see if the results of the OWEZ turbines match the Flex5 results.

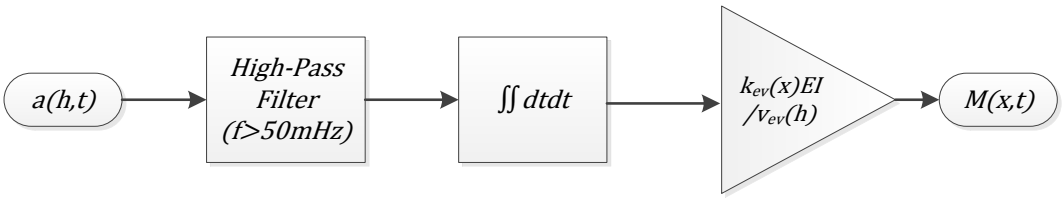

Figure 7-2 Flow chart for finding the bending moment at (x) from the acceleration at (h)

7.1.1 Fore-Aft direction

The ratio between the equivalent loads from the estimated (BM_{est}) and the measured (BM_{meas}) Fore-Aft bending moments, equation (7.2), are given in Figure 7-3. In section 2.1.2 an explanation about the equivalent loads can be found, together with how they are calculated.

$$R_{\Delta Feq(BM)} = \frac{\Delta F_{eq}(BM_{est})}{\Delta F_{eq}(BM_{meas})} \tag{7.2}$$

The estimated bending moment is calculated from equation (7.1), the process is shown in Figure 7-2.

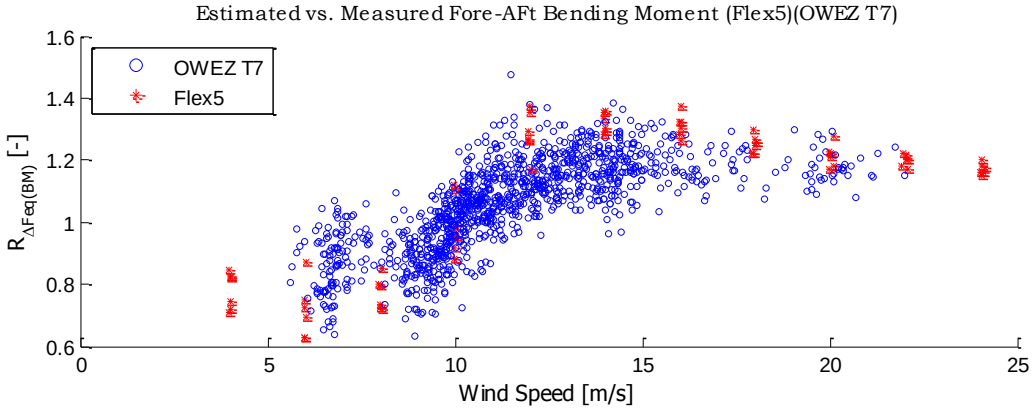

Figure 7-3 Ratio of equivalent loads between estimated and measured Fore-Aft bending moment, where the bending moment is estimated from integration of the filtered tower top acceleration (Flex5)(OWEZ T7)(Ratio=Estimated/Measured)

The scatter is a lot bigger than for the Flex5 results, but the results are comparable. That means the also for the OWEZ turbine straightforward integration leads to over- and underestimation of the bending moments. The bending moments are overestimated above rated wind speed because of the gravity measured by the sensor. The under estimation below rated wind speed comes from the missed low frequency cycles.

The overestimation seen in the Flex5 results looks bigger than in the OWEZ results. That could be explained by the fact that the acceleration sensor in Flex5 is mounted higher than the OWEZ sensors. The rotation of the accelerometer will then also be bigger. This means that more gravity is measured, leading to a larger overestimation of the bending moments.

The overestimation from the measured gravity can be corrected by iteration between the measured and estimated acceleration.

The underestimation can be corrected by adding the low frequency cycles from the thrust to the integrated acceleration. The thrust can be estimated from the rotor speed, pitch angle and undisturbed wind speed. The biggest difference between Flex5 and OWEZ in this case is that the undisturbed wind speed is unknown and therefore the wind speed from the nacelle measurements is used. The necessary corrections are summarised in

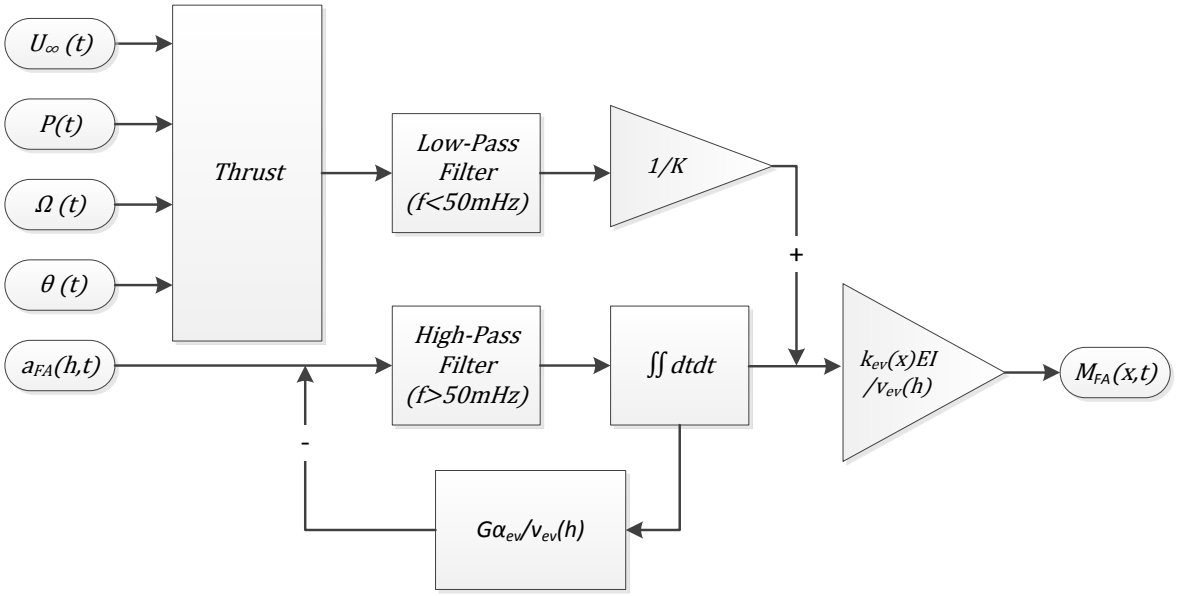

Figure 7-4 Flow chart for finding the bending moment at (x) from the acceleration at (h), with the necessary thrust and gravity correction

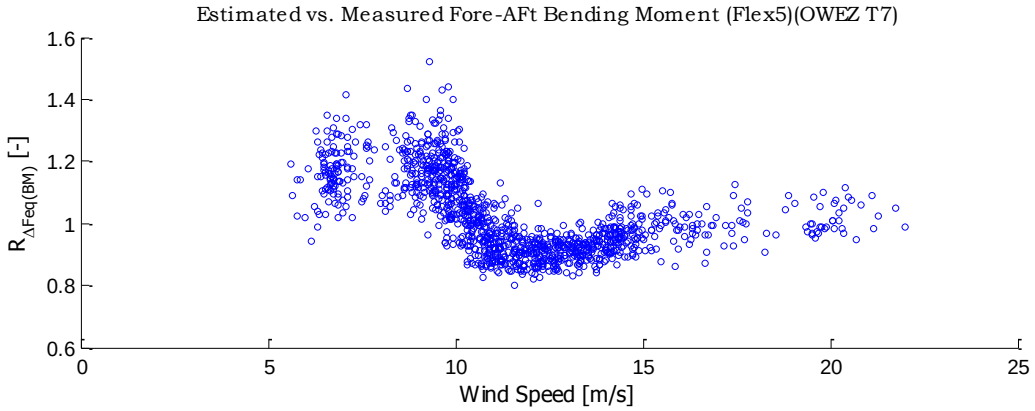

Figure 7-5 Ratio of equivalent loads between estimated and measured Fore-Aft bending moment, where the bending moment is estimated from integration of the filtered tower top acceleration, with low frequency compensation and gravity correction (OWEZ T7)(Ratio=Estimated/Measured)

In Figure 7-5 the corrections derived from the theory and validated by Flex5 are applied to the measurements. At low wind speeds the overestimation is significant, which implies that the low frequency compensation is too dominant. The overestimation at higher wind speeds is not very significant; the bending moments are even underestimated slightly for some cases above rated wind speed. It is therefore believed that the gravity correction can also be reduced.

The best results are found when the influence of the thrust compensation is reduced by 60% and the amount of iteration steps is reduced to 3. Due to the gravity correction the bending moments are underestimated by about 10%. The corrected results are shown in Figure 7-6 together with the results without any corrections, ('Direct').

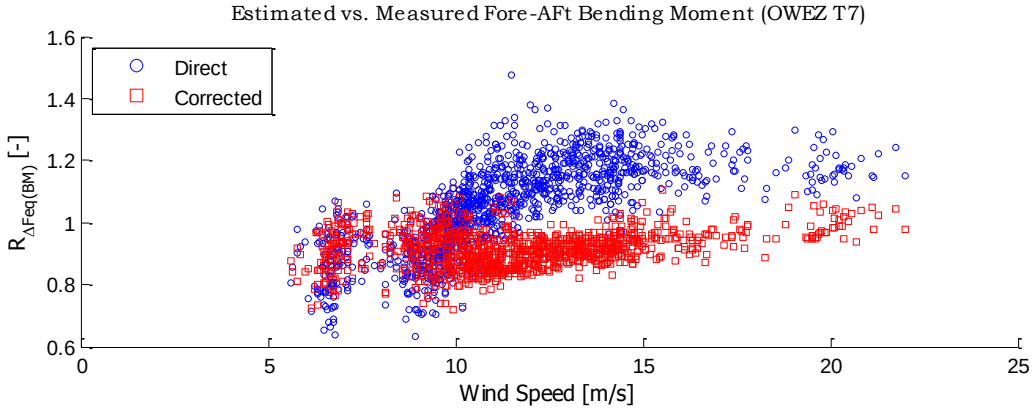

Figure 7-6 Ratio of equivalent loads between estimated and measured Fore-Aft bending moment, where the estimated values are given with the corrections shown in Figure 7-4 ('Corrected') and without any corrections('Direct') (OWEZ T7)(Ratio=Estimated/Measured)

To conclude on the measurements in the fore-aft direction, please note that these are the results, results of Figure 7-5, where the approach derived with Flex5 was used, Figure 7-4:

- The equivalent load range (10 min. 1 Hz) of the tower base bending moment from the tower top acceleration is overestimated by 3% with a standard deviation of 12.7%
- The 1 year equivalent load range of the tower base bending moment from the tower top acceleration is under estimated by 2%.

The results can be improved by adjusting gains of the proposed corrections. The gain was adjusted with $K = 1.7K$ the number of iteration steps was decreased to 2.

With the adjusted values the Fore-Aft bending equivalent loads are underestimated by 8% with a standard deviation of 6%.

7.1.2 Side-Side direction

The results for the Side-Side bending moment are given in Figure 7-7, together with the Flex5 results. Equations (7.1) and (7.2) were used, i.e. the approach from Figure 7-2. That means that no additional corrections are applied to the results.

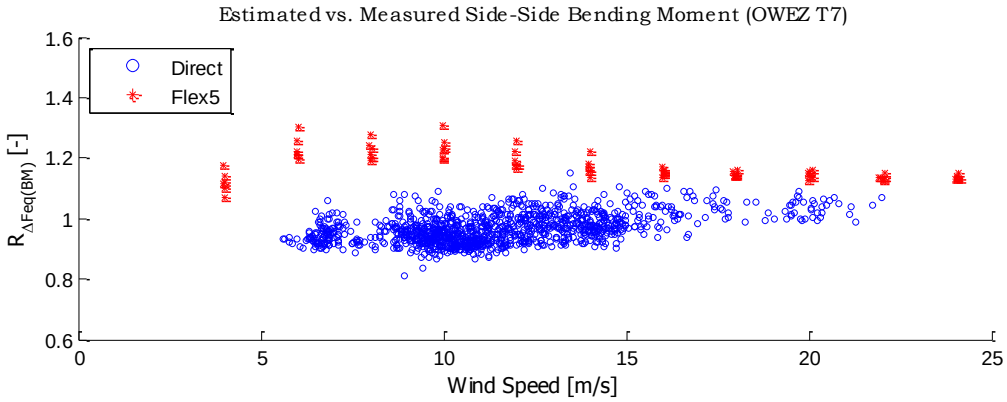

Figure 7-7 Ratio of equivalent loads between estimated and measured Side-Side bending moment, where the bending moment is estimated from integration of the filtered tower top acceleration (Flex5)(OWEZ T7)(Ratio=Estimated/Measured)

In the side-side direction the results from the OWEZ turbine are even better than those found with Flex5. In Flex5 the biggest error came from the measured gravity by the accelerometer. There is reason to believe that this phenomenon has a smaller effect on the OWEZ sensors because they are mounted lower. This was also visible in the fore-aft direction.

With the gravity correction the scatter can be reduced, but this has as side effect that the equivalent loads are underestimated. It seems that with more iteration steps the standard deviation decreases, but the underestimation also becomes larger. It can therefore be concluded that the best results are found without any corrections, i.e. the results from Figure 7-7.

For the approach shown in Figure 7-8 without the feedback loop, the following can be concluded: For the measurements in the side-side direction:

- The equivalent load range (10 min. 1 Hz) of the tower base bending moment from the tower top acceleration is underestimated by 3% with a standard deviation of 4.8%
- The prediction of the 1 year equivalent load range of the tower base bending moment from the tower top acceleration is overestimated by 0.3%

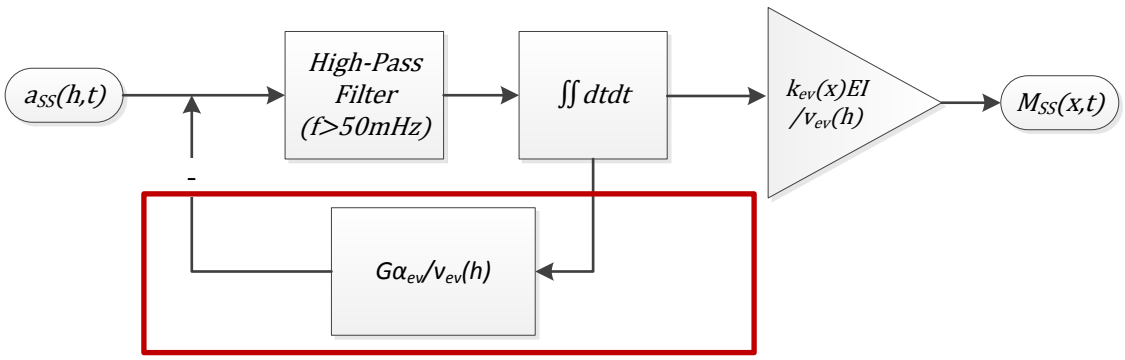

Figure 7-8 Flow chart for finding the side-side bending moments, the gravity correction does not lead to significant improvement of the results

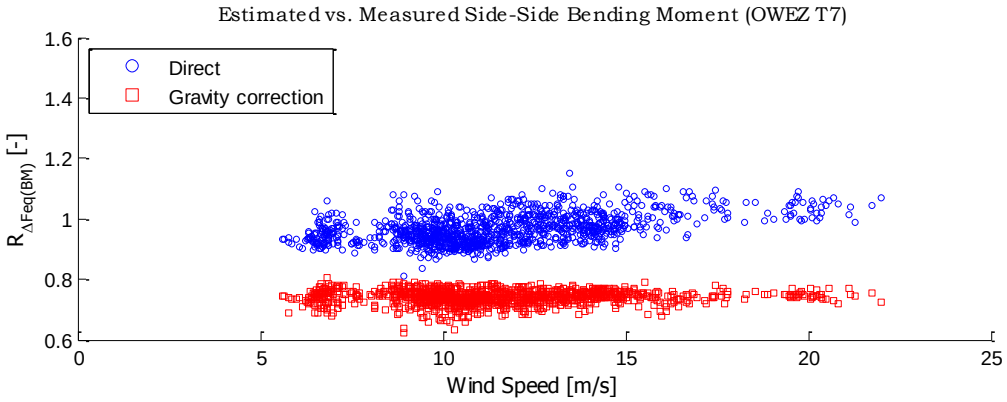

Figure 7-9 Ratio of equivalent loads between estimated and measured Side-Side bending moment, where the bending moment is estimated from integration of the filtered tower top acceleration ('Direct') and is corrected for gravity ('Gravity correctin') (Flex5)(OWEZ T7)(Ratio=Estimated/Measured)

The standard deviation can be reduced to 2.1%, but this means that the equivalent loads in the side-side direction are underestimated by more than 25%, Figure 7-9.

7.2 Validation (Turbine 8)

The number of 10 min periods that will be used for validating the results of turbine 7 is 939, i.e. 156.5 h of data, Figure 7-10.

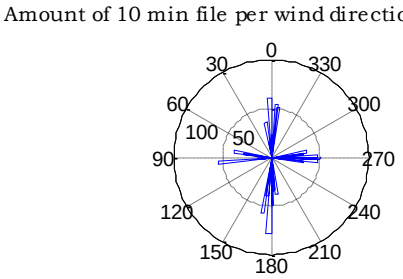

Figure 7-10 Amount of data used for the validation turbine (T8), the radius of the circle gives the amount of files, where the circle represents the corresponding yaw angle. The yaw angle is measured counterclockwise, i.e. East = 270^{O} (OWEZ T8)

The validation for turbine 8 will be done by applying the approach that gave the best results for turbine 7, Figure 7-11.

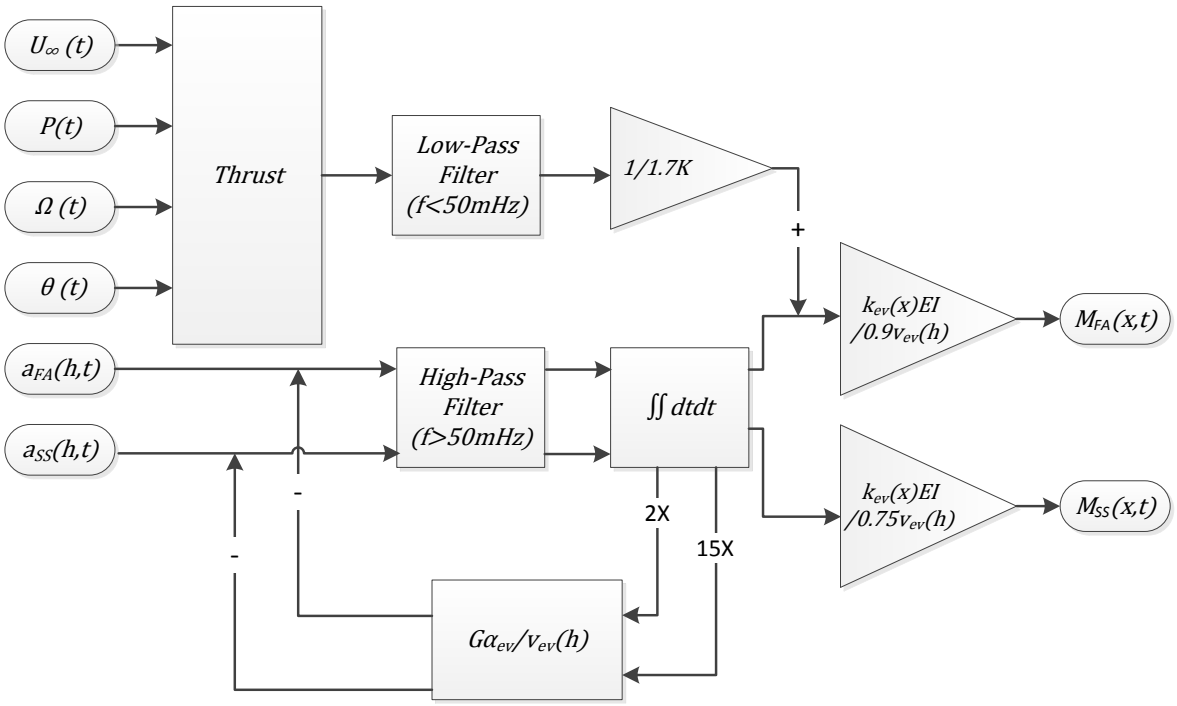

Figure 7-11 Flow chart for finding the fore-aft and side-side bending moments of the OWEZ turbines, with the accelerations measured at (h) and the bending moments at (x)

In the fore-aft direction the best results where found if the influence of the thrust compensation was reduced by 60% by increasing the tower stiffness ($K = 1.7K$ (with respect to the Flex5 results) and the amount of iteration steps needed for the gravity correction is 2. The equivalent loads are underestimated by 10%, therefore the mean will also be corrected for turbine 8.

For the side-side direction the best results were found if 15 iteration steps were used for the gravity correction. The equivalent loads are underestimated by 25%, therefore the mean wil also be corrected for the side-side results.

The results for this approach are given in the figure below.

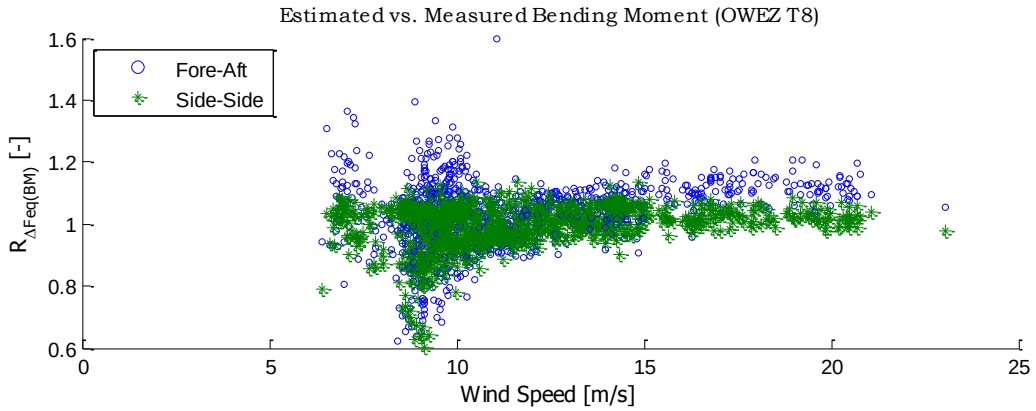

Figure 7-12 Ratio of equivalent loads between estimated and measured Fore-Aft and Side-Side bending moment, where the bending moment is estimated with the proposed approach from the test turbine, i.e. T7. (OWEZ T8)(Ratio=Estimated/Measured)

The scatter is very large at just below rated wind speed. This could mean that the thrust estimator distorts the results and the method is not transferable. This was also seen in Figure 7-5, where the Flex5 input was directly transferred to turbine 7. The error however leads to both over-and underestimation of the loads, whereas for turbine 7 the thrust estimator only led to overestimation.

Additionally the scatter is also visible in the side-side direction, there where no thrust correction is applied. The scatter could come from malfunctioning sensors.

Sensor faults were found by removing the time series with extreme high (or low) sensor output (section 6.3.2). In all other cases it was assumed that they perform as they should. This might not be the case. Only the files used for the validation are investigated.

The mean acceleration should as well as the mean bending moment coincide with the yaw angle. This is checked in Figure 7-13, where the mean strain and acceleration are plotted against the yaw angle.

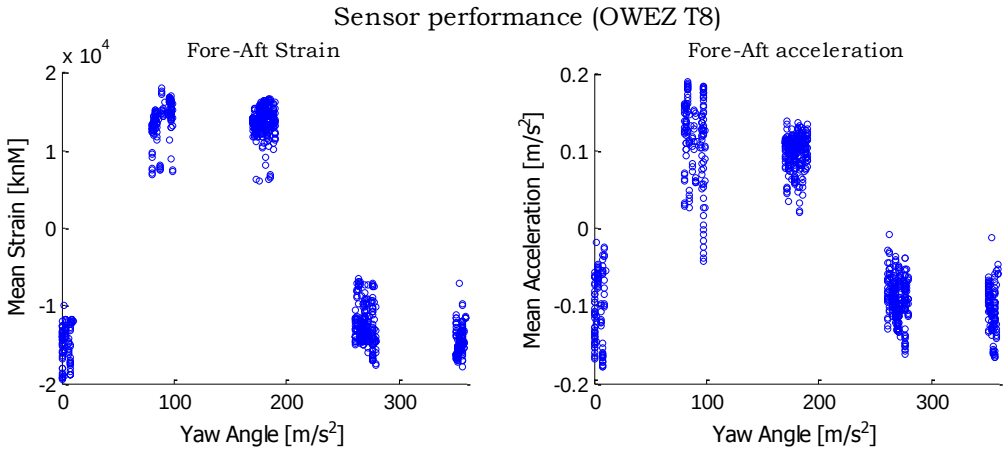

Figure 7-13 Mean fore-aft strain and acceleration vs. yaw angle (OWEZ T8)

The strain gauges perform as expected, positive bending is measured for 90^O and 180^O angles and negative for $0^O/360^O$ and 270^O angles. Similar behaviour is expected from the acceleration sensors. For positive bending the tower top will rotate and the accelerometers will measure gravity. The mean of the measured signal gives an indication of the size of the rotation. Positive gravity is measured for 90^O and 180^O angles and negative for $0^O/360^O$ and 270^O angles. However, the scatter at 90^O angles is very large. This could mean that one of the sensors does not perform well.

The acceleration is measured with 2 sensors. A combination of the two makes the complete acceleration signal. In Figure 7-14 the mean of the each sensor signal from the whole measurement campaign is plotted.[24] Sensor 1 (left plot) shows results as expected, but with sensor 2 (right plot) a lot of scatter is present.

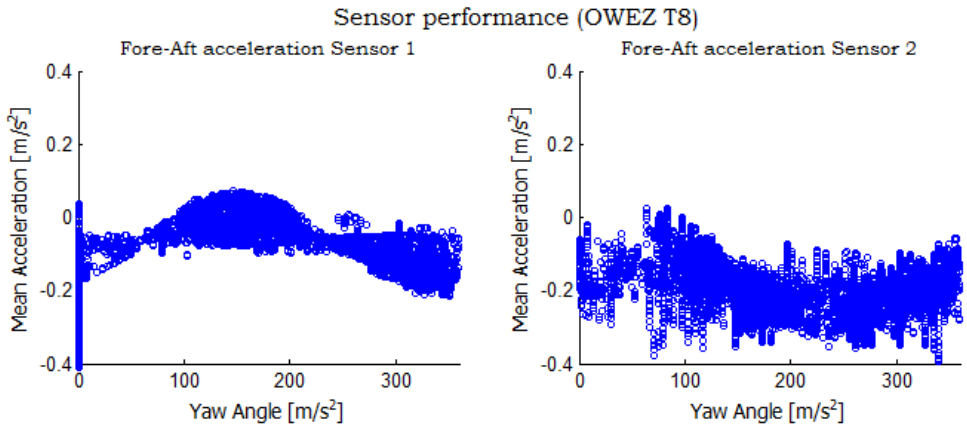

Figure 7-14 Mean acceleration from the tower top sensors vs. yaw angle (OWEZ T8)

[24] This means that there are over 50,000 data points plotted in this figure, the word processor had trouble coping with that, explaining the low quality of the figure.

From the offset of sensor 2 it is expected that sensor is installed under a relative large tilt angle (i.e. ~ 1.1^{O} vs. less than 0.1^{O} for the biggest offset from the sensors at Turbine 7, (not shown here). With Flex5 it was shown that gravity has a significant influence on the acceleration signal. If 1 sensor measures more than 10 times more gravity than the other sensors an increase in scatter may be expected.

From this it is concluded that the extra scatter in the results from turbine 8 comes from an acceleration sensor that is not performing well, or that it is installed wrong. That means that the transferability of the approach applied to turbine 7 cannot be properly evaluated, at least not for all yaw angles. The right plot of Figure 7-13 suggests the influence is the biggest for 90^{O} angles. Omitting that load case might reduce the scatter and something can be said about the transferability of the proposed method.

The scatter is reduced, but it seems that it is more a result of using less data than that it solves the problem.

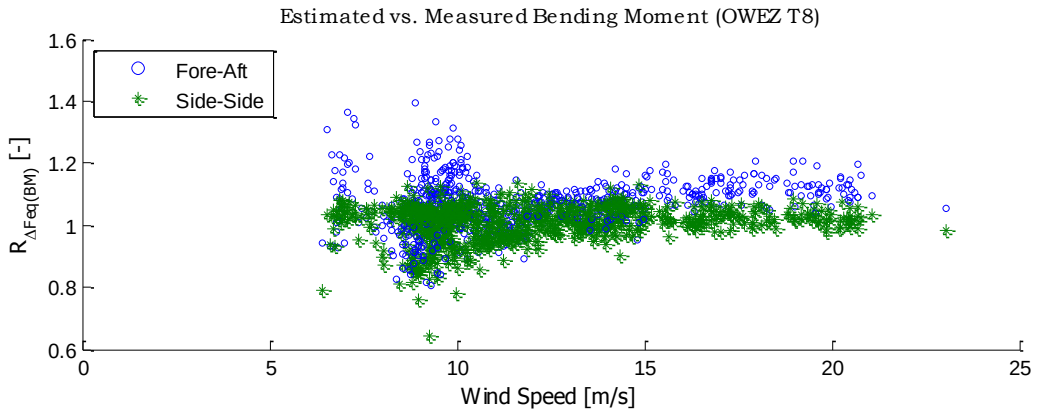

Figure 7-15 Ratio of equivalent loads between estimated and measured Fore-Aft and Side-Side bending moment, where the bending moment is estimated with the proposed approach from the test turbine, i.e. T7 and 90^{O} winds are omitted. (OWEZ T8)(Ratio=Estimated/Measured)

For the conclusion on validation the approach from Figure 7-11, the results presented in Figure 7-12 are used.

The equivalent load range of the tower base bending moment from the tower top acceleration is:

- Overestimated with 4% with a standard deviation of 11% in the fore-aft direction
- Underestimated by 0.5% with a standard deviation of 7% in the side-side direction

The 1 year equivalent load ranges of the tower base bending moment from the tower top acceleration is:

- overestimated by 7% in the fore-aft direction
- overestimated by 3% in the side-side direction

NB. The validation is done on a turbine where it is believed that one of the sensor used is installed in such a way that good results cannot be guaranteed.

8 Conclusions and recommendations

8.1 Main conclusions

The objective of this thesis was to provide an accurate prediction of the tower base bending moment equivalent fatigue loads (10 min. 1 Hz and 1 year equivalent load ranges) by using the acceleration of the tower top.

The following steps were taken:

- The possibility of determining the tower bending moment from the tower top deflection is investigated with a homogeneous massless beam.
- It is investigated which steps need to be taken to find the tower top displacement from the tower top acceleration.

The results were validated with the aero-elastic code Flex5 and with measurements performed at two OWEZ turbines

With the approach shown in the flow chart of Figure 8-1 the following results are found for the OWEZ measurements of turbine 8.

The equivalent load range (10 min. 1 Hz) of the tower base bending moment from the tower top acceleration is:

- overestimated by 4% with a standard deviation of 11% in the fore-aft direction.
- underestimated by 0.5% with a standard deviation of 7% in the side-side direction.

The prediction of the 1 year equivalent load range of the tower base bending moment from the tower top acceleration is possible:

- with an accuracy of 95% in the fore-aft direction.
- with an accuracy of 98%in the side-side direction.

Bending moment from tower top deflection

It is shown that for a homogeneous massless beam predictions on the basis of tower top deflection and the first eigenmode are exact if the only load is a horizontal force at the tower top. If moments or distributed loads are present, errors are introduced. These errors can be significant if the size of the moment or distributed load is large with respect to the horizontal force at the tower top. However, at $1/3^{th}$ of the beam length the error from the bending moment is zero and at $1/4^{th}$ of the beam length the error from the distributed load is zero.

For wind turbine loadings the following was concluded about the bending moments and the tower top deflection. If the first eigenmode is assumed:

- a linear relationship may be assumed between the deflection of the tower top and the bending moment at the tower base in the fore-aft direction.
- a linear relationship will lead to overestimation of the bending moment in the side-side direction.
    - The error in the side-side direction can be compensated with the torque.

Integration of acceleration to deflection

Integration of the acceleration signal leads to significant errors. The low frequencies present in the signal are blown up by integration, so-called drift. This problem can be overcome by using a high-pass filter prior to the integration. A cut in frequency of 50 mHz gives the best results.

The negative side effect of a filter is information is lost, since the frequencies below 50 mHz are thrown away. This will lead to underestimation of the loads.

- In the fore-aft direction the underestimation can be as big as 40%.
- In the side-side direction the underestimation is about 15%.
    - The problem in the fore-aft direction can be overcome by adding low frequencies from the thrust.
    - The problem in the side-side direction can be overcome by adding low frequencies from the torque.

If the thrust and torque are estimated the equivalent load range (10 min. 1 Hz) of the tower top deflection from integration of the top acceleration is:

- overestimated by 1% with a standard deviation of 3% in the fore-aft direction
- estimated exact with a standard deviation of 1.9% in the side-side direction

Prediction of tower loads with measured acceleration (Flex5)

In the fore-aft direction a thrust estimator is needed to compensate the information loss from the high-pass filter. In the side-side direction a torque estimator needs to be used to do so. However, a torque estimator is also used in the side-side direction to correct for the errors introduced by the assumed mode shape. These two corrections counteract each other and the influence of the torque estimator is therefore hardly visible; estimating the torque is thus not necessary.

The acceleration sensor also measures gravity, which can have a significant influence on the results.

- In the fore-aft direction the loads can be overestimation by about 40%
- In the side-side direction the overestimation can be as big as 20%
    - This problem can be overcome with iterative process between the estimated displacement and the measured acceleration.

NB. It was noticed that gravity only influences the acceleration signal for frequencies up to the eigenfrequency of the tower. With a more aggressive high-pass filter the measured and the horizontal tower top acceleration give the same results. This will however lead to an even bigger loss of information.

The equivalent load range (10 min. 1 Hz) of the tower base bending moment from the tower top acceleration is for the simulations:

- overestimated by 6% with a standard deviation of 3.5% in the fore-aft direction.
- Overestimated by 3% with a standard deviation of 1.4% in the side-side direction.

The 1 year equivalent load range of the tower base bending moment from the tower top acceleration is for the simulations:

- overestimated by 5% in the fore-aft direction
- overestimated by 3% in the side-side direction

Prediction of tower loads with acceleration (OWEZ Measurements)

For the measurements the same problems occur as with the simulations. If the same approach is applied, prediction of the equivalent load range (10 min. 1 Hz) of the tower base bending moment from the tower top acceleration is for the measurements possible:

- overestimated by 3% with a standard deviation of 12.7% in the fore-aft direction
- underestimated by 3% with a standard deviation of 4.8% in the side-side direction

The prediction of the 1 year equivalent load range of the tower base bending moment from the tower top acceleration is for the measurements possible:

- with an accuracy of 98% in the fore-aft direction
- with an accuracy of 99% in the side-side direction

The approach was optimized, which meant that some of the proposed corrections were applied with different parameters. The optimized approach, given in Figure 8-1, was validated with the independent data from a second turbine in the same wind farm.

NB. The validation of the fine-tuned approach is done on a turbine where it is believed that one of the sensor used is installed in such a way that good results cannot be guaranteed. The prediction of the tower base bending moment will thus probably be better than the figures suggest.

With the fine-tuned approach from the test turbine the prediction of the equivalent load range (10 min. 1 Hz) of the tower base bending moment from the tower top acceleration is possible:

- with an accuracy of 96% with a standard deviation of 11% in the fore-aft direction
- with an accuracy of 99% with a standard deviation of 7% in the side-side direction

With the fine-tuned approach from the test turbine the prediction of the 1 year equivalent load ranges of the tower base bending moment from the tower top acceleration is f possible:

- with an accuracy of 95% in the fore-aft direction
- with an accuracy of 98%in the side-side direction

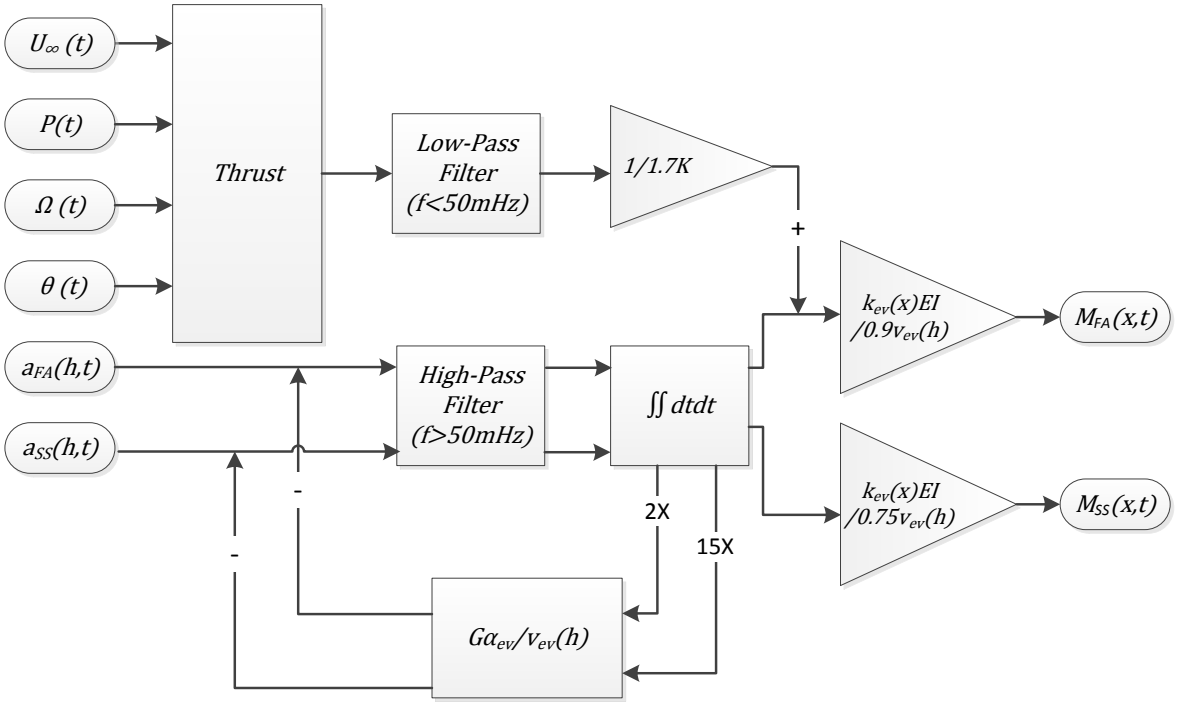

Figure 8-1 Flow chart for finding the fore-aft and side-side bending moments of the OWEZ turbines, with the accelerations measured at (h) and the bending moments at (x)

8.2 Recommendations

The biggest uncertainty in the prediction of the tower base bending moment is found in the fore-aft direction and is ascribed to the way the thrust was estimated. Results can be improved if more effort is put into thrust estimation.

Additionally, if the thrust can be estimated for values up to the eigenfrequency of the tower, the influence of gravity on the measured acceleration can be neglected.

The iteration needed to remove the influence of gravity is sensitive to the amount of iteration steps. Ideally the iteration converges to the right displacement. However, it was shown that the displacement converges to much lower values. This iterative approach might be too simplistic. Besides, the influence of assuming small angles as well as the influence of the high pass filter has not been investigated.

This process deserves more attention because it already gives promising results with limited effort.

Ringing and ripple from the (inverse) Fourier could lead to additional errors. This phenomenon was not investigated.

Furthermore, measuring the tower top with triaxial accelerometers allows for quantifying the amount of gravity measured and may give better results.

9 Bibliography

[1] Justin, J. Wilkes and J. Moccia, "http://www.ewea.org," February 2013. [Online]. Available: http://www.ewea.org/fileadmin/files/library/publications/statistics/Wind_in_power_annual_statistics_2012.pdf. [Accessed 20 May 2013].

[2] "NWEA," 2009. [Online]. Available: http://www.nwea.nl/windenergie-de-feiten. [Accessed 20 May 2013].

[3] International Energy Agency, *Tracking Clean Energy Progress 2013,* Paris: http://www.iea.org/publications/freepublications/publication/TCEP_web.pdf, 2013.

[4] N. Cosack, "Fatigue Load Monitoring with Standard Wind Turine Signals," Universität Stuttgart. Dr.-Ing. Thesis, Stuttgart, 2010.

[5] D. Inaudi, *Overview of 40 bridge structural health monitoring projects,* Canada: Roctest Ltd.

[6] V. Giurgiutiu, "Multifunctional Vehicle Structural Health Monitoring Opportunities With Piezoelectric Wafe Active Sensors," University of South Carolina, Columbia, 2002.

[7] Verbruggen, T.W., "Load monitoring for wind turbines. Fibre optic sensing and data processing.," ECN Windenergie, 2010.

[8] G. W. Roberts, X. Meng and H. A. Dodson, "Integrating a Global Positioning System and Accelerometers to Monitor the Deflection of Bridges," *Journal of Surveying Engineering,* no. 130, pp. 65-72, 2004.

[9] F. G. Polanco, "Estimation of Structural Component Loads in Helicopters: A review of Current Methodologies," Aeronautical and Maritime Research Laboratory, Melbourne, 1999.

[10] T. S. Obdam, L. W. Rademakers and H. Braam, "Flight Leader Concept for Wind Farm Load Counting: Offshore evaluation," in *European Offshore Wind Conference*, Stockholm, 2009.

[11] R. Dittmar, S. Müller and S. Schwartz, "Restlebensdauer von Windenergieanlagen bestimmen," *Erneuerbare Energien,* no. 3, pp. 20-22, 2005.

[12] C. Hofemann, G. Van Bussel and D. Veldkamp, "Artificial Neural Networks for SCADA based Load Reconstruction (PO.313_A)," in *EWEA*, Brussels, 2011.

[13] M. Hau, "Promising Load Estimation Methodologies for Wind Turbine Components," UPWIND Project D5.2, Kassel, 2002-2006.

[14] B. Jasniewicz, "Online estimation of mechanical loads for wind turbines," UPWIND project D5.3, Kassel, 2002-2006.

[15] C. A. Ochoa Algarín, "Root Blade Load Estimation by Measurement Database for the Implementation in a SCADA System," Delft University of Technology, Eindhoven University of Technology, MSc. Thesis , 2012.

[16] D. Veldkamp, *Personal correspondance,* 2013.

[17] S. Frandsen, "Turbulence and turbulence generated structural loading in wind turbine clusters," PhD. Thesis, Risø National Laboratory, Roskilde, Denmark, 2007.

[18] D. Veldkamp, "Chances in Wind Energy: A Probabilistic Approach to Wind Turbine Fatigue Design," DUWIND, PhD. Thesis; Delft, 2006.

[19] K. Thomsen, "The Statistical Variation of Wind Turbine Fatigue Loads," Risø National Laboratory, Roskilde, Denmark, 1998.

[20] D. Veldkamp, *Standards and load calculations,* Delft: TU Delft; Lecture notes, 2011.

[21] W. Bierbooms, *Introduction to wind energy,* Delft: Lecture slides TU Delft, 2011.

[22] D. Veldkamp, "Estimation of bending moments in the tower," Personal correspondence, 2013.

[23] L. D. Slifka, "An Accelerometer Based Approach to Measuring Displacement of a Vehicle Body," University of Michigan-Dearborn, M.Sc. Thesis, Dearborn, 2004.

[24] T. S. Edwards, "Effects of aliasing on numerical integration," *Mechanical Systems and Signal Processing,* vol. 21, no. 1, pp. 165-176, 2007.

[25] M. Rasila, "Torque- and Speed Control of a Pitch Regulated Wind Turbine," Chalmers University of Technology, Göteborg, Sweden, 2003.

[26] NoordzeeWind, "Off shore Windfarm Egmond aan Zee," NoordzeeWind, 2008.

[27] H. Kouwenhoven, "User manual data files meteorological mast Noordzee Wind," NoordzeeWind, 2007.

[28] "Agentschap NL," [Online]. Available: http://www.agentschapnl.nl/sites/default/files/sn_bijlagen/bep/80-Windparken/Zuidlob/Fase1/4_Aanvragen/bouwaanvragen/Bouwaanvraag-Vestas-V90-27aug09-311230.pdf. [Accessed 5 05 2013].

[29] J. F. Manwell, J. G. McGowan and A. L. Rogers, Wind Energy Explained, Chichester: John Wiley & Sons Ltd, 2002, p. 161.

[30] G. R. /. KMS, "DW," 13 09 2012. [Online]. Available: http://www.dw.de/calculating-the-true-cost-of-electricity/a-16235063. [Accessed 21 May 2013].

[31] T. Burton, N. Jenkins, D. Sharpe and E. Bossanyi, Wind Energy Handbook, 2 ed., Chicester: John Wiley & Sons Ltd, 2011.

[32] D. Cerda Salzmann and J. van der Tempel, "Aerodynamic Damping in the Design of Support Structures for Offshore Wind Turbines," in *Copenhagen Offshore Wind*, Copenhagen, 2005.

[33] A. T. Myers and V. Valamanesh, *Aerodynamic Damping and Seismic Response of Wind Turbine Structures,* Boston, Massachusetts: Northeastern University, 2012.

[34] EWEA, "European Wind Energy Association," 2010. [Online]. Available: http://www.ewea.org/fileadmin/ewea_documents/documents/publications/factsheets/EWEA_FS_Economics.pdf. [Accessed 20 June 2013].

[35] International Electrotechnical Committee, "IEC 61400-1 Ed.3: Wind turbines - Part 1: Design requirements," IEC, 2005.

[36] D. M. Frangopol, A. Strauss and S. Kim, "Bridge Reliability Assessment Based on Monitoring," *Journal of bridge engineering,* vol. 3, no. 13, pp. 258-270, May/June 2008.

Appendix A Flex5

Flex5 has been developed at the Technical University of Denmark, to model the behaviour of horizontal axis wind turbines. It has got a few important degrees of freedom and does fully non-linear load and response calculations. It is used and modified by turbine manufacturers to comply with their needs and turbines. Some basic features from the original version are:

- Superposition of deterministic and stochastic wind
- Aerodynamic loads from unsteady BEM-theory
- Viscous damping for all degrees of freedom
- Beam model with distributed mass and stiffness for blades and tower
- Stiff body with mass and mass moments of inertia for Hub, Nacelle and Foundation
- First order models for Generator, Brake and Yaw system
- Second order model for pitch system

Mode shape functions are used for the modelling of structural dynamics of the tower and the blades. For the nacelle, rotor shaft and hub, stiff bodies connected by flexible hinges are used. There is no coupling in terms of stiffness assumed for the generalised mass and stiffness of these subsystems.

Explicit 2^{nd} order Runge-Kutta method based on numerical integration in the time domain is used to calculate the response of the structure. Constant acceleration between steps is assumed. For the calculation of the aerodynamic loads Blade-Element-Momentum (BEM) theory is used. To account for the effects not captured with BEM, like dynamic wake and inflow and tip losses, additional models are used.
From [4]

Appendix B Fourier Analysis

A Fourier transform (FT) is built on the idea that every signal can be decomposed into a set of oscillating functions, i.e. sines and cosines. A simple example is shown in Figure B-1. The signal on top is the sum of the two signals below, in essence an inverse Fourier transform (IFT).

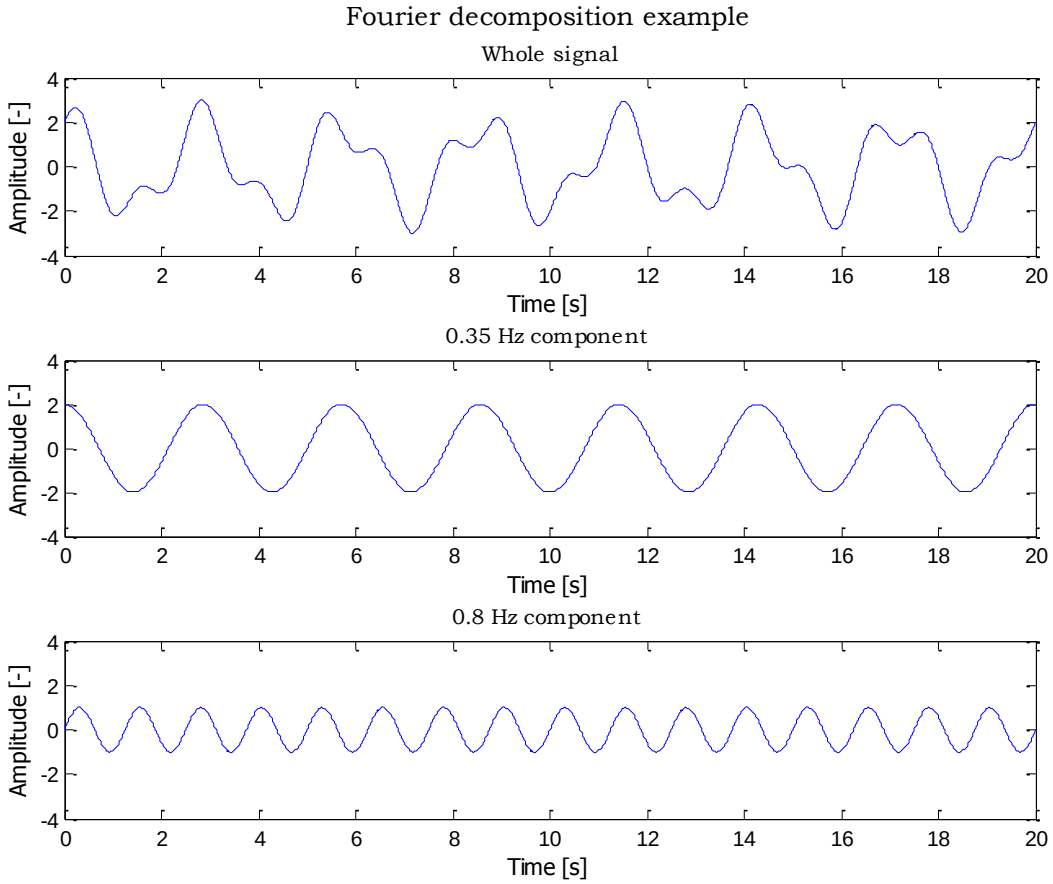

Figure B-1 Example of a Fourier decomposition. The signal on top consits out of a 0.35 Hz and 0.8 Hz components below.

The opposite can also be done. In that case the signal given in the time domain, as is the case in this example, can be rewritten in its so called frequency domain. The signal is then represented as a list of frequencies with corresponding amplitudes, which can be visualised in a so called power spectral density. E.g. the time series in the top plot in Figure B-1 has the corresponding power spectral density as shown in Figure B-2. It gives amplitudes of 2 and 1 at respectively 0.35 Hz and 0.8 Hz, as expected[25].

[25] Note that the ripple is due to the finite length of the signal. Increasing the signal's length will reduce the size of the ripple.

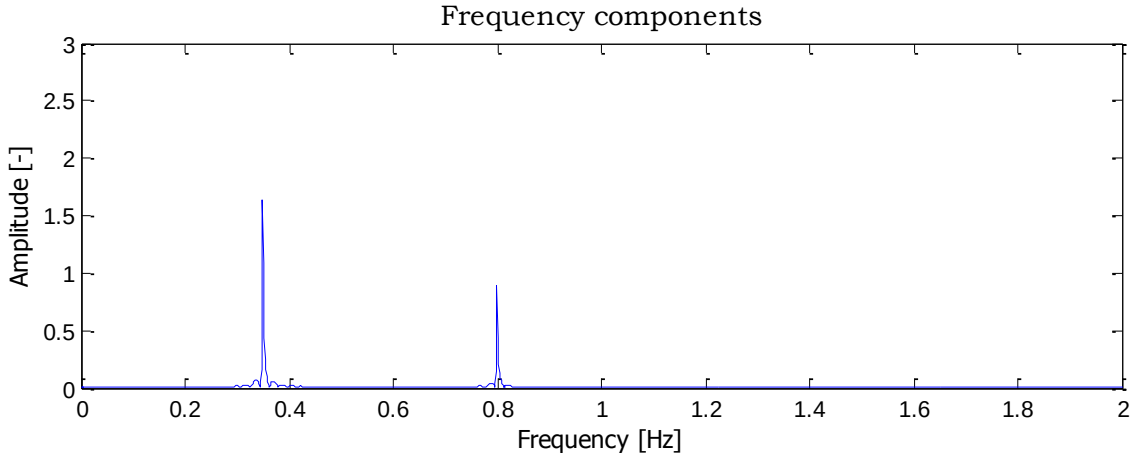

Figure B-2 The power spectral density from example in Figure B-1. It shows the frequencies in the signal with their corresponding amplitudes.

B.1 Filter and integration

The switch from time to frequency domain makes it easy to integrate a signal, because it is easy to integrate a sinusoid. Double integration of a sinusoid is done in the next equation[26].

$$\iint a(t)\,dt^2 = x(t) = -\left(\frac{1}{2\pi\omega}\right)^2 Ampl * \sin(2\pi\omega t) \qquad (9.1)$$

Where,

a	Acceleration $[m/s^2]$
t	Time $[s]$
$Ampl$	Amplitude $[-]$
ω	frequency $[Hz]$
x	Displacement $[m]$

Fourier assumes that all signals can be written as a sum of sines and cosines. Equation (9.1) shows that integrating a sine (or cosine for that matter) is the same as dividing the sine's amplitude by its frequency. Integration within the frequency domain is thus nothing more than dividing each amplitude by its corresponding frequency. The inverse Fourier transform will then give the integrated signal.

This also shows that integration is very sensitive to low frequencies. All frequencies below $1/2\pi$ i.e. ~ 0.16 Hz will result in increasing amplitudes. This can result in unwanted errors if some very low frequencies are present in the signal. These should be filtered.

This directly leads to the second advantage of the Fourier transform. In the frequency domain it is very easy to filter a signal for certain frequencies. The list of frequencies can be manipulated very easy to create any filter desired, i.e. the amplitudes of unwanted signals are simply set to zero. Performing an inverse Fourier transform will then give the filtered signal.

Fourier can thus be very handy to combine integration and filtering. Integration and filtering can thus be done with the aid of Matlab in 4 simple steps, shown below.

- Perform a Fourier transform to transform a time signal to its frequency domain
- Set all amplitudes corresponding to unwanted frequencies to 0
- Divide all remaining amplitudes by their corresponding frequency

[26] The integration constants are neglected. It should always be checked if this is valid.

- Perform an inverse Fourier transform to return to the time domain

$$a(t) \rightarrow a(\Omega) \rightarrow \overset{\curvearrowright}{\sim} \rightarrow \frac{a(\Omega)}{\Omega^2} \rightarrow x(\Omega) \rightarrow x(t)$$

B.2 OWEZ Results

The integration of the Fore-Aft and Side-Side acceleration signal with this Fourier approach leads to the same results as the trapezoidal integration. Remember that for the trapezoidal integration also a Fourier filter was used to remove the low frequencies that lead to integration errors.

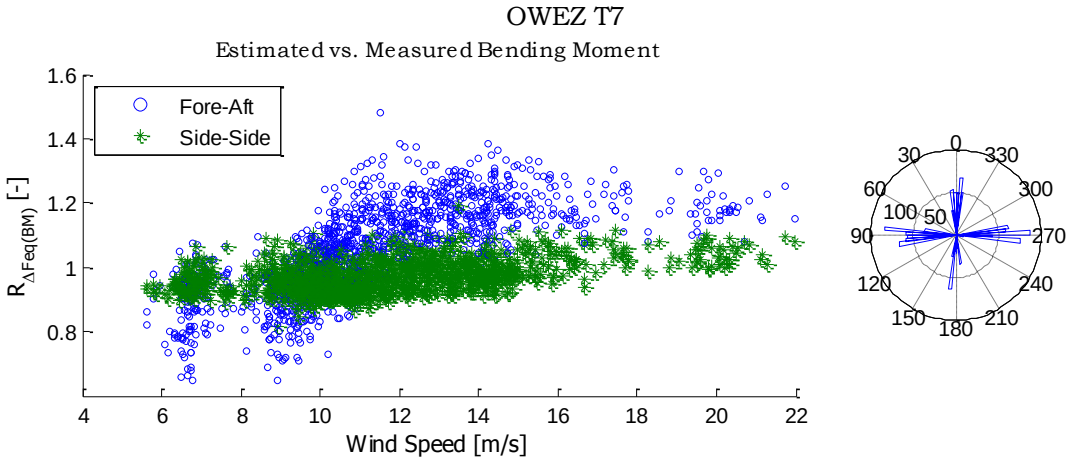

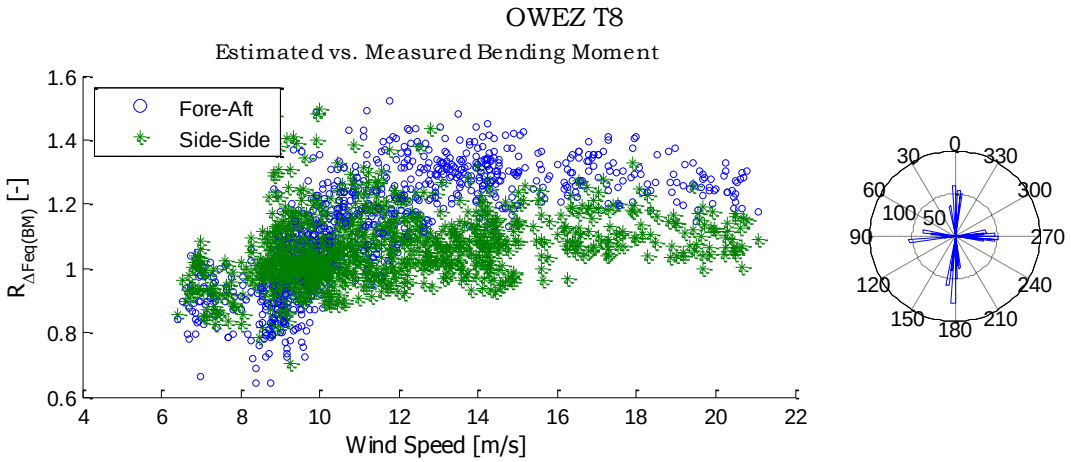

Appendix C Finding the Eigen mode of a Beam

When a blade (basically a clamped beam) is vibrating in its eigenmode, the load is determined by its mass and the local acceleration only - there are no external loads Suppose that the eigenmode (deflection) is described by *u(x) = ev(x)* and the amplitude at the tip *u(x=R) = 1*, then the force per metre *p(x)* is given by:

$$p(x) = m(x)ev(x)\ddot{u}(R)$$

This expression gives a way of finding the eigenmode, as follows. If the blade is moving in its eigenmode, the load is *p(x)*. However the shape under load *p(x)* can be found with beam theory. If the shape is a true eigenmode, it must of course be the same as the mode shape that was used to determine *p(x)* in the first place!

The above can be programmed in s simple recipe (for example in a spreadsheet or in Matlab) to find the eigenmode, the generalised mass, the frequency and the generalized stiffness.

As an exercise try this for a homogeneous steel tower of L = 100 m height without nacelle. The diameter is D = 3 m, and the wall thickness is t = 0.020 m. Steel density is ρ = 7850 kg/m^3 and Young's modulus is E = 2.1e11 Pa. Assume the distance between stations to be Δx (for example Δx = 1 m)

The relevant stiffness is:

$$EI = \frac{E\pi}{64}\left(D^4 - \left(D - 2t\right)^4\right) \approx \frac{E\pi}{8} D^3 t$$

1 Guess the first eigenmode $ev_0(x)$, for example a parabola $ev_0(x) = (x/L)^2$. Deflection at the top must be 1.
2 At the tower stations (say $x = 0, 1, .., L$), find the load $p(x) = m(x)\, ev_0(x)$ where $m(x)$ is the mass per metre.
3 Starting at the top with $F(L) = 0$, determine the shear force $F(x)$ at every station:

$$F(x - \Delta x) = F(x) + \frac{p(x - \Delta x) + p(x)}{2}\Delta x$$

4 Also find the bending moment. $M(L) = 0$ and for every other station:

$$M(x - \Delta x) = M(x) + F(x)\Delta x + \frac{p(x - \Delta x) + 2p(x)}{6}\Delta x^2$$

5 Find the local curvature $k(x) = M(x)/EI(x)$
6 Next find the angle $v(x)$ ($v(x)$ = 0 at the tower base)

$$v(x) = v(x - \Delta x) + \frac{k(x - \Delta x) + k(x)}{2}\Delta x$$

7 Find the deflection $u(x)$:

$$u(x) = u(x-\Delta x) + v(x-\Delta x)\Delta x + \frac{2k(x-\Delta x)+k(x)}{6}\Delta x^2$$

8 The current estimate of the frequency is now $\omega_0 = 1/\sqrt{u_L}$.
9 Normalise the deflection to unity at the top ($x = L$). This deflection is the new eigenvector $ev_1(x)$. Restart at step 1.
10 Continue until $ev(x)$ has converged. The generalized (effective) mass for the first mode is:

$$GM_1 = \int_0^L m(x)[ev(x)]^2\,dx$$

Which should come out to about 25% of the beam mass (if your calculation is correct). The exact solution for the first eigenfrequency of a homogeneous beam is:

$$\omega_1 = \frac{\lambda_1^2}{L^2}\sqrt{\frac{EI}{m}}$$

With λ_1 = 1.8751041. The approximate answer should be off by less than 1%.

The same method can be used for finding the eigenmodes of a blade.

2007.03.12/HFV

Appendix D Influence of waves (Flex5)

Waves and current create an additional loading to the base of the tower. The current is a constant distributed loading and the waves are a cyclic low-frequency loading. The response of the turbine is investigated with a PSD plot of the bending moments and the tower top deflection at 6 m/s wind speed, Figure D-1.

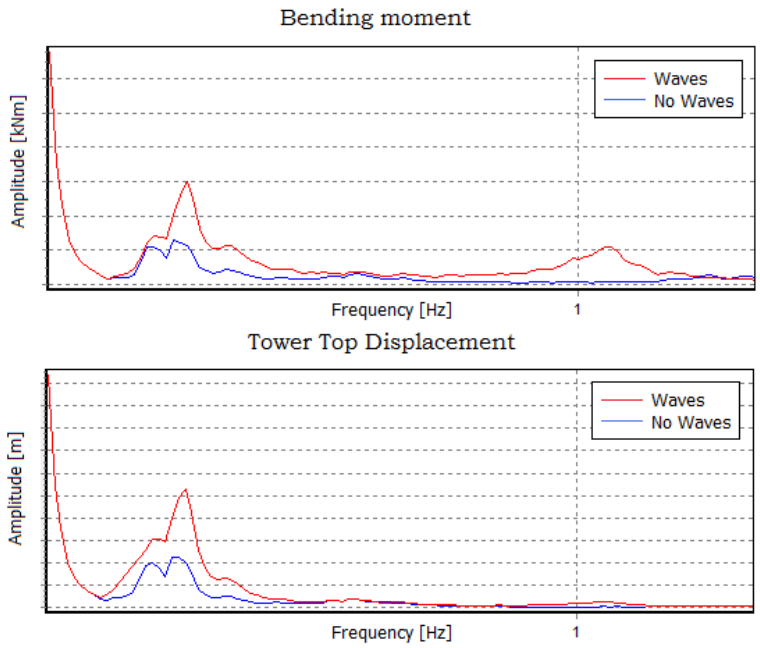

Figure D-1 Power spectral density plot of the bending moment and tower top displacement with and without wave loading

It shows that the amplitude at the 1st Eigen mode is much bigger with waves and current than without and there is an additional peak at just above at just above 1 Hz. The PSD's of the bending moment and the tower top displacement look alike except for the peak at 1 Hz. This might distort the linear relationship between the tower top deflection and the bending moment. In Figure D-2 the ratio between the equivalent loads calculated from the tower top displacement and the actual bending moment are given with respect to maximum wave height.

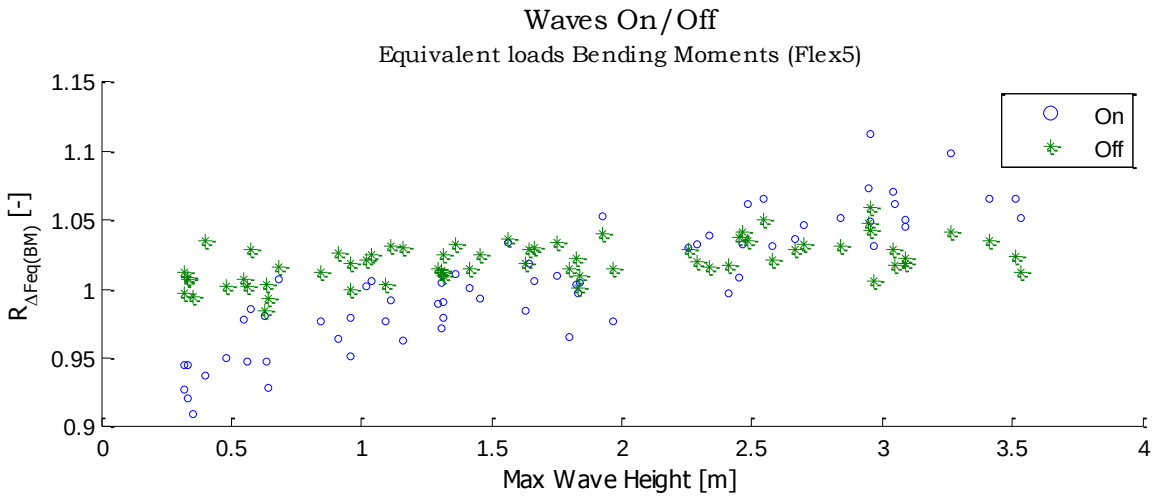

Figure D-2 Equivalent loads ratio between estimated bending moment from tower displacement and acutal bend moment (Flex5) (Ratio=Estimated/Measured)

It becomes visible that the tower top displacement is underestimated at low wave heights and over estimated at high wave heights. The same holds for wind speeds, since the wave height is very strongly correlated with the wind speed.

At the point where the thrust force is at its maximum (Figure D-3), the ratio is closer to zero, i.e. around 1.5 m max wave height. At the point where the wave loading is at its max and the thrust force is has become lower again the bending moments are even over predicted. It seems that whenever the wave loading is becoming more significant the mode shape is not able to describe the loading of the tower very well.

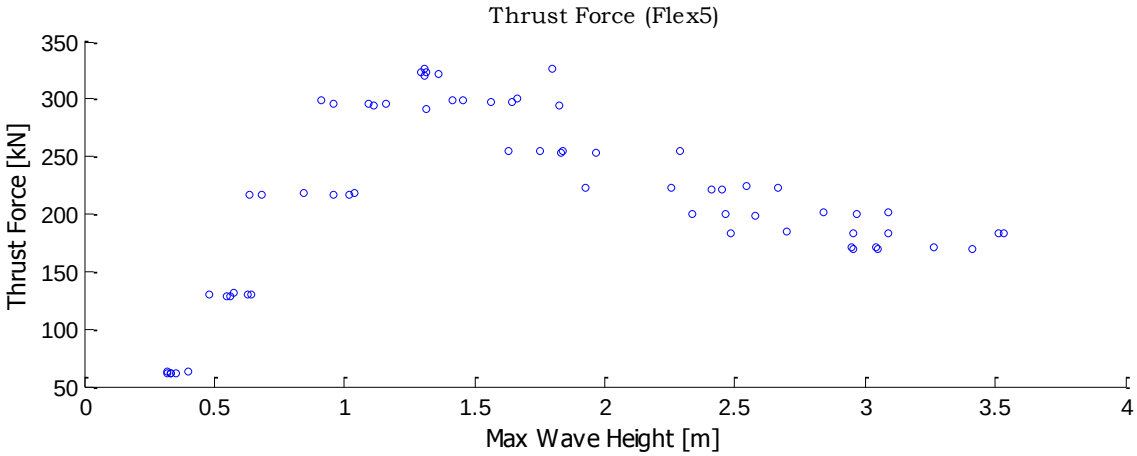

Figure D-3 Thrust force vs. wave height (Flex5)

A wind speed/wave height correction might thus necessary to predict the tower base bending moments from the tower top deflection in an offshore environment. It is not expected that this phenomenon will be visible in the Side-Side direction since the waves, current and wind are all aligned with the F-A direction.